

See discussions, stats, and author profiles for this publication at: <https://www.researchgate.net/publication/344606344>

# Damage and equivalent load definition for durability of vehicle

Thesis · August 2018

DOI: 10.13140/RG.2.2.20834.96969

---

CITATIONS

0

READS

2,494

1 author:



Benegúz Dániel Lévai

Linköping University

1 PUBLICATION 0 CITATIONS

SEE PROFILE

Linköping University | Department of Management and Engineering  
Master's thesis, 30 credits | Master's Mechanical Engineering programme  
Spring/ autumn 2018 | LIU-IEI-TEK-A--18/03044—SE

# Damage and equivalent load definition for durability of vehicle

Bendegúz Dániel Lévai

Company Supervisor, Mehdi Mehrgou (AVL Graz)  
University Supervisor, Dr. Joakim Holmberg  
Examiner, Jonas Stålhand



Linköping University  
SE-581 83 Linköping, Sweden  
+46 013 28 10 00, [www.liu.se](http://www.liu.se)

## **Upphovsrätt**

Detta dokument hålls tillgängligt på Internet – eller dess framtida ersättare – under 25 år från publiceringsdatum under förutsättning att inga extraordinära omständigheter uppstår.

Tillgång till dokumentet innebär tillstånd för var och en att läsa, ladda ner, skriva ut enstaka kopior för enskilt bruk och att använda det oförändrat för ickekommersiell forskning och för undervisning. Överföring av upphovsrätten vid en senare tidpunkt kan inte upphäva detta tillstånd. All annan användning av dokumentet kräver upphovsmannens medgivande. För att garantera äktheten, säkerheten och tillgängligheten finns lösningsmedel av teknisk och administrativ art.

Upphovsmannens ideella rätt innehåller rätt att bli nämnd som upphovsman i den omfattning som god sed kräver vid användning av dokumentet på ovan beskrivna sätt samt skydd mot att dokumentet ändras eller presenteras i sådan form eller i sådant sammanhang som är kränkande för upphovsmannens litterära eller konstnärliga anseende eller egenart.

För ytterligare information om Linköping University Electronic Press se förlagets hemsida <http://www.ep.liu.se/>.

## **Copyright**

The publishers will keep this document online on the Internet – or its possible replacement – for a period of 25 years starting from the date of publication barring exceptional circumstances.

The online availability of the document implies permanent permission for anyone to read, to download, or to print out single copies for his/hers own use and to use it unchanged for non-commercial research and educational purpose. Subsequent transfers of copyright cannot revoke this permission. All other uses of the document are conditional upon the consent of the copyright owner. The publisher has taken technical and administrative measures to assure authenticity, security and accessibility.

According to intellectual property law the author has the right to be mentioned when his/her work is accessed as described above and to be protected against infringement.

For additional information about the Linköping University Electronic Press and its procedures for publication and for assurance of document integrity, please refer to its www home page: <http://www.ep.liu.se/>.

# Abstract

The thesis aims to investigate adequate techniques to evaluate and estimate fatigue damage in the durability analysis of vehicles.

The thesis implements stress based linear damage accumulation rules e.g. Miner's modified. Multiple methods are tested to connect external loads to internal i.e. stress. These methods are quasi-static superposition method, modal superposition method, and frequency response approach. For the testing several loading signals are defined and applied to the same simple geometry (in this case a beam). The methods are compared across the different loadcases which supposed to enforce different behaviour from the body that is of interest in a vehicle durability analysis e.g. excitations of eigenmodes. From the results of the investigation, modal superposition is further used to evaluate stress from a multiple body simulation (MBS) of a passenger car. The MBS uses several virtual road-profiles representing non-stationary random, deterministic periodic, and deterministic single event load signal types. The representation of vehicle uses flexible bodies. The results from MBS are modal participation factors and acceleration signals from 34 locations defined on the car in all 6 degrees of freedom. The modal participation factors are used in the model superposition method to calculate stress and used separately to estimate the location of critical points. These estimations are compared against the actual critical point locations calculated from stress. The acceleration signals are used to define pseudo damage. Which is used to reduce data size and compare measurements i.e. simulations. The method's additional applicability is investigated in terms evaluation of load severity correlating with real damage. For that purpose, previously calculated damage is used as reference and pseudo damage definition is modified to have better agreement. The changes in definition include the selection of acceleration signals, combination of several signals and the optimization of parameters. The parameter optimization is done using genetic optimization algorithm.

From the methods tested for internal load calculation, modal superposition method was used, due to the quicker implementation into MBS, and because it captures increased stress responses due to excitation of eigenfrequencies.

The estimation of critical points has the potential for accuracy with the implementation of added suggestions discussed in the thesis. A reduced model including only the critical points saves substantial computational time. In the examples of this thesis from several hours to few minutes.

From the results of this thesis damage estimations from pseudo damage can be improved. However, the accuracy is not satisfactory for final evaluation fatigue.

## Acknowledgement

I would like to thank AVL List GmbH, Graz with special thanks to Mehdi Mehrgou giving me the opportunity for this project and providing me working space, literature, and all the necessary resources for the success of this thesis.

I express my gratitude towards the entire staff of Linköping University for accepting me and enabling me to learn and grow as an engineer. I am particularly grateful for the continuous support, guidance, and encouragement from my supervisor, Dr. Joakim Holmberg.

I also wish to thank Andreas Benjamin Ofner and André Dinis master students for their valuable insights related to my thesis, and for all the coffee table conversations not so related to the thesis.

# Content

Abstract .....	i
Acknowledgement.....	ii
Content .....	iii
List of figures .....	v
List of tables .....	vii
Nomenclature.....	viii
1. Introduction .....	1
1.1. Background .....	1
1.2. Objectives.....	2
1.3. Methods.....	2
1.4. Limitations .....	3
2. Theory.....	4
2.1. Methods to evaluate internal loads from complex models .....	4
2.1.1. Quasi-static superposition method (QSSM) .....	4
2.1.2. Modal superposition method (MSM) .....	5
2.1.3. Frequency response approach (FRA).....	7
2.2. Critical plane method .....	8
2.3. Damage definitions.....	9
2.4. Pseudo damage.....	11
3. Beam model .....	12
3.1. Model description.....	12
3.2. Application of Quasi-static superposition .....	12
3.3. Application of Modal superposition .....	14
3.4. Application of Frequency response approach.....	16
3.5. Case studies .....	17
3.5.1. Load cases .....	17
3.5.2. Results & discussion.....	19
4. Body in white model .....	24
4.1. Model description.....	24
4.2. Method to evaluate stress .....	28
4.3. Analysis .....	28
4.3.1. Modal participation factors .....	28
4.3.2. Critical points.....	35
4.3.3. Prominent modeshapes.....	36
4.3.4. Damage .....	39

4.4. Equivalent Pseudo damage definition.....	41
4.4.1. Pseudo damage and stress.....	42
4.4.2. Evaluation of channels .....	45
4.4.3. Evaluation of loadcases .....	50
4.4.4. Evaluation of parameters.....	52
5. Conclusion .....	57
6. Future work .....	58
References .....	59
Appendix A .....	61
A.1. Modes and frequencies of constrained beam.....	61
Appendix B.....	62
B.1. Modes and frequencies of BIW .....	62
B.2. BIW hotspots, critical points, and prominent modes .....	63
B.2.1. Hotpots .....	63
B.2.2. Critical points.....	64
B.2.3. Mode 1 .....	66
B.2.4. Mode 2 .....	68
B.2.5. Mode 28 .....	70
B.2.6. Mode 110 .....	72
B.2.7. Mode 114 .....	74
Appendix C .....	76
C.1. Accelerometer locations and channels.....	76
Appendix D .....	81
D.1. Results of optimization .....	81

# List of figures

Figure 1 Critical plane .....	8
Figure 2 S-N curves of different damage models .....	10
Figure 3 Beam model with boundary conditions .....	12
Figure 4 Workflow of Quasi-static superposition method.....	13
Figure 5 System response of Beam model to unit Tx load.....	13
Figure 6 System response of Beam model to unit Fy load.....	14
Figure 7 Workflow of Modal superposition method .....	15
Figure 8 Modeshapes of unconstrained Beam model.....	16
Figure 9 Workflow of Frequency response approach.....	17
Figure 10 Load-history of Subcase 1-4 (partial) .....	18
Figure 11 PSDs of Tx Subcase 1-4.....	18
Figure 12 PSDs of equivalent stress at critical point from QSSM .....	19
Figure 13 PSDs of equivalent stress at critical point from MSM .....	19
Figure 14 PSDs of equivalent stress at critical point from FRA.....	20
Figure 15 Fatigue damage from Subcase 1-4 .....	21
Figure 16 RFM of stress cycles from Subcase 1 (QSSM) .....	21
Figure 17 RFM of stress cycles from Subcase 1 (MSM) .....	21
Figure 18 RFM of stress cycles from Subcase 1 (FRA).....	21
Figure 19 PSDs of equivalent stress at critical point from QSSM .....	22
Figure 20 PSDs of equivalent stress at critical point from MSM .....	22
Figure 21 PSDs of equivalent stress at critical point from FRA.....	22
Figure 22 Fatigue damage from Subcase 5-8 .....	23
Figure 23 RFM of stress cycles from Subcase 8 (MSM) .....	23
Figure 24 RFM of stress cycles from Subcase 8 (FRA).....	23
Figure 25 Finite element model of Body in white .....	24
Figure 26 Virtual vehicle model of Body in white .....	25
Figure 27 Rough road and Cobblestone roadprofiles .....	25
Figure 28 In-phase and Out-of-phase Washboards .....	25
Figure 29 Potholes, Curb island and Bumps roadprofiles .....	26
Figure 30 Alternative workflows for stress evaluation on BIW .....	28
Figure 31 2 <sup>nd</sup> and 51 <sup>st</sup> modal participation factors from Lc 5 .....	29
Figure 32 All modal participation factors from Lc 5.....	30
Figure 33 Pseudo damage from modal participation factors .....	30
Figure 34 Summed pseudo damage from modal participation factors .....	31
Figure 35 Maximum Von Mises stress from modeshapes .....	31
Figure 36 Summed pseudo damage from scaled modal participation factors .....	32
Figure 37 Relative summed pseudo damage .....	32
Figure 38 Pseudo damage from modal scaled participation factors .....	33
Figure 39 Pseudo damage from scaled modal participation history of Lc 5 .....	33
Figure 40 Pseudo damage from scaled modal participation history of Lc 5 (Re-ordered modes) ..	34
Figure 41 Pseudo damage from scaled modal participation history of Lc 4 .....	37
Figure 42 PSD of equivalent stress at critical point from Lc 4 .....	37
Figure 43 Computational time saving .....	38
Figure 44 Fatigue Damage of BIW .....	39
Figure 45 RFM from FEMFAT .....	39
Figure 46 RFM from WAFO .....	39

Figure 47 Modified S-N curves of critical points .....	40
Figure 48 Miner modified dmg and Pseudo dmg from modal participation factors .....	40
Figure 49 Accuracy of pseudo damage from modal participation factors.....	41
Figure 50 Equivalent stress history at critical point from Lc 11.....	43
Figure 51 Acceleration history at channel 45 from Lc 11 .....	43
Figure 52 Acceleration history at channel 105 from Lc 11 .....	43
Figure 53 PSD of equivalent stress at critical point from Lc 11 .....	44
Figure 54 PSD of acceleration at channel 45 from Lc 11 .....	44
Figure 55 RFM of equivalent stress at critical point from Lc 11 .....	44
Figure 56 RFM of acceleration at channel 45 from Lc 11 .....	45
Figure 57 RFM of acceleration at channel 105 from Lc 11 .....	45
Figure 58 Relative pseudo damage from acceleration .....	46
Figure 59 Relative Miner modified damage .....	46
Figure 60 Comparison of Miner modified damage and Pseudo damage from channel 195 .....	47
Figure 61 $f_{max}$ from selected Chs .....	48
Figure 62 Comparison of Miner modified dmg and summed Pseudo dmg from all Chs.....	49
Figure 63 Deviation of summed Pseudo dmg from all Chs .....	49
Figure 64 Deviation of summed Pseudo dmg from all Chs (reduced Lcs) .....	49
Figure 65 Miner modified dmg and summed Pseudo dmg from all Chs (reduced Lcs).....	49
Figure 66 Modified S-N curves of critical points (enlarged from Figure 47) .....	50
Figure 67 Best/Average/Worst channels across loadcase groups .....	51
Figure 68 Comparison of Miner modified dmg and parametrized Pseudo damage from <i>Ch7,36</i> ..	55
Figure 69 Comparison of Miner modified dmg and parametrized Pseudo damage from <i>Ch8,36</i> ..	55
Figure 70 Comparison of Miner modified dmg and parametrized Pseudo damage from <i>Ch9,36</i> ..	56
Figure 71 Modes and frequencies of constrained beam .....	61
Figure 72 Hotspots of BIW.....	63
Figure 73 Critical points of BIW (1/4) .....	64
Figure 74 Critical points of BIW (2/4) .....	64
Figure 75 Critical points of BIW (3/4) .....	65
Figure 76 Critical points of BIW (4/4) .....	65
Figure 77 Mode 1 with hotspot and critical point (1/3) .....	66
Figure 78 Mode 1 with hotspot and critical point (2/3) .....	66
Figure 79 Mode 1 with hotspot and critical point (3/3) .....	67
Figure 80 Mode 2 with hotspot and critical point (1/3) .....	68
Figure 81 Mode 2 with hotspot and critical point (2/3) .....	68
Figure 82 Mode 2 with hotspot and critical point (3/3) .....	69
Figure 83 Mode 28 with hotspot and critical point (1/3) .....	70
Figure 84 Mode 28 with hotspot and critical point (2/3) .....	70
Figure 85 Mode 28 with hotspot and critical point (3/3) .....	71
Figure 86 Mode 110 with hotspot and critical point (1/3) .....	72
Figure 87 Mode 110 with hotspot and critical point (2/3) .....	72
Figure 88 Mode 110 with hotspot and critical point (3/3) .....	73
Figure 89 Mode 114 with hotspot and critical point (1/3) .....	74
Figure 90 Mode 114 with hotspot and critical point (2/3) .....	74
Figure 91 Mode 114 with hotspot and critical point (3/3) .....	75
Figure 92 Locations of accelerometers (1/3).....	76
Figure 93 Locations of accelerometers (2/3).....	77
Figure 94 Locations of accelerometers (3/3).....	77

## List of tables

Table 1 Loadcases of Beam analysis .....	17
Table 2 Loadcase description of BIW analysis.....	27
Table 3 Most prominent modes .....	34
Table 4 Comparison of predicted and actual critical points .....	35
Table 5 Channels located near to critical points.....	46
Table 6 $f_{max}$ from summed pseudo dmgs of different sets of Chs .....	48
Table 7 Loadcase groups.....	50
Table 8 Best $f_{max}$ from loadcase groups .....	52
Table 9 Optimum objective values.....	54
Table 10 Over and under estimations of optimized pseudo damage .....	54
Table 11 Modes and frequencies of BIW .....	62
Table 12 Accelerometer channels .....	80
Table 13 Parameters of optimized pseudo damage definition from <i>Ch7,12</i> .....	81
Table 14 Parameters of optimized pseudo damage definition from <i>Ch7,36</i> .....	82
Table 15 Parameters of optimized pseudo damage definition from <i>Ch7,102</i> .....	85
Table 16 Parameters of optimized pseudo damage definition from <i>Ch8,12</i> .....	85
Table 17 Parameters of optimized pseudo damage definition from <i>Ch8,36</i> .....	86
Table 18 Parameters of optimized pseudo damage definition from <i>Ch8,102</i> .....	89
Table 19 Parameters of optimized pseudo damage definition from <i>Ch9,12</i> .....	89
Table 20 Parameters of optimized pseudo damage definition from <i>Ch9,36</i> .....	90
Table 21 Parameters of optimized pseudo damage definition from <i>Ch9,102</i> .....	93
Table 22 Optimization parameters .....	93

# Nomenclature

## Mathematical style

Representation	Description	Meaning
$a$	Italic	Number
$\bar{a}$	Overbar	Vector
$\bar{\bar{a}}$	Double overbar	Matrix
$\{a\}$	Curly brackets	Vector, in finite element representation
$[a]$	Square brackets	Matrix, in finite element representation
$\{a\}^T, [a]^T$	Superscript T	Vector transpose, Matrix transpose
$[a]^{-1}$	Superscript -1	Inverse matrix
$\dot{a}$	Dot	First time derivative
$\ddot{a}$	Double dot	Second time derivative
$a(x)$	Followed by $(x)$	Function of spatial position
$a(t)$	Followed by $(t)$	Function of time
$a(f)$	Followed by $(f)$	Function of frequency
$S_i(a(t))$	$S_i(\dots)$	Cycle count of time signal

## Symbols

Symbol	Description
$a$	Acceleration
$\alpha$	Proportional constant
$\beta$	Damage exponent (slope of S-N curve)
$D$	Fatigue damage
$d$	Pseudo damage
$e$	Unit load
$f$	Symmetric distance measure
$L$	External loading (force/moment)
$l$	Numerical values of external loading
$p$	Dirlik probability density function
$\Phi$	Modal shape
$\Psi$	Modal stress
$q$	Modal participation factor
$S$	Amplitude of a cycle
$\sigma$	Stress
$u$	Displacement

## Abbreviations

---

BIW	Body in white
Ch	Channel
dmg	Damage
FEA	Finite Element Analysis
FRA	Frequency Response Approach
Lc	Loadcase
MB	Multi-Body
MBS	Multi-Body Simulation
MSM	Modal Superposition Method
PSD	Power Spectral Density
QSSM	Quasi-Static Superposition Method
RFM	Rainflow Matrix
VPD	Virtual Product Development
VPG	Virtual Proving Ground

---

# 1. Introduction

## 1.1. Background

Since the car's mass production has begun in the early 20<sup>th</sup> century its role become increasingly integral to society. The car provides mobility, comfort, and access to remote places, which result in increased economic and social interactions. It is hard to imagine modern life without these benefits. However, automotive use also brought many negative consequences such as: pollution, exploitation of non-renewable resources, and accidents. [1] Therefore, the goals of the automotive industry must include mitigating these negative effects, in addition to expanding the benefits what a car can provide. One aspect which can play an important role in this is durability.

Durability is the question of whether a structure can remain functional under its intended use case. In this question fatigue is big factor, as it is considered the reason for 60- 90% of all mechanical failures. [2] [3] Therefore, the evaluation of fatigue life is essential to ensure safety. Moreover, increased accuracy and speed in the process raise potential for sustainable designs. Longer working lives can be safely ensured, and/or with fewer resources. However, there are several angles from which the evaluation of fatigue can be approached.

One approach is by modelling the vehicle. An increasing trend in the automotive industry is the implementation of Virtual Product Development (VPD) which has the potential to eliminate physical testing from the development of vehicle. [4] However, to create good designs, accurate modelling of the car is necessary. This can be a very complex process. Decisions must be made about how many components should be included or what can be neglected, how to represent contacts (idealized joints, nonlinear contact, spot-welds), what tire model to use, should the elasticity of car body be included and so on. [4] [5] The determination of critical points is also essential since fatigue is a local phenomenon. [2] Adequate FEA modelling in these points are especially important. Fortunately, today it is most likely possible to find accurate modelling techniques for all these questions, however with increased complexity comes increased computational time. This problem can easily become a limiting factor in decades from now. Gordon Moore, cofounder of Intel said in an interview "I see Moore's Law dying here in the next decade or so" [6] where he referred to the observation (named after him) that the number of transistors in dense integrated circuits double in every two years. Therefore, waiting for technology to catch up to complex problems is inadvisable. Thus, simplifying FEA models while keeping fatigue related aspects intact is important. In this process, the key aspect to keep is the amplitude of stress cycles. [2] Therefore, one question of this thesis is how to arrive to stresses (internal loads) from the applied forces or displacement (external loads) most efficiently.

Another approach for durability analysis is via psychical testing. In this case, it needs to be verified that a component meets its design targets. Design targets are phrased as e.g. 1 million kilometres driven distance in Europe without failure. However, the loading is varied by the quality of roads in a specific region, speed limits, driving style, cargo, and by climate as well. [7] This would mean multiple tests to cover the entirety of customer usage. Furthermore, if testing is done using 'representative' loads e.g. driving in the intended customer region for 1 million kilometres, this becomes an extremely long and expensive process. [7] [8] Thus, there is a need for defining verification loads. Ideally, the verification loads should represent the design targets but in a much shorter time. Another important aspect of the verification load is that it does not alter the failure mechanism of design targets, e.g. high cycle fatigue. The definition of such equivalent load relies

on relating the test scenario to the design scenario i.e. establishing how much more severe the verification load is compared to the design target. [7] Relating verification loads to design targets is fairly straight forward by modelling the whole vehicle and evaluating stresses. However, if such an accurate model exists, testing is no longer necessary and VPD can be implemented instead. Thus, another big question of this thesis is to determine the severity of loads relative to each other, based on external loads e.g. accelerations.

## 1.2. Objectives

As mentioned before, there are several angles from which the evaluation of fatigue can be approached from. Navigating through them requires good understanding of the underlying principles to select the most suitable way. This thesis aims to contribute to this area by elaborating on how to implement different methods and examine their merits and limitations.

The specific goals for this thesis are:

- Evaluate multiple methods for stress calculation applicable to complex models (due to some form of simplification)
- Investigate the possibility of predicting critical points
- Fatigue life calculation from internal loads i.e. stresses on a vehicle's body in white (BIW)
- Investigate ways to relate severity of loadcases to each other on BIW based on external loads i.e. accelerations

## 1.3. Methods

The problem of calculating stress will be investigated by testing three methods which are applicable to complex models. These three methods are: Quasi-static superposition, Modal superposition, and Frequency response approach. These methods will be compared against each other analysing a simple beam model to reveal their advantages and disadvantages.

One method will be selected to calculate damage on BIW from several different loadcases. The selection will be based on which method is the most applicable to analysis of vehicle. The loadcases will be defined as virtual road profiles in a multi-body simulation (MBS). The simulations will include straight line events, and flexible body representations.

Alongside MBS the possibilities of making predictions for the location of critical points will be tested. The accuracy of these predictions will be evaluated. In case of mismatches recommendations will be made for improvements.

In addition, time savings will be investigated in case of a reduced BIW model. The model reduction will be based on estimated critical points by excluding rest of the geometry from stress evaluation.

The possibility of estimating the relative severity of different loadcases based on measurable acceleration signals will be investigated using pseudo damage. Pseudo damage is a commonly used method for data reduction and as way to compare measurements. [7] The relative severity of loadcases based on pseudo damage will be extensively compared to the ones based on real damage (calculated from stress previously).

## **1.4. Limitations**

- a) Modal superposition method relies on modal transient analysis. This type of analysis is only applicable when no damping or only modal damping is used. [9]
- b) In 3.5.1 the load definition for the Frequency response approach were power spectral densities (PSDs) calculated from the time signals in MATLAB using Welch's method. Due to windowing the frequency band which contains the power of signal widened compared to the theoretical PSD. [3]
- c) In 4.3.1-4.3.3 the estimation of critical points is based on modal participation factors. The interaction of modal participation factors was neglected, therefore these predictions can be less accurate dependent on influence of interactions.
- d) A limitation of the performed analyses on BIW is that the accuracy of vehicle model was not verified (done by real life testing). Suspension parameters, structural damping, spot-weld representations and excluded structural components and masses can have a big influence on the results. Therefore the damage values do not reflect the fatigue life of the real vehicle.
- e) Pseudo damage is not commonly used to evaluate the severity of loads. It is only a basis comparing measurements. [7] However in Section 4.4 it was used to investigate the possibility of not just measurement comparison, but equivalent load i.e. damage prediction as well.

## 2. Theory

### 2.1. Methods to evaluate internal loads from complex models

In the following 3 methods are going to be introduced to calculate internal loads e.g. stress. Later in Section 3.2-3.4, the implementation of these methods will be detailed.

On a side note, most FEA solvers are displacement-based and not stress-based. However, the strain field of a structure can be extracted from the displacement field by partial derivatives, and assuming linear elasticity the strain field describes the stress field based on Hook's law. This means that calculating the displacement field of a structure also acquires a description of the stress field. Consequently, the following methods will not necessarily be formulated for stress, but often for displacement. [10]

#### 2.1.1. Quasi-static superposition method (QSSM)

The underlying assumption for this method is that the subject is a stiff component. That is, the highest frequency of external loads is much smaller than the lowest eigenfrequency of the structure. In this case internal stresses linearly depend on external loads which makes the following representation of linear combination possible: [7]

$$\bar{\sigma}(x, t) = \sum_{i=1}^n \bar{c}_i(x) l_i(t) \quad (1)$$

where

$x$  – Point of structure

$i = 1, \dots, n$  - Number of external loads (integer) [-]

$\bar{\sigma}(x, t)$  – Local stress tensor at point  $x$  of the structure in time  $t$  (e.g. in Voigt notation) [MPa]

$\bar{c}_i(x)$  – Linear coefficient for load  $i$  [-]

$l_i(t)$  – Individual external load value in time [-]

The determination of  $\bar{c}_i$  is possible by means of static FEA, however, in practice it is rarely calculated explicitly, instead the following formulations are used.

The following equation needs to be solved:

$$[K] * \{u\}(t) = \{L\}(t) \quad (2)$$

where

$[K]$  – Stiffness matrix [-]

$\{u\}(t)$  – Displacement in time [mm]

$\{L\}(t)$  - External loads in time (vector function) [N] and/or [Nm]

The external load vector  $\{L\}(t)$  is composed of individual load vectors  $\bar{L}_i(t)$  expressed as:

$$\bar{L}_i(t) = l_i(t) * \bar{e}_i \quad (3)$$

where

$\bar{L}_i(t)$  – Individual external loads [N] or [Nm]

$l_i(t)$  - Numerical values in time of individual external loads [-]

$\bar{e}_i$  – Unit load [N] or [Nm]

Instead of solving (2) directly in QSSM each unit load is evaluated in a separate static FEA.

$$[K] * \{u\}_i = \{e\}_i \quad (4)$$

where

$\{u\}_i$  – Displacement in response to unit load  $i$  [mm]

The total system response can be expressed by superposing the results of each static analysis  $\{u\}_i$  (expressed as  $\bar{u}_i(x)$ ) and multiplied by loads' time signals: [7]

$$\bar{u}(x, t) = \sum_{i=1}^n l_i(t) \bar{u}_i(x) \quad (5)$$

The distinction between  $\{u\}_i$  and  $\bar{u}_i(x)$  is that  $\{u\}_i$  is a vector containing displacements for all nodes of the discretized structure i.e. finite element model while  $\bar{u}_i(x)$  is a vector function of  $x$  containing displacements for only point  $x$ .

The benefit of this method is that after evaluating the unit loads by FEA, any loading can be evaluated by just applying new time signals in Eq. (5), without any further FEA. Furthermore, if the critical location of a structure is known, then only these spots need to be evaluated.

$$\bar{u}(x_{crit}, t) = \sum_{i=1}^n l_i(t) \bar{u}_i(x_{crit}) \quad (6)$$

where

$x_{crit}$  – The position of critical point [mm]

### 2.1.2. Modal superposition method (MSM)

The modal superposition method describes the deformation of a structure by its vibrational mode shapes  $\Phi_i(x)$ . Modeshapes are calculated in a modal analysis by solving the following equation of motion for undamped vibrations: [9]

$$[M]\{\ddot{u}\} + [K]\{u\} = 0 \quad (7)$$

where

$[K]$  – Stiffness matrix [-]

$[M]$  – Mass matrix [-]

$\{u\}$  - Displacement [mm]

$\{\Phi\}$  is defined as: [9]

$$\{u\} = \{\Phi\} \sin(\omega t) \quad (8)$$

where

$\{\Phi\}$  – Modeshapes i.e. eigenvectors [mm]

$\omega$  - circular natural frequency [rad/s]

$\{\Phi\}_i$  are determined by the non-trivial solutions of the following eigenequation: [9]

$$([K] - \omega_i^2 [M])\{\Phi\}_i = 0 \quad (9)$$

A useful characteristic of  $\{\Phi\}_i$  is that the deflection of a linear elastic structure can be expressed as the linear combination of modeshapes at any given time: [7]

$$\bar{u}(x, t) = \sum_{i=1}^n q_i(t) \Phi_i(x) \quad (10)$$

where

$q_i(t)$  – Modal participation factor for mode  $i$  [-]

This formulation is the basis of MSM. It also bears resemblance with Eq. (5),  $q_i$  are scalar time signals, like  $l_i$ . However, it is more abstract, and unfortunately cannot be measured. The calculation of modal participation factors is done by a modal transient FEA, where the following equation of motion is solved (ignoring damping): [9]

$$[M]\ddot{\{u\}}(t) + [K]\{u\}(t) = \{L\}(t) \quad (11)$$

If modeshapes are expressed as a matrix  $[\Phi]$  where each column is  $\{\Phi\}_i$  and  $q_i(t)$  is written as vector  $\{q\}(t)$ , then (10) can be rewritten as: [9]

$$\{u\}(t) = [\Phi] \{q\}(t) \quad (12)$$

Inserting (12) into (11) and multiplying by  $[\Phi]^T$  gives

$$[\Phi]^T [M] [\Phi] \ddot{\{q\}}(t) + [\Phi]^T [K] [\Phi] \{q\}(t) = [\Phi]^T \{L\}(t) \quad (13)$$

The following quantities can be defined: [9]

$[m] = [\Phi]^T [M] [\Phi]$  - Modal (generalized) mass matrix

$[k] = [\Phi]^T [K] [\Phi]$  - Modal (generalized) stiffness matrix

$\{p\}(t) = [\Phi]^T \{L\}(t)$  - Modal force vector

$[m]$ ,  $[k]$  are diagonal matrices, which means that equation (13) is uncoupled. Therefore  $q_i(t)$  for (10) can be easily determined by just solving: [9]

$$m_{ii} \ddot{q}_i(t) + k_{ii} q_i(t) = p_i(t) \quad (14)$$

where

$m_{ii}$  - Modal mass for the  $i^{\text{th}}$  mode

$k_{ii}$  - Modal stiffness for the  $i^{\text{th}}$  mode

$p_i$  - Modal force for the  $i^{\text{th}}$  mode

An advantage of MSM is the reduction of computational cost. The entire system's response is described by modal shapes and modal participation factors in Eq. (10).  $\Phi_i$  only need to be calculated once in a modal analysis as in Eq. (9) and  $q_i$  can be easily determined by Eq. (14) for any new loading definition.

In addition, MSM is nicely implementable into the definition of flexible bodies in Multi-body simulations (MBS). The goal of flexible body definition is to describe the relative displacements of coupling points, which are the points where joints and forces are defined in MBS. These displacements are defined by modeshapes by Eq. (10). However,  $\Phi_i$  in this context can be different to vibrational modes i.e. normal modes. The mode shapes can also come from the structure's response to the application of a unit load i.e. static modes. Applying only static modeshapes is equivalent with QSSM. When both normal and static modes are included the method is called Craig-Bampton method. [7]

### 2.1.3. Frequency response approach (FRA)

The formulation of this approach also bears a resemblance to QSSM, since here too the system's response to unit loads are scaled and superposed. However, in this case the loads are expressed in the frequency domain, and the structure's response  $\sigma_i(f)$  is a function of frequency too. [11]

$$\bar{\sigma}(x, f) = \sum_{i=1}^n \bar{\sigma}_i(x, f) l_i(f) \quad (15)$$

where

$\bar{\sigma}(x, f)$  - Total stress response at point  $x$  [MPa]

$\bar{\sigma}_i(x, f)$  - Stress response at point  $x$  to unit load  $i$  [MPa]

$l_i(f)$  - Individual external load in the frequency domain [-]

$\bar{\sigma}_i(x, f)$  (expressed as  $\{\sigma\}_i(f)$ ) are calculated by the following:

$$\{\sigma\}_i(f) = [\Psi] \{T\}_i(f) \quad (16)$$

where

$[\Psi]$  - Modal stress [MPa] from

$$\{\sigma\}(t) = [\Psi] \{q\}(t) \quad (17)$$

$\{T\}_i(f)$  - Transfer function (vector) [-] from

$$\{T\}_i(f) = (-(2\pi f)[m] + i2\pi f[d] + [k])^{-1}[\Phi]\{e\}_i \quad (18)$$

and

$[d] = [\Phi]^T [D] [\Phi]$  - Modal (generalized) damping matrix

In practice the unit loads  $e_i$  are evaluated in a modal frequency response analysis [9]. The response of the system is dependent on the frequency of the unit load, which is encapsulated in the transfer function  $\{T\}_i(f)$ . This combined with the PSD of external loads describes the total system response  $\{\sigma\}(f)$  in the frequency domain as a stress PSD. The advantage of this method is, again, that after the first initial FEAs, any new loading can be evaluated by just Eq. (15). Further details about the application of FRA is in Section 3.4.

## 2.2. Critical plane method

In fatigue related applications the definition of an equivalent stress becomes especially important. The accumulated damage is based on stress cycles. In case the stress is multiaxial the use of equivalent stress is necessary. However, the commonly used von Mises stress cannot by definition Eq. (19) produce negative values, which property would skew the results. This is the easiest to see, in a uniaxial case, ( $\sigma_1 \neq 0, \sigma_2 = \sigma_3 = 0$ ) when one cycle of  $\sigma_1$  produces tension (positive sign) and compression (negative sign) in its extreme points. Using von Mises stress, the negative signs would disappear from the compressing part of the cycle, taking its absolute value. Therefore, the original cycle would be cut into two smaller cycles. Thus, there is a need for another equivalent stress definition.

$$\sigma^{VM} = \sqrt{\frac{(\sigma_1 - \sigma_2)^2 + (\sigma_2 - \sigma_3)^2 + (\sigma_3 - \sigma_1)^2}{2}} \quad (19)$$

where

$\sigma^{VM}$  – von Mises stress

$\sigma_1, \sigma_2, \sigma_3$  – principal plane stresses

At the surface of components, the stress can be treated as a two-dimensional tensor. Cracks usually initiate from the outer surface with a preferred orientation. Therefore, there exists a critical plane normal to the surface (Figure 1) at which the definition of an equivalent stress is suitable for fatigue related applications. [7]

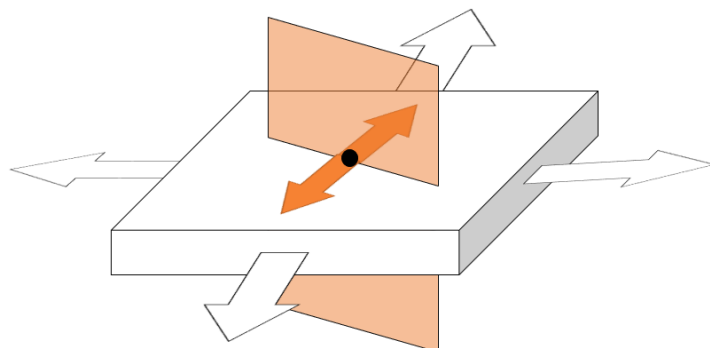


Figure 1 Critical plane

The method which is used in this thesis is one that is implemented in the commercial software FEMFAT. [11] The definition of equivalent stress is a modified version of the following equation. [12]

$$\sigma^{Eq} = sign(\sigma_n) \sqrt{\sigma_n^2 + \left(\frac{\sigma_a}{\tau_a}\right)^2 \tau_n^2} \quad (20)$$

where

$\sigma^{Eq}$  - Equivalent stress

$\sigma_n$  - Amplitude of normal stress in critical plane

$\tau_n$  - Amplitude of shear stress in critical plane

$\sigma_a$  - Alternating tensile/compressive strength

$\tau_a$  - Shear alternating stress limit

On a side note, here the word “alternating” refers to the loading characteristic of which the material property was derived from. Alternating, or fully reversed stress has zero mean value, i.e.  $\sigma_m = 0$  &  $\sigma_a \neq 0$ . [2]

The modification of Eq. (20) is documented in the software manual of FEMFAT as “Modified equivalent stress in the critical cutting plane”. [11] The manual and its content is bound to software license therefore the modification is not published here.

The process of determining the orientation of critical plane depends on the stress history.  $\sigma^{Eq}(t)$  is evaluated in several planes creating multiple equivalent stress definitions. The one which results in most damage is selected as critical. [12]

### 2.3. Damage definitions

According to [2] the rate or form (e.g. sine wave or square wave) at which internal loading is applied to a structure has no effect on the fatigue life. Therefore, once the internal loading of a structure is known, it is possible to evaluate the fatigue life of components by just the number and amplitude of stress cycles. The extraction of these cycles from a time signal can be done by several different counting methods e.g. rainflow counting. [7]

The evaluation of fatigue relies on fatigue life tests. In these tests, a cyclic load is applied to a test specimen with constant amplitude  $S_i$ . The number of cycles  $N_i$  is counted until failure. The test is repeated with other values of amplitude. A typical representation is the S-N curve shown in Figure 2. One of the simplest and most popular fatigue model is the Palmgren-Miner linear damage accumulation rule: [7]

$$D = \sum_{i=1}^k \frac{n_i}{N_i} \quad (21)$$

where

$D$  - is the total accumulated damage.

$n_i$  - is the number of applied load cycles at a constant amplitude

$N_i$  - is the number of applied load cycles at a constant amplitude at failure

$k$  - is the number of distinct  $S$  amplitude values

The criteria of failure is  $D = 1$

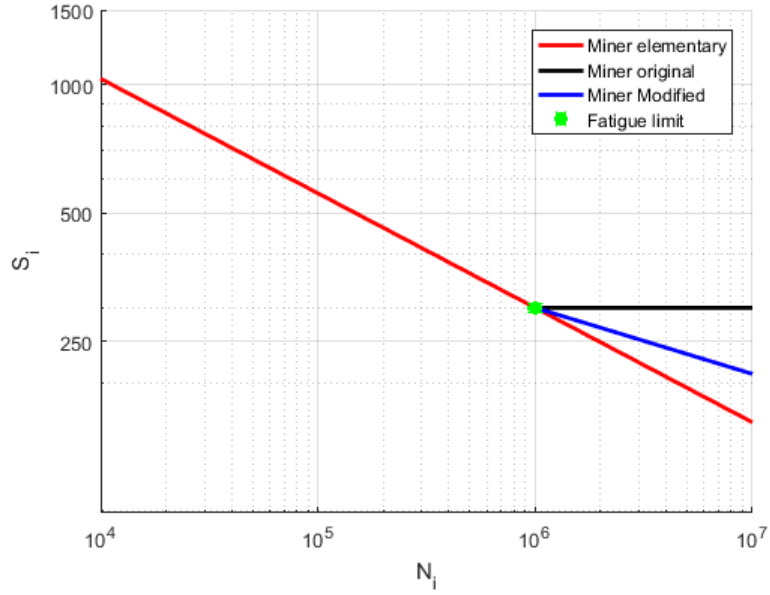


Figure 2 S-N curves of different damage models

There are three common ways to describe the S-N curve for Palmgren-Miner's model: miner elementary, miner original, and miner modified (see Figure 2). The S-N curve of the miner elementary damage model can be described by

$$N_i = \alpha * S_i^{-\beta} \quad (22)$$

where

$\alpha$  - Proportional constant

$S_i$  – Cycle amplitude

$\beta$  - Damage exponent i.e. slope of S-N curve

Based on linear damage accumulation rule the damage from one cycle ( $n_i=1$ ): [7]

$$D = \sum_{i=1}^k \frac{1}{N_i} = \frac{1}{\alpha} * \sum_{i=1}^k S_i^{-\beta} \quad (23)$$

According to [13] the life predictions of this model are usually nonconservative. More accurate damage estimation can be achieved by nonlinear models, which take into account the sequence of load cycles. However, these models usually follow an iterative process [14], which is more expensive computationally. Therefore, for the purposes of this thesis Palmgren-Miner's damage models will be used.

The damage model is additionally corrected by the modification of S-N curves based on mean stress and stress gradient following "2.7 Influence factors" in [11].

## 2.4. Pseudo damage

Pseudo damage is another tool to investigate the damage potential of external loads. The formulation of pseudo damage is based on linear damage accumulation and the elementary representation of an S-N curve. However, it is less reliant on material properties, therefore  $\alpha$  is left out. [7]

$$d = \sum_{i=1}^k S_i^\beta \quad (24)$$

where

$d$  - Pseudo damage

It is important to note that in case of Palmgren-Miner's damage  $S_i$  is interpreted as the amplitude of stress, since the corresponding S-N curves were determined by material testing based on stress. However,  $S_i$  in the formula of pseudo damage can be a cycle from any measured signal. Usually it is force or acceleration. This means the stress-based S-N curves are not applicable. Therefore, that the numerical value of pseudo damage does not provide information on how much of the fatigue life has been consumed.

The applicability of pseudo damage lies in the reduction of data. In case of a hundred acceleration sensor per measurements, the evaluation of each registered signal using rainflow matrices (RFMs) or PSDs would be unfeasible due to the sheer number of them. Using pseudo damage, each signal or channel provides just one number. This number due to  $\beta$  will be sensitive to high amplitudes the same way real damage is. That is, cycles twice as big generate  $2^\beta$  times the damage.

$$S^\beta = d$$

$$(2 * S)^\beta = 2^\beta * d$$

Therefore, despite the reduction of information, important fatigue related aspect of the signal is captured. However, it is generally not suitable to evaluate the fatigue life of a component, rather to provide comparisons between measurements. [7]

### 3. Beam model

The aim with this chapter is to investigate what type of behaviour is captured in response to the loading of a simple structure with practical applications of three different methods, described in Section 2.1.1-2.1.3.

#### 3.1. Model description

To make the analyses easy to run and/or reproduce, a simple I-beam will serve as the base geometry, see Figure 3.

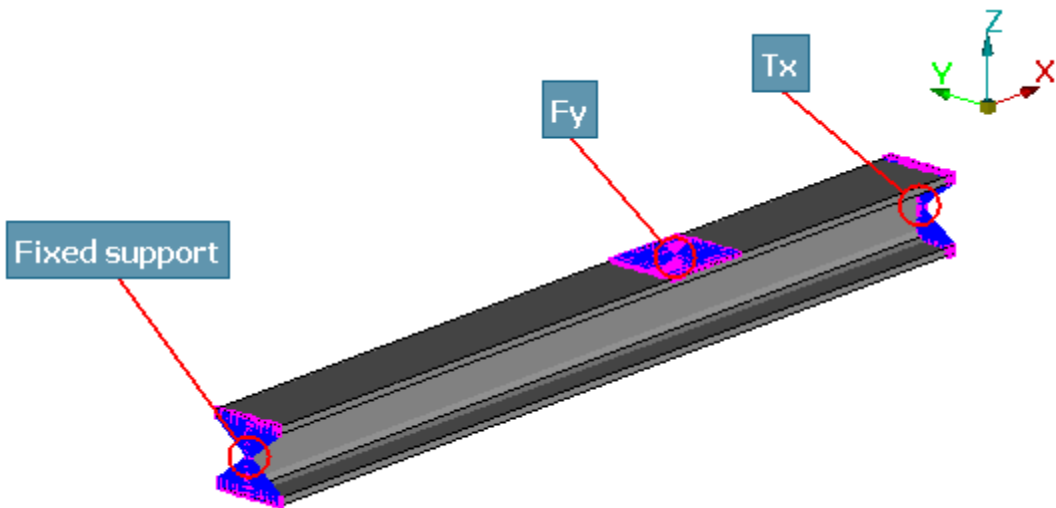


Figure 3 Beam model with boundary conditions

Using NASTRAN's element terminology [15], the model is composed by 7680 CHEXA elements, and 11982 nodes. Furthermore, several RBE2 rigid elements (blue in Figure 3) which connect the nodes of a specified area to a single centre node for the definition of boundary condition. This structure of rigid elements will be referred as spider webs. The structure is fixed at one end. The defined external loads are a force along the y axis ( $F_y$ ), applied at the top surface of the beam, and a moment ( $T_x$ ) around the x axis applied at the other end of the beam. The material properties were defined as: 210000 MPa Young's modulus, 0,3 Poisson ratio and 7,85 g/cm<sup>3</sup> density.

#### 3.2. Application of Quasi-static superposition

The workflow of QSSM is illustrated in Figure 4. The first step generally is the decomposition of external loads to unit forces and moments and determining their descriptive scalar time signals. Since in the following, the external loads will be defined specifically to test the available methods this process is skipped. However, in general applications one might need to gather this information from measurements or MBSs. In these cases, the definition of boundary conditions and applied forces might not be self-evident. In numerous cases a component is capable to rigid body motion.

The technique for handling such a loadcase is called inertia relief (available in most finite element solvers), whereby the outside forces are balanced out by equivalent body forces, as if the body would freely accelerate in space. [7]

The first actual step in the current application is the definition of time signals in MATLAB, and applying corresponding unit loads in a FEA (using MSC NASTRAN). The system's response is a stress tensor for each unit load (Figure 5 and Figure 6). During the superposition these will be scaled by the corresponding time signals. A summation will then result in a stress tensor such that all distinct loads were applied at the same time. From the complete stress tensor equivalent stress will be calculated at the surface of the geometry by the critical plane method. The superposition and calculation of equivalent stress is done by FEMFAT, in addition with the specification of the critical point where the most amount of damage is accumulated. FEMFAT also modifies the material's S-N curve based on mean stress and other factors. Next cycle counting is done on the equivalent stress history. From the cycle count and the modified S-N curve, damage is calculated either by FEMFAT or MATLAB.

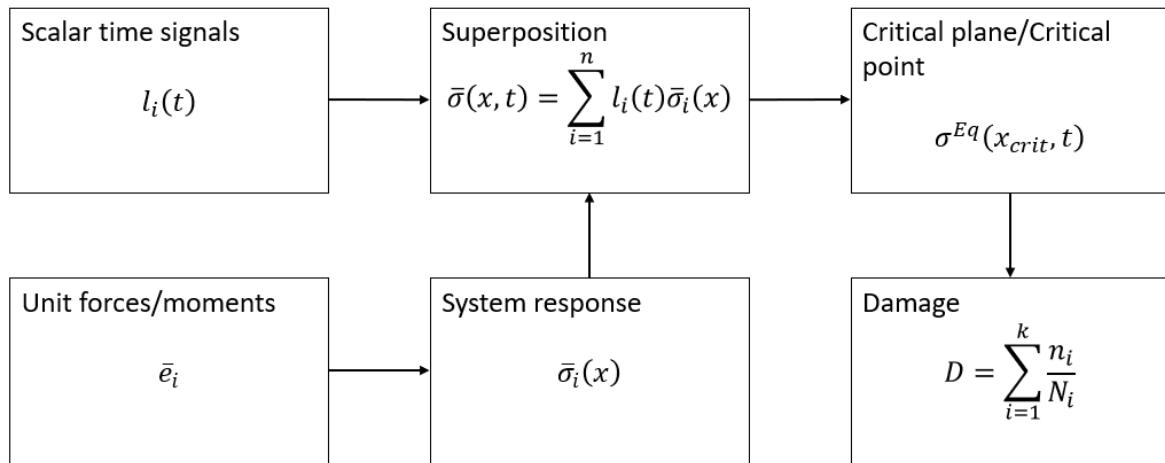


Figure 4 Workflow of Quasi-static superposition method

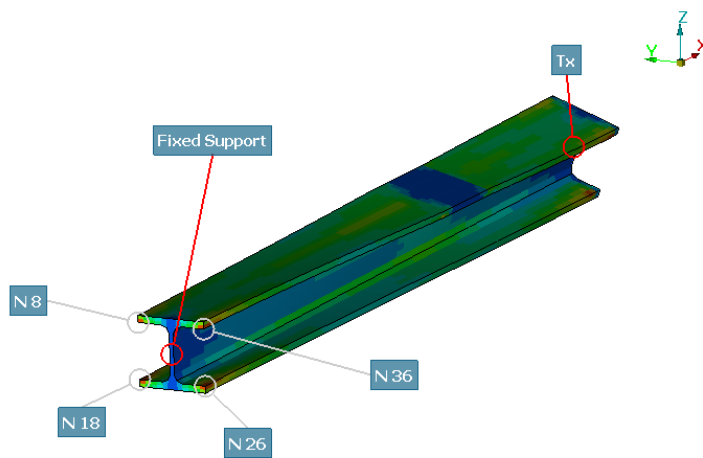


Figure 5 System response of Beam model to unit Tx load

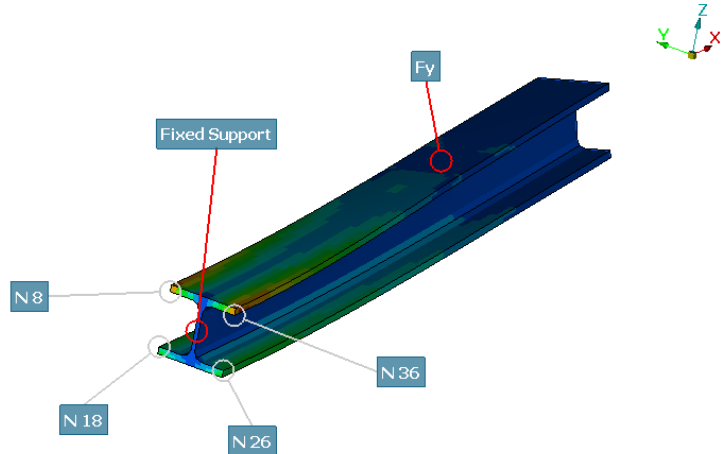


Figure 6 System response of Beam model to unit  $F_y$  load

### 3.3. Application of Modal superposition

The workflow of MSM or ‘modal transient solution technique’ as it is also being referred to is shown in Figure 7. The process starts with a modal FEA (in NASTRAN). The results are the unconstrained eigenfrequencies and modal shapes, of which the first few can be seen in Figure 8. In case of an unconstrained structure there are 6 so called rigid-body modes (1 for each degree of freedom). [9] These modes have no significance in the current application of MSM, therefore, they are neglected.

One thing to consider at the first step of MSM is the number of included mode shapes, for which there is no exact answer, at least not without some previous knowledge about the structure. A rule of thumb is to examine the PSD of external loads and include all modes with a frequency at least twice of the highest load peak.

The next step starts with a so-called condensation which transforms the previous modal shapes into a format which then can be imported and used in a multi-body software (MSC ADAMS). This condensation file is necessary to create a flexible body model. [16] Due to the multi-body environment the boundary conditions need to be singular nodes. Therefore, RBE2 spider webs were defined at the loaded areas, then the centres of the webs were constrained and loaded inside ADAMS. The loading is defined in time, which is then evaluated in a modal transient FEA to calculate the modal participation history.

The use of a multi-body software in case of a single body problem might seem counterintuitive. However, it grants benefit in case of the BIW when this workflow will not need to change.

It can be noted that if the modal FEA is performed on the constrained structure, the frequencies as well as the mode shapes change. This is shown in the Appendix A.1, Figure 71. For the implementation of flexible body constraints are unnecessary, since the constraint are going to be defined in the MBS.

The next step is the summing the stress responses defined by the modeshapes scaled by  $q_i(t)$ . The result is the entire structure’s stress tensor history. Thanks to the modal transient analysis this method can capture structural vibrations, due to the presence of accelerations and a mass matrix in Eq. (11). Therefore, MSM is applicable to non-stiff components. The evaluation of equivalent stress and damage is done the same way as in the application of quasi-static method.

However, with this method one needs to consider the computational cost. Even though the modal FEA needs to be performed only once, the number of stress responses to be superposed is governed by the number of mode shapes, which is often higher than the number of applied forces. Also, more importantly, to determine  $q_i(t)$  a modal transient analysis needs to be performed, where the entire structure is evaluated in several timesteps. The timesteps needs to be in such high number that the sampling frequency covers the important frequency content of the load signals.

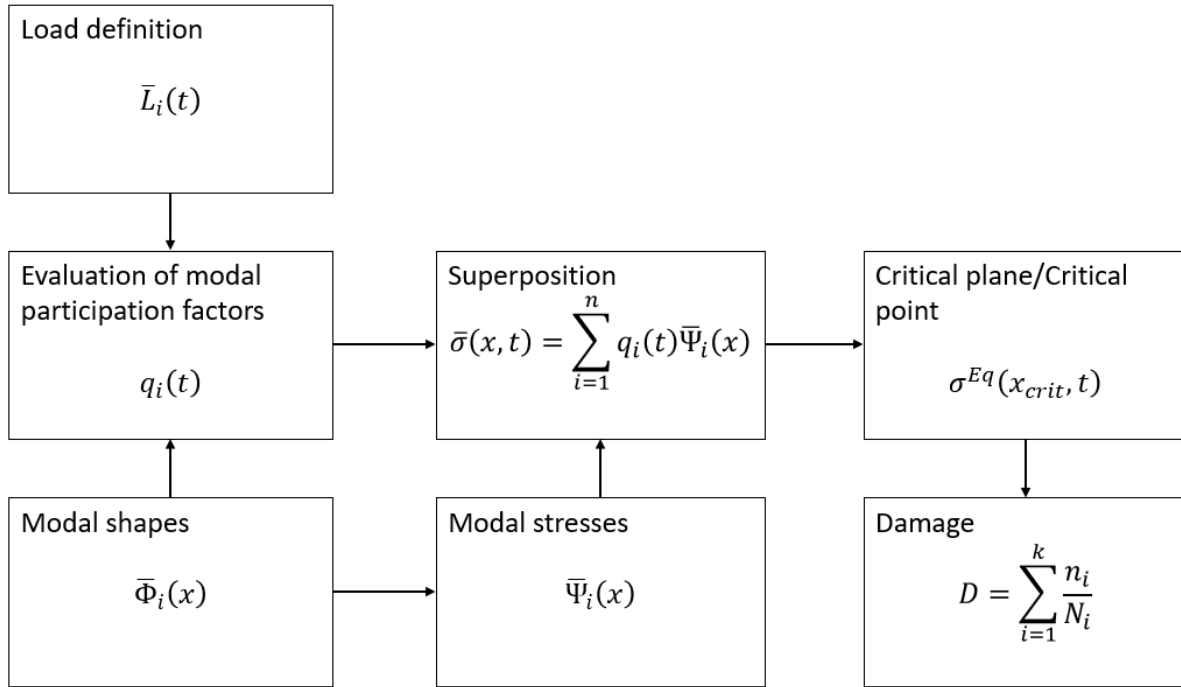


Figure 7 Workflow of Modal superposition method

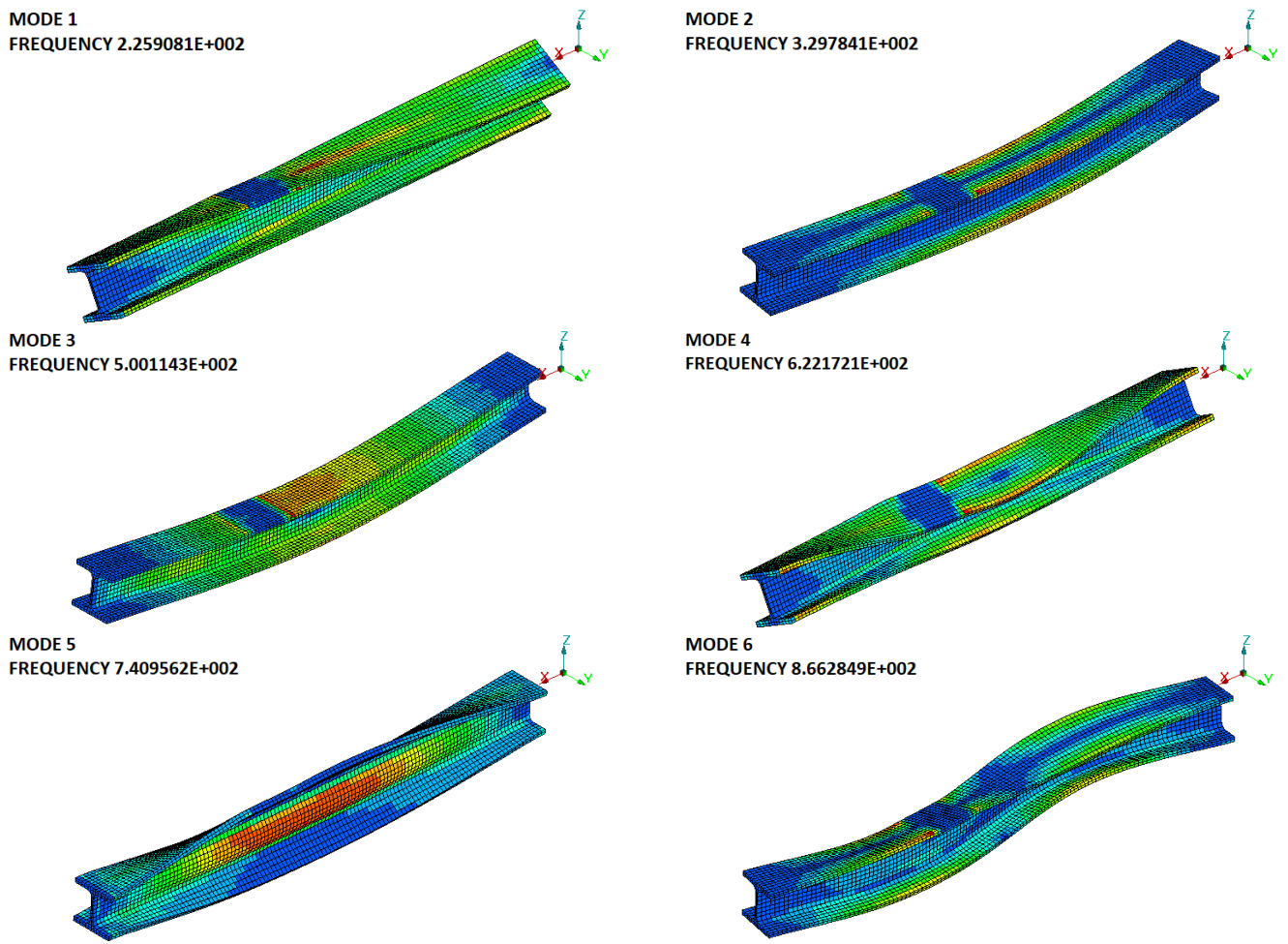


Figure 8 Modeshapes of unconstrained Beam model

### 3.4. Application of Frequency response approach

The workflow of FRA is shown in Figure 9. The process begins with a frequency response analysis (NASTRAN) of the same unit loads as in case of the static superposition method. The results are so called frequency transfer functions  $\bar{T}_i(f)$  which describes the relation between stress tensors i.e. the system's response and the frequency of load.

In the following step the external loading is defined in form of a PSD alongside with the duration of time. In case of multiple load components, additional Cross-PSDs and Phase-PSDs are specified, which describes the load's relation to each other. All of which is defined as input in FEMFAT.

From this an equivalent stress PSD is computed which is a description of the complete stress tensor in the frequency domain. Next the equivalent stress is calculated in the critical points, followed by the definition of cycle counts. The number of cycles as well as their amplitudes is determined by the duration of load, and Dirlik probability density function  $p$ . [3]

This method due to the load's expression in the frequency domain, should capture the increased system response in case of excitation near natural frequencies.

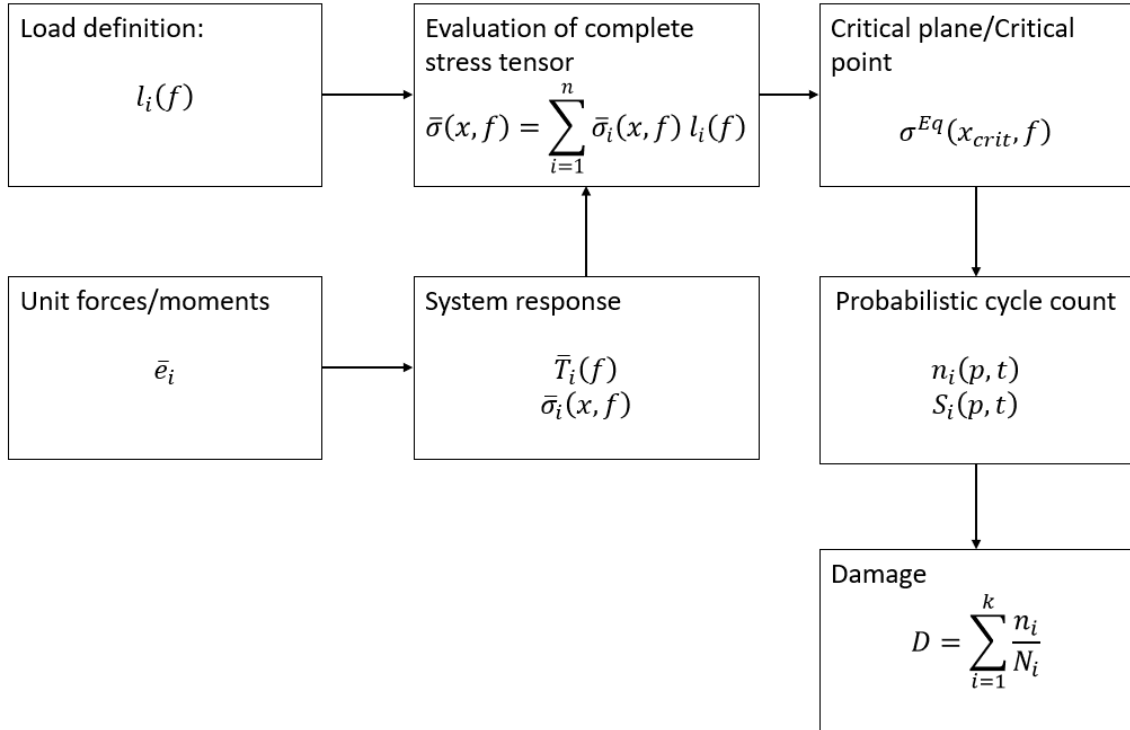


Figure 9 Workflow of Frequency response approach

### 3.5. Case studies

#### 3.5.1. Load cases

The purpose of the following load cases is to investigate the excitation near eigenfrequencies. From Appendix A.1 Figure 71 it can be seen that the first 3 modes of the constrained structure have eigenfrequencies around 50, 81 and 123 Hz which are going to be excited in separate subcases.

There are 8 subcases. Every subcase has the same fixed-end boundary condition and every applied load is defined as a sine function. The parameters are detailed at Table 1 below.

	Applied as	Magnitude	Frequency [Hz]	Number of cycles
Subcase 1	Tx	550 [Nm]	15	200
Subcase 2			50	
Subcase 3			81	
Subcase 4			123	
Subcase 5	Fy	3.4[kN]	15	
Subcase 6			50	
Subcase 7			81	
Subcase 8			123	

Table 1 Loadcases of Beam analysis

The magnitude of Tx and Fy where defined so the resulting von Mises stress would be at the magnitude of ~100 MPa in case of static loading.

Short segments of Subcases 1-4 are presented below in the time domain. This formulation of loads is used in the QSSM and at the beginning of the MSM. For the frequency response method, the same loads need to be defined in the frequency domain. The PSDs of the same first 4 functions are also presented in Figure 11.

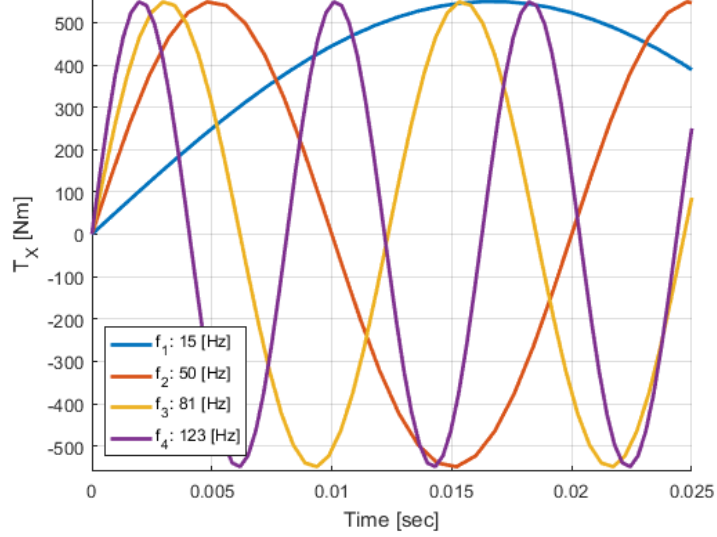


Figure 10 Load-history of Subcase 1-4 (partial)

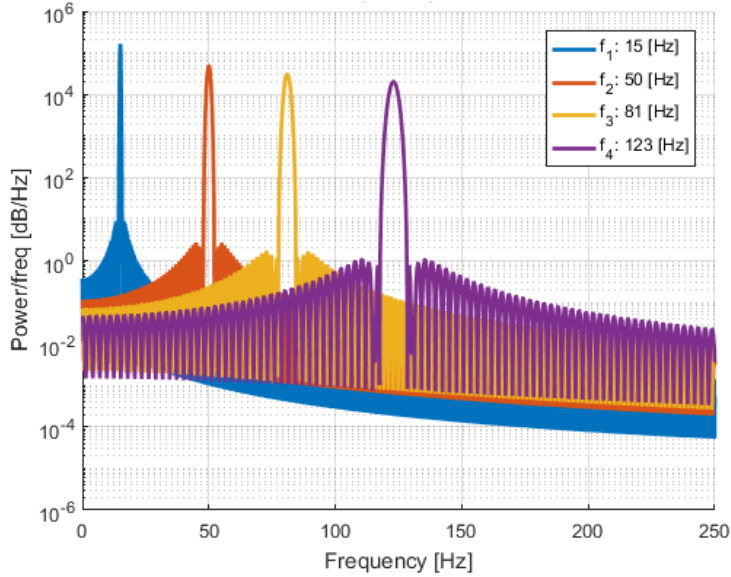


Figure 11 PSDs of Tx Subcase 1-4

Note the PSD of a perfect sine signal is theoretically a delta function with the only one nonzero value at its frequency. [3] The PSD was calculated from the time signals in MATLAB using Welch's method. Due to windowing the frequency band which contains the power of signal increased.

### 3.5.2. Results & discussion

The PSDs of equivalent stress at the critical point are plotted from the results of the three tested methods in Figure 12-Figure 14. The critical points from all subcases are shown in Figure 5 and Figure 6.

The basic assumption when using QSSM is that the loading frequency is lower than any of the eigenmode's of the constrained structure e.g. the structure can be regarded stiff. Therefore, the power content in a frequency is determined by the loading signal only. This can be seen in the similarity of power distribution of external loads (Figure 11) and equivalent stress (Figure 12). However, the assumption is only true for Subcase 1 and 5 (See Table 1). From the results of MSM and the FRA (Figure 13 and Figure 14) the stress response is much higher in other subcases. The highest is at 123 Hz which is the eigenfrequency of the 3rd mode. That modeshape can be described by twisting around the x axis. The applied moment is creating similar twisting deformation, which excites the mode resulting in excessive stress. It is also interesting to note that in the modal results of subcase 1-3, despite the external loads have no peaks at 123 Hz, there are peaks at 123 Hz in the response.

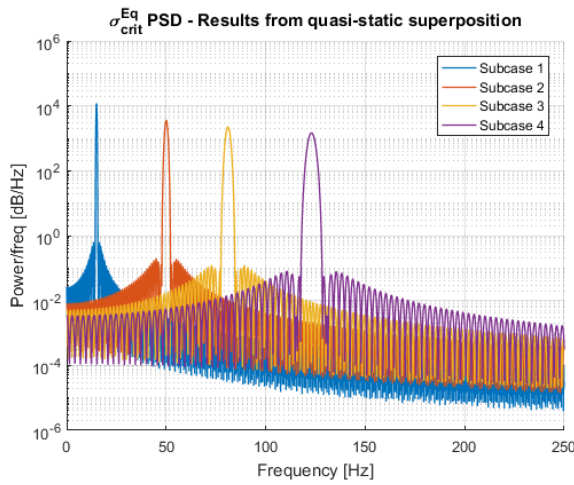


Figure 12 PSDs of equivalent stress at critical point from QSSM

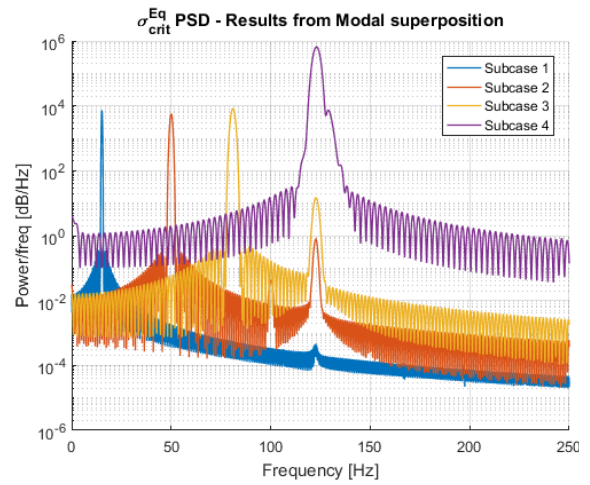


Figure 13 PSDs of equivalent stress at critical point from MSM

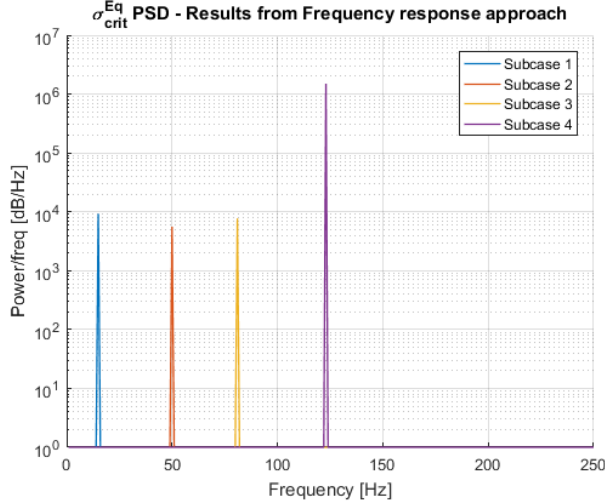


Figure 14 PSDs of equivalent stress at critical point from FRA

On a side note, exporting the PSDs from FRA was not available in FEMFAT at the time of writing this thesis. The peaks of frequency response were therefore read manually and recreated in MATLAB, hence the lack of detail in this type of plots.

Miner's modified model was used to calculate damage from each loadcase, (Figure 15). In case of QSSM the damage is independent of the external loading's frequency. The cycle count of subcase 1 (Figure 16) is identical to subcases 2-4. MSM and the FRA both produce higher damage the closer the loading frequency is to 123 Hz, at which the damage is more than 1, which means failure. However, there is a difference between the results of two methods especially in subcase 1. The cycle count of MSM (Figure 17) as well as the resulting damage is almost identical to the quasi-static's. The RFM of FRA is however quite different (Figure 18). This is due to the probability density function which estimates the distribution of cycle amplitudes. The relation of damage with stress amplitudes is exponential, therefore the individual cycles of high amplitudes skewed the results. The increased frequency bands of input PSDs could also play a role here. However, in Figure 11 the band is increasingly wider from Subcase 1 to 4, while in Figure 15 the difference between damage from QSSM and FRA are the biggest in subcase 1 and smallest in subcase 3. This defies correlation between the wider bands and difference in damage estimations.

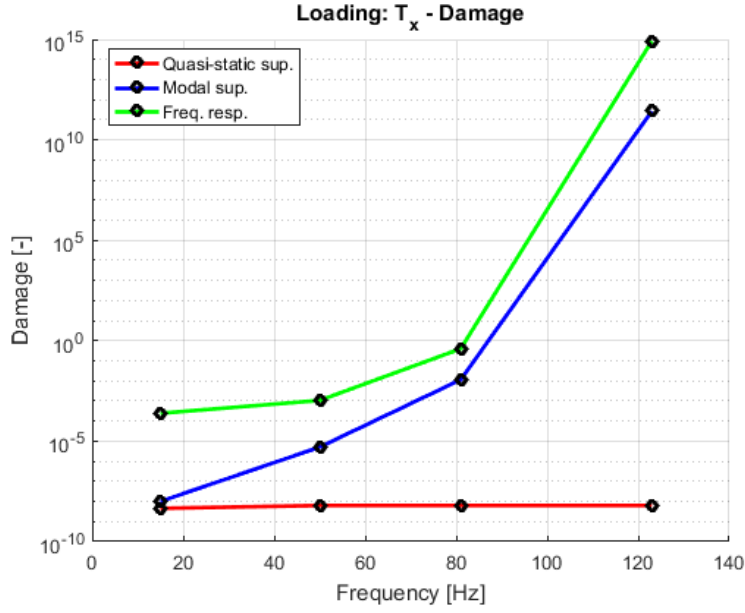


Figure 15 Fatigue damage from Subcase 1-4

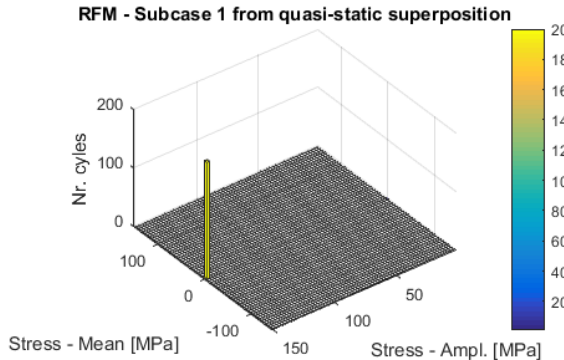


Figure 16 RFM of stress cycles from Subcase 1 (QSSM)

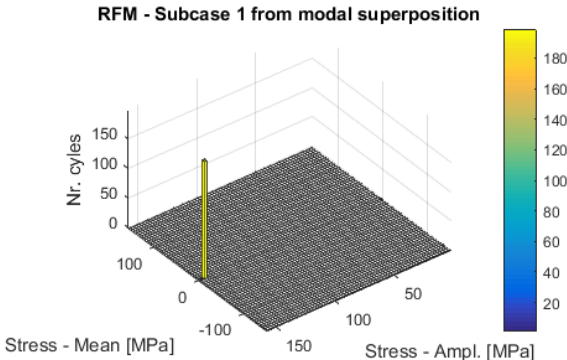


Figure 17 RFM of stress cycles from Subcase 1 (MSM)

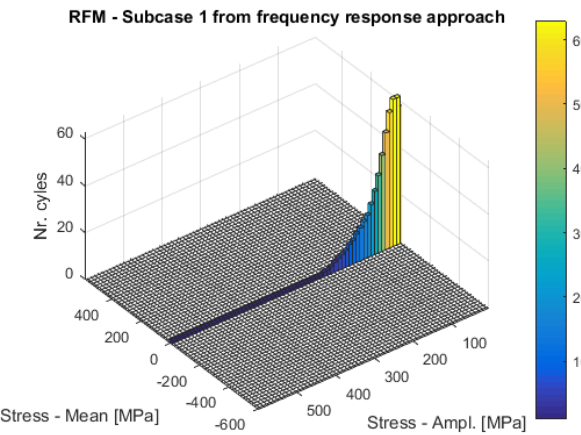


Figure 18 RFM of stress cycles from Subcase 1 (FRA)

In subcase 5-8 the applied load is  $F_y$  in the same frequency ranges as before. The PSDs from quasi static superposition (Figure 19) similarly to before is a linearly scaled variant of the external load's. From the other two methods (Figure 20 and Figure 21) two peaks need to be mentioned. The one at 50 Hz is the eigenfrequency of the 2<sup>nd</sup> mode. This mode is described by bending in the x-y plane. Its excitation by a force in y direction makes sense. The other peak is at 123 Hz, therefore the 3<sup>rd</sup>

mode is excited again. This is due to that  $F_y$  is not applied at the centreline of the beam but at the top surface of it. Therefore, this loading also generates twisting deformation. Which is amplified not only at 123Hz but at 81 Hz as well, although to a smaller degree.

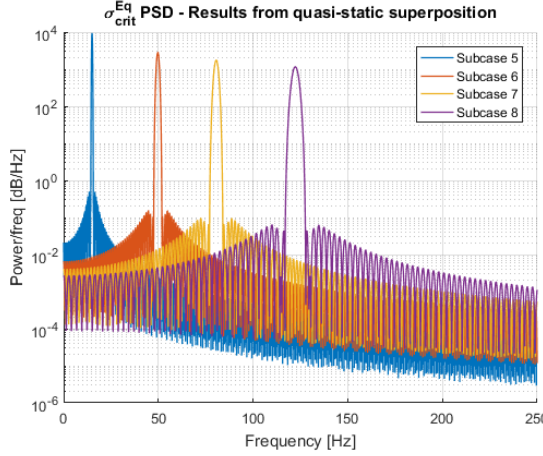


Figure 19 PSDs of equivalent stress at critical point from QSSM

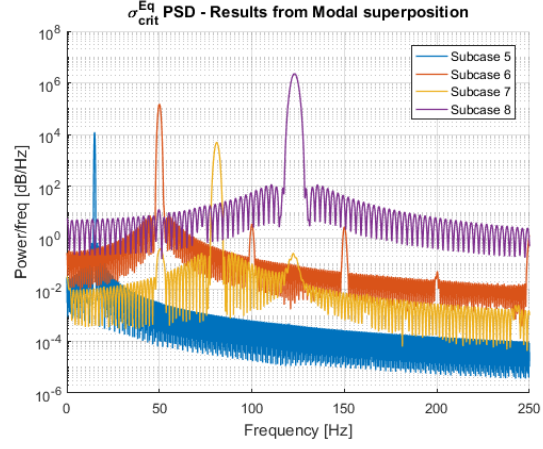


Figure 20 PSDs of equivalent stress at critical point from MSM

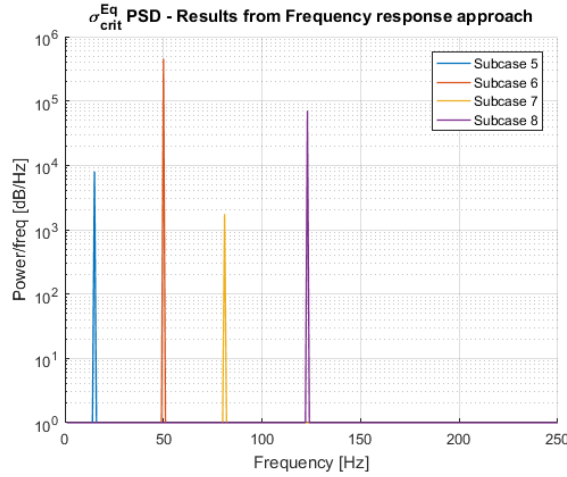


Figure 21 PSDs of equivalent stress at critical point from FRA

Due to the amplified stress response the damage is substantially higher at 50 and 123 Hz. At both of which failure would occur. However, the severity of loading at 123 Hz is deemed different by MSM and FRA. From the PSDs of FRA, the power at 123 Hz is less than the MSM's. Consequently, the distribution of stress amplitudes is at a much lower level (Figure 23 and Figure 24).

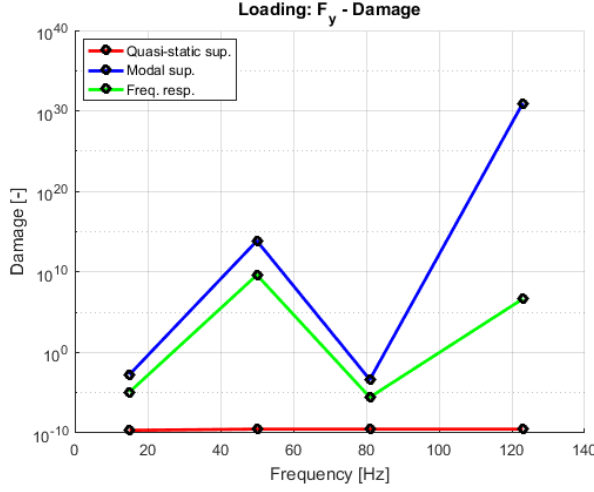


Figure 22 Fatigue damage from Subcase 5-8

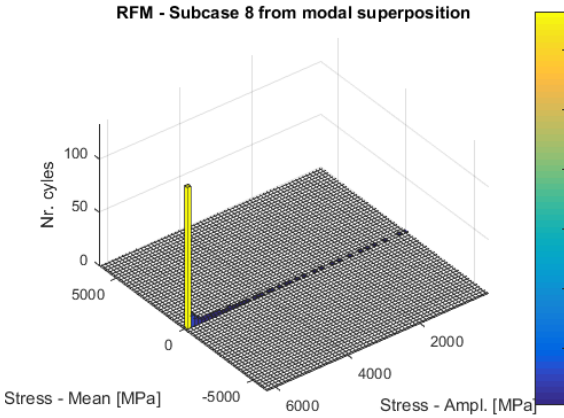


Figure 23 RFM of stress cycles from Subcase 8 (MSM)

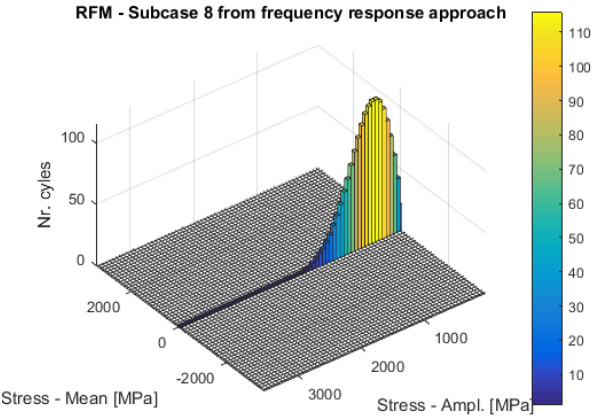


Figure 24 RFM of stress cycles from Subcase 8 (FRA)

To summarize, the danger of structural vibrations was shown. Excitations increased damage even outside the direct frequency range of an eigenmode (Subcase 2 and 3). Excitations occurred even if the enforced deformation just partially resembles a modeshape (Subcase 8).

The QSSM does not capture structural vibrations.

The MSM capture these excitations but a transient analysis is needed with high enough sampling frequency.

The FRA also captured the damage potential of vibrations but gave varying predictions of damage compared to MSM. The reason for this is most likely due to that the probability density function is best suited for random loads and long-time signals which is not true for the investigated load signals. [3]

## 4. Body in white model

### 4.1. Model description

The investigated geometry is a model of a vehicle's Body in white (BIW) shown in Figure 25. The model contains 689071 PSHELL elements and 698000 nodes. [15] The model is an assembly of 314 parts connected with spot-welds. The spot-weld representations in FEA can have big effect on stress concentrations. For the investigated BIW, SPIDER2 representation was chosen based on [5]. The applied material is steel ETG 100, SAE1144, 44.

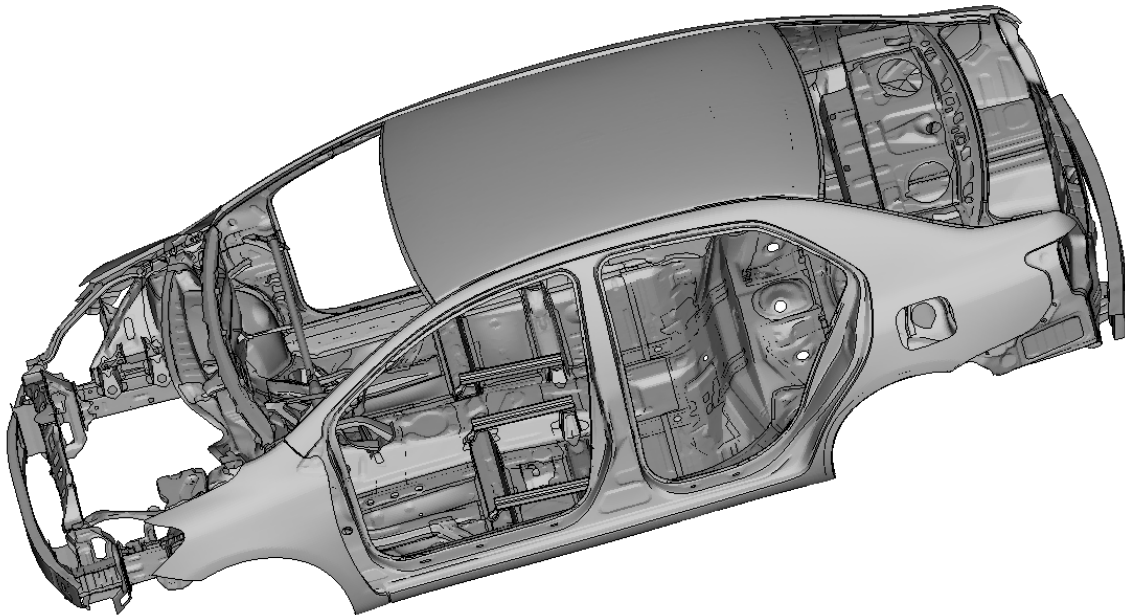
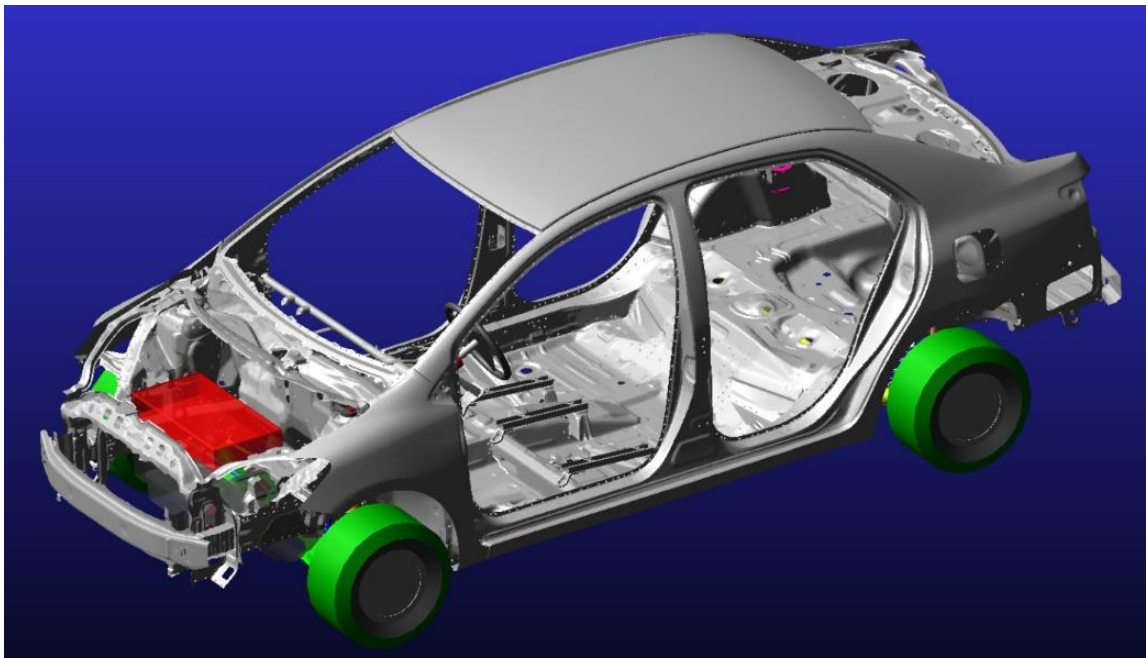


Figure 25 Finite element model of Body in white

The model is evaluated by the virtual proving ground method (VPG), which has the benefit that real life testing is not essential to evaluate a vehicle. The loading on BIW is not from measured forces or accelerations, but it will be calculated in a multi-body analysis. For this there is a need for a virtual vehicle model of the car, as well as virtual road profiles. The forces acting on the BIW will be the results of the car driving on a virtual road.

The multi-body model of vehicle including the investigated BIW was created by authors of [4] and is shown in Figure 26. The model has a front McPherson and rear twist beam suspension. Most bodies in the model are flexible, the control arms, subframe, steering tie-rods and BIW. However, windshields, exhaust pipe, doors and seats are excluded from the model. [4] For the tires the PAC202 Pacejka tyre model is used

For the flexible model of BIW 130 modeshapes were used. The list of modeshapes with their corresponding natural frequency is listed in Appendix B.1 Table 11.



*Figure 26 Virtual vehicle model of Body in white*

The used road profiles in Figure 27-Figure 29 represent a wide range of loading scenarios [4]:

- Random non-stationary loads by different class of rough roads, and cobblestone road profile

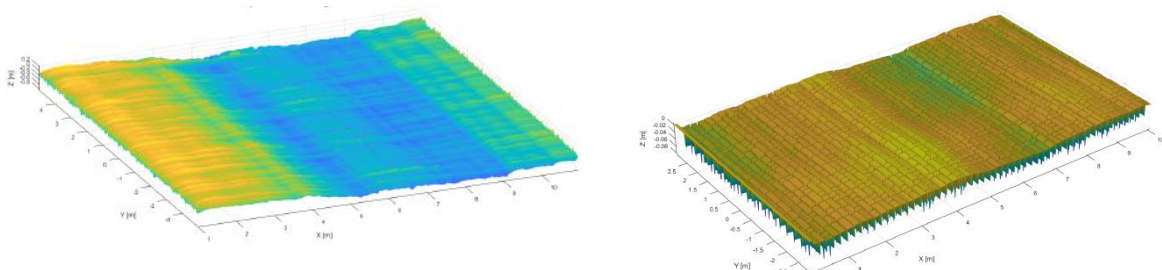


*Figure 27 Rough road and Cobblestone roadprofiles*

- Deterministic periodic loads by two variations of washboards

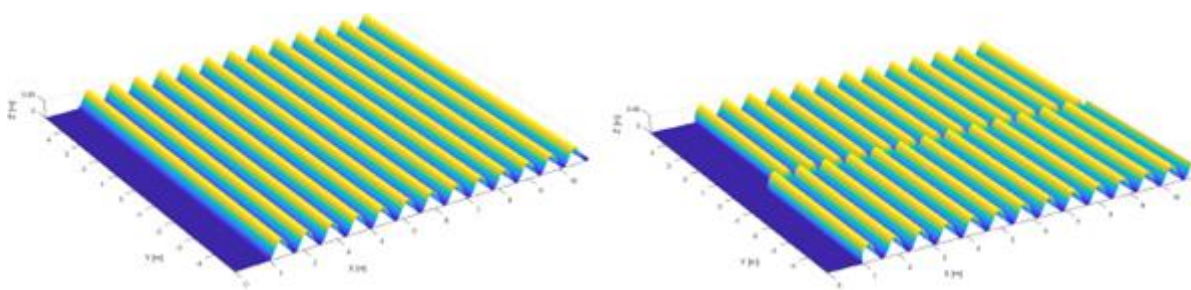


*Figure 28 In-phase and Out-of-phase Washboards*

- Deterministic single event loads by potholes, curb island and bumps

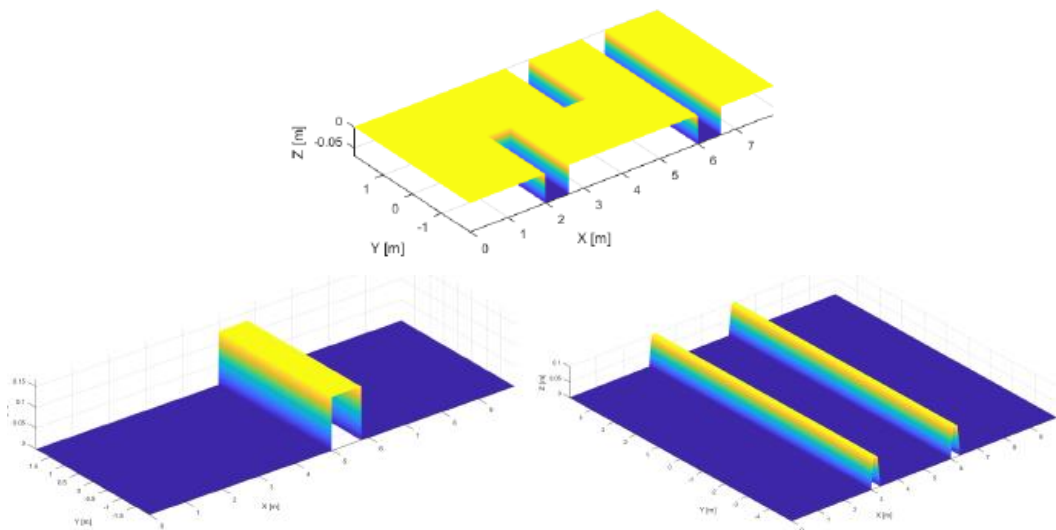


*Figure 29 Potholes, Curb island and Bumps roadprofiles*

Table 2 list all Loadcases with the different variations of these road profiles as well as driving speed, simulated time, and distance. The classes of A-D in case of rough roads refer to an increasingly rougher road profile. [4] [17]

Loadcase number	Road profile	Road profile variation	Car's velocity	Simulated distance[m]	Simulated time[s]
1	Rough road	Class: A	75	208,33	10
2	Rough road	Class: B	75	208,33	10
3	Rough road	Class: C	65	180,56	10
4	Rough road	Class: D	50	138,89	10
5	Cobblestone	-	40	100	9
6	Washboard	In-phase	45	200	16
7	Washboard	Out-of-phase	45	200	16
8	Curb Island	Height: 90 [mm]	40	35	3,15
9	Curb Island	Height: 110 [mm]	22,5	35	5,6
10	Curb Island	Height: 130 [mm]	15	35	8,4
11	Bump	Height: 55 [mm]	30	35	4,2
12	Bump	Height: 77 [mm]	25	35	5,04
13	Bump	Height: 110 [mm]	20	35	6,3
14	Pothole	Depth: 70 [mm]	25	35	5,04
15	Pothole	Depth: 85 [mm]	37,5	35	3,36
16	Pothole	Depth: 100 [mm]	50	30	2,16

Table 2 Loadcase description of BIW analysis

## 4.2. Method to evaluate stress

In the previous Sections 2.1.1-2.1.3, and 3.2-3.4 methods were evaluated to how calculate internal loads (stress), which is the base of fatigue calculations. For the BIW, Figure 30 illustrates how the workflow needs to be extended to create all necessary input in each method. Green arrows indicate when all input is ready for a method to evaluate stresses. Since the multi-body model uses flexible bodies the modal analysis is already finished before MBS. Therefore, using the MSM, after MBS only the modal participation factors need to be extracted to have all necessary quantities. For QSSM and the FRA, unit loads must be calculated from the BIW's coupling points. These are the points where the BIW interacts with the rest of the bodies (subframe, suspension components, etc). Also, the corresponding time signal or PSD must be defined for each unit load. These loads need to be further processed in either static or frequency response FEA. The time savings of these methods are not manifesting since the multi-body analysis must be performed either way. Furthermore, in this application they require more FEA calculations than MSM.

In consequence, the MSM is used for the easy implementation to analyse BIW, and for the benefit of capturing structural vibrations.

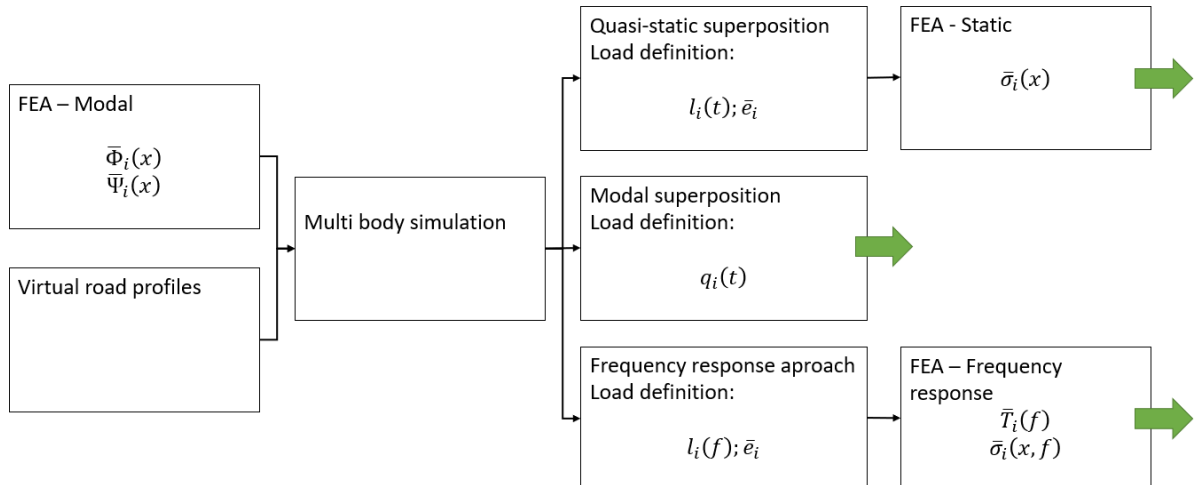


Figure 30 Alternative workflows for stress evaluation on BIW

## 4.3. Analysis

### 4.3.1. Modal participation factors

Modal participations will be the base of later calculations for equivalent stress histories and therefore damage. However, it is worth some time to look for other possible application for this data.

One idea is to investigate the relevance of every modeshape from the perspective of damage. The goal is to describe the response of the structure by just a small set of modeshapes. If it is possible the information can be very useful during a development process. From prominent modeshapes one can have a better understanding on how to reinforce the body. In addition, if not all

modeshapes are necessary to describe the model mathematically, then by reducing the number of used modes computational expenses can be saved.

But first it is important to note that the values of modal participations are the result of the mathematical representation for the analysed body. The formulation sums stress tensors together dependent on the participation factors. By analysing the participation factors alone, their interaction is neglected. However, this simplification can still provide useful information in case one of the natural frequencies is excited, and/or the final shape is mostly described by a just a few modeshapes.

First have a look on modal participation histories of two arbitrary selected modeshapes under the same loading. In Figure 31 the 2<sup>nd</sup> and 51<sup>st</sup> modal participation is shown from the analysis results on Cobblestone road profile.

Numerically  $q_2$  has much higher values than  $q_{51}$ . From this it seems that not all modes contribute at the same degree.

Figure 32 shows a representation of all  $q_i$  in time during the same loadcase. It can be seen after the first few modes the value of  $q_i$  decrease drastically the entire time.

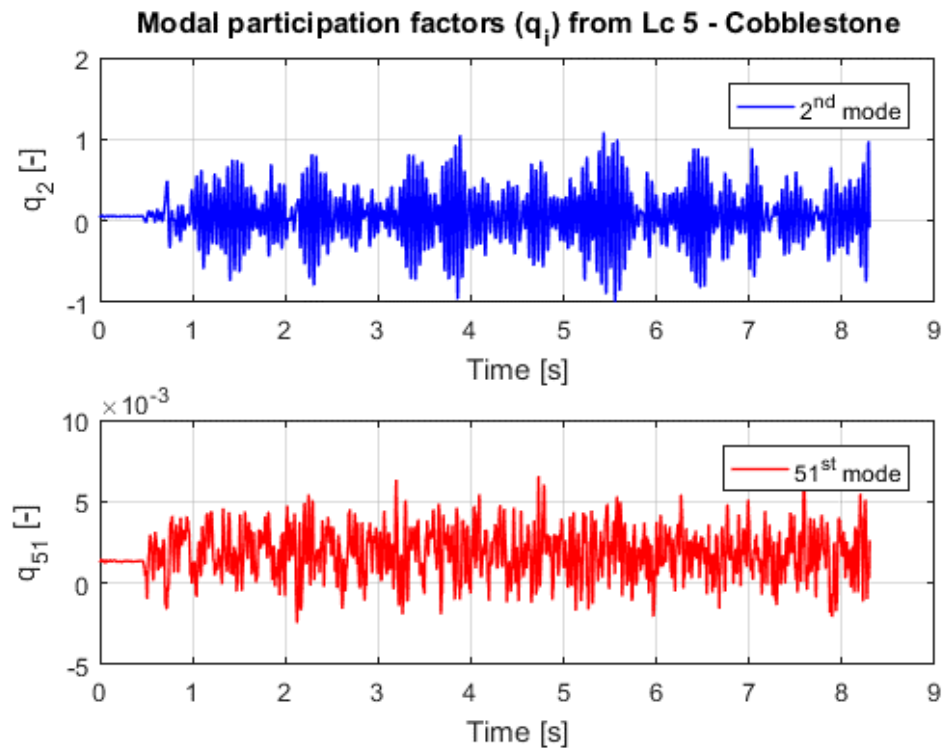


Figure 31 2<sup>nd</sup> and 51<sup>st</sup> modal participation factors from Lc 5

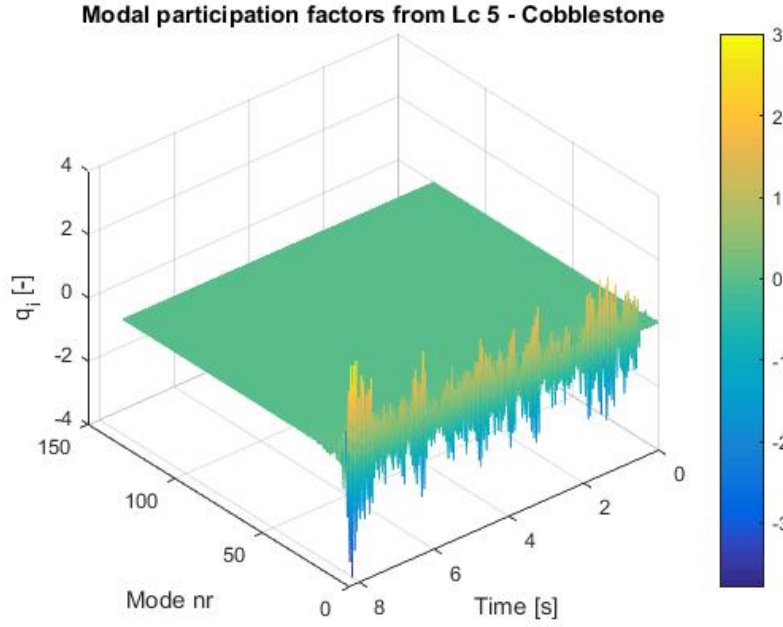


Figure 32 All modal participation factors from Lc 5

Since  $q_i$  are time signals, it is possible to calculate pseudo damage after rainflow counting.

$$d_{ij}^\phi = \sum_k S_k(q_{ij})^\beta \quad (25)$$

where

$i = (1, \dots, 130)$  – Mode number

$j = (1, \dots, 16)$  – Loadcase number

$q_{ij}$  – modal participation history of mode  $i$ , from Lc  $j$

$S_k$  – Amplitude of cycle  $k$

$k$  – Cycle number

$d_{ij}^\phi$  – Pseudo damage based on modal participation factor of mode  $i$ , from Lc  $j$

In Figure 33 pseudo damage values are shown from all load cases for every  $q_i$ . For the pseudo damage calculation  $\beta = 5$  was used as a damage exponent. It can be seen that there are damage values above 1. However, it is important to remember that the pseudo damage definition does not guarantee damage numbers between 0 and 1 for a working component. The numbers are useful for the relative comparison between loadcases and modes. One comparison is that it seems that the higher modes are participating less than the lower ones.

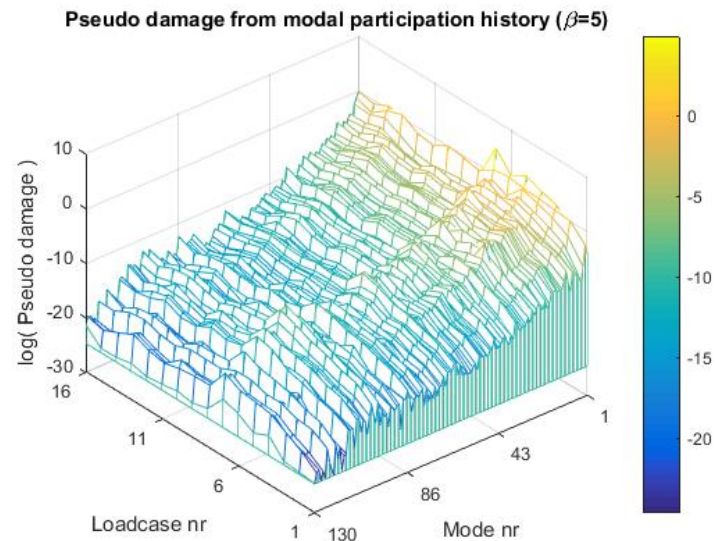


Figure 33 Pseudo damage from modal participation factors

But to make comparison between loadcases as well, the 16x130 individual pseudo damage number need to be reduced to just 16. For simplicity this will be achieved by a simple sum over the modes.

$$d_j^\phi = \sum_i d_{ij}^\phi \quad (26)$$

From (25), it is

$$d_j^\phi = \sum_i \sum_k S_k(q_{ij})^\beta \quad (27)$$

The results are shown in Figure 34. This is the first estimation of the different load's relative severity. Regarding the first 4 loadcases which are rough road class A to D (where each class is increasingly rougher), they produce increasingly higher pseudo damage values. The highest pseudo damage numbers come from Loadcase 7 which is the out-of-phase washboard. The accuracy of this estimation is however is yet to be tested.

Here the interaction of modes is still neglected because the damage values were calculated separately, and then summed. In addition, an assumption was made that each mode has the same damage potential. This means that one cycle with the same amplitude from  $q_k$  produces the same damage as  $q_l$  ( $k \neq l$ ).

However, by looking at the maximum von Mises stress values (Figure 35) from each mode (when  $q_i=1$ ), it is obvious that the highest modes are more damaging due to their higher stresses.

In the following, the mode's different damage potential will be included. This is done by the multiplication of  $q_{i(t)}$  with the corresponding scalar values of maximum Von Mises stress  $\max(\sigma_i^{VM})$ . After that scaled pseudo damage  $d_j^{sc,\phi}$  is calculated similarly as before, see Figure 36.

$$d_j^{sc,\phi} = \sum_i \sum_k \max(\sigma_i^{VM}) * S_k(q_{ij})^\beta \quad (28)$$

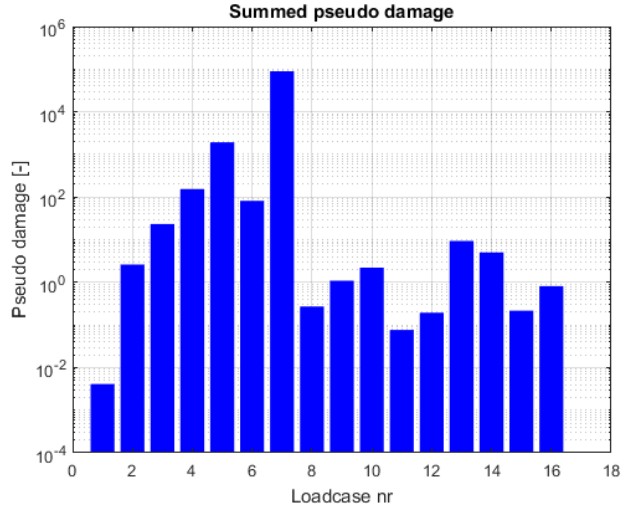


Figure 34 Summed pseudo damage from modal participation factors

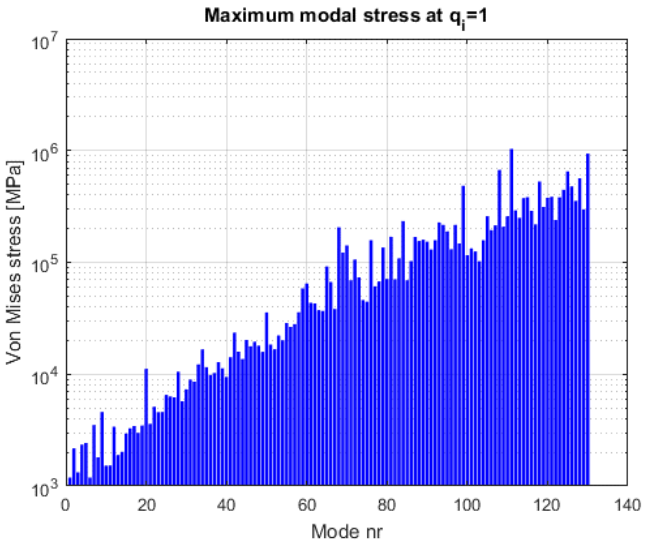


Figure 35 Maximum Von Mises stress from modeshapes

However due to the scaling the magnitude of pseudo damages is entirely different than before. For comparison between the previous and the scaled results the total damage is calculated from all loadcases by a summation. The total damage is the same in both cases, since the loadcases did not change just the way of evaluating them. Therefore, if pseudo damage from one loadcase is expressed as a percentage of the total damage, different methods become comparable. The results are relative pseudo damage numbers shown in Figure 37.

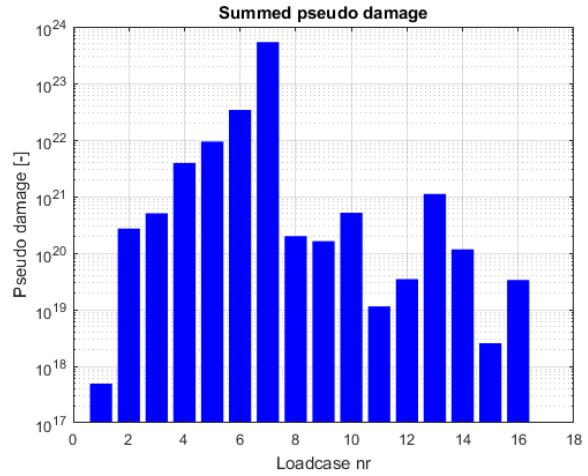


Figure 36 Summed pseudo damage from scaled modal participation factors

$$d_j^{rel} = \left( \frac{1}{\sum_j d_j} \right) d_j \quad (29)$$

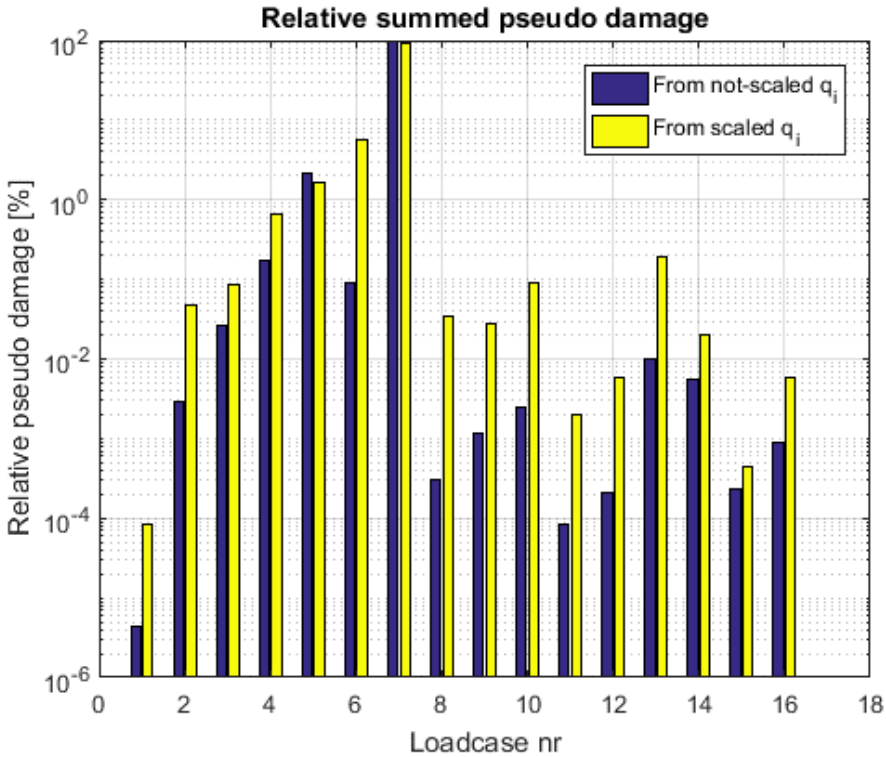


Figure 37 Relative summed pseudo damage

The scaled pseudo damages have less variance, since the range between the most and least damaging loadcase shrunk. From scaled results the fractions of the total damages are higher in all but two cases (Lc 5 and 7). Therefore, due to the scaling the damage potential of higher modes is now shown to have more significant effect. Also, since the relative damage values are generally

not the same from the two sets of results, the conclusion of how much more damaging is on Lc compared to another differs substantially. This would also mean different fatigue life predictions.

Other than comparing damage between Lcs what is also important is to examine if the importance of modes changed due to scaling (Figure 38).

The damage values are much higher numerically, which could be expected due to the scaling. But more importantly now it is not just the first few modes that are resulting in significant damage. However, the distribution still has noticeable peaks and valleys, therefore there are differences between how much damage is contributed by one mode.

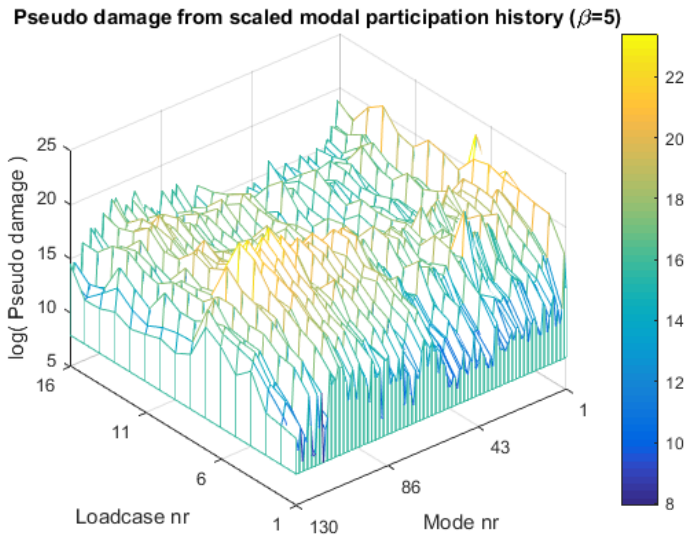


Figure 38 Pseudo damage from modal scaled participation factors

Using the total damage from Lc 5, Cobblestone the results from all 130 modes are normalized (by  $d_5^{sc,\phi}$ ) and expressed as percentages in Figure 39.

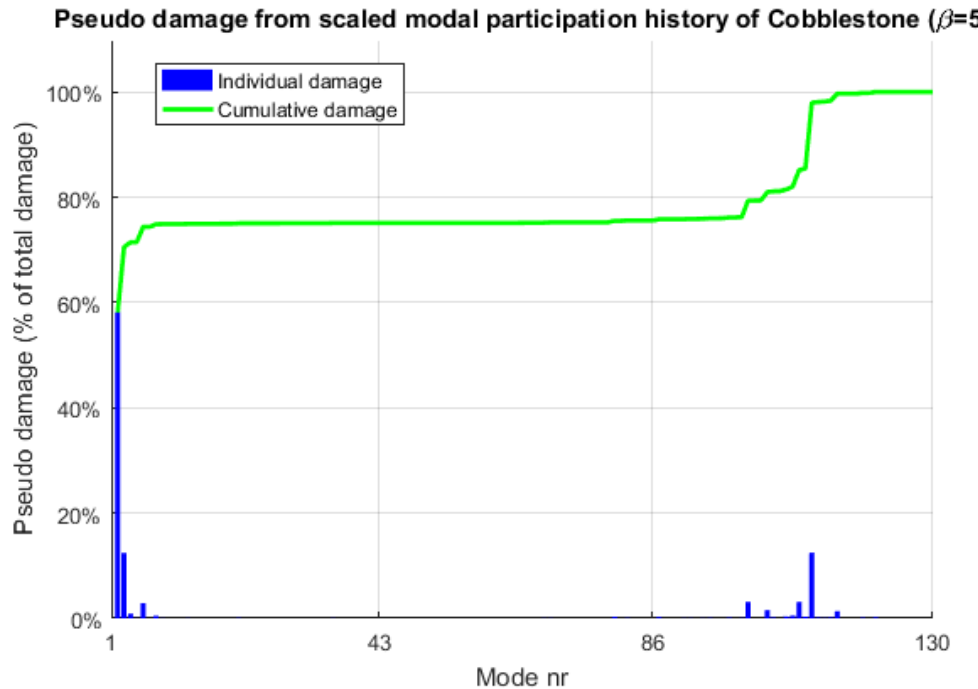


Figure 39 Pseudo damage from scaled modal participation history of Lc 5

It is clear that only a few modes create the majority of the total damage. In Figure 40 the modes are reordered by their percentage value. It can be seen that 6 modes are enough to accumulate more than 90% of the total damage.

With this approach the most prominent modes can be defined for each loadcase. Table 3 presents these modes. The single most important modes are highlighted in green at every Lc.

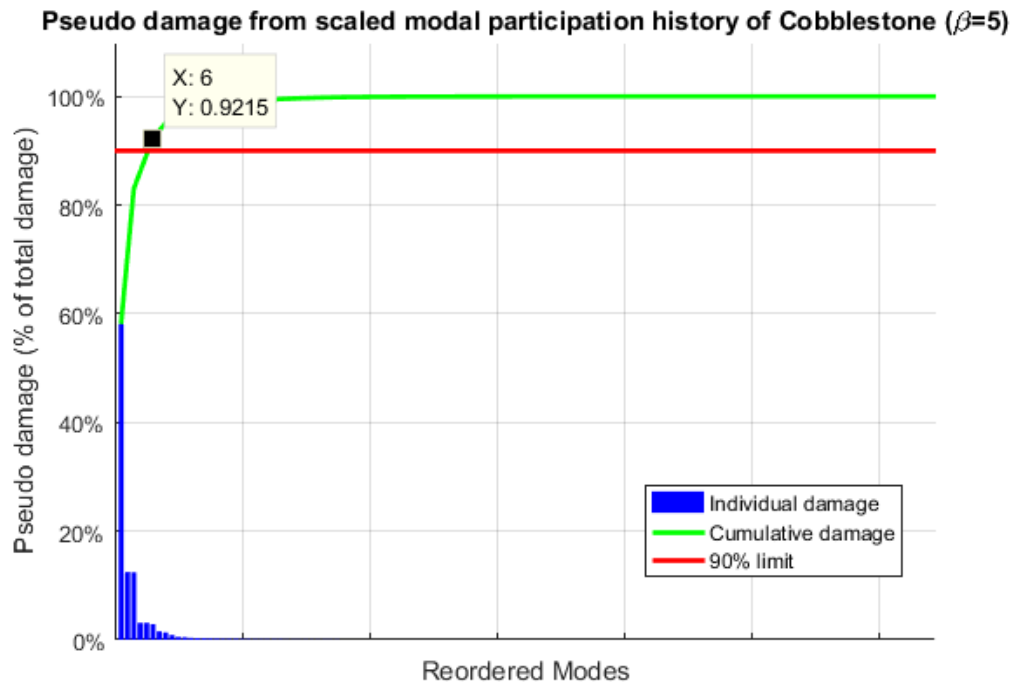


Figure 40 Pseudo damage from scaled modal participation history of Lc 5 (Re-ordered modes)

Limit: 90%												
Lc1	2	108	110									
Lc2	2											
Lc3	1	2										
Lc4	1	2	20	26	28	90	100	108	110			
Lc5	1	2	5	100	108	110						
Lc6	2	94	100	103	110	114						
Lc7	1	100	110	114								
Lc8	2	79	86	100	103	107	108	109	110	112	114	
Lc9	2	100	108	109	110	112	114					
Lc10	2	108	109	110	111	112	114					
Lc11	2	65	69	99	100	108	109	110	112	114		
Lc12	2	69	79	100	103	108	109	110	112	114		
Lc13	2	108	109									
Lc14	1	2	110									
Lc15	1	2	5	69	94	99	100	103	108	109	110	114
Lc16	1	2	99	100	107	108	109	110				

Table 3 Most prominent modes

### 4.3.2. Critical points

Knowing the location of critical points is essential to improve a design. It is also key to understanding the relations between loads and damage. Not to mention how much computational time can be saved if only a small set of nodes need to be evaluated instead of the full model. In the previous subsection, the most prominent modes were determined from the perspective of damage. It is reasonable to think that this information can be used to predict the location of critical points.

The rating of modes was based on the maximum stress of each modeshape therefore their hotspots are defined as the prediction for the critical points. Nonetheless, the entire model (with all nodes) was evaluated, therefore, the actual critical points are known. The comparison between predictions and actual results are shown in Table 4. The location of nodes in Table 4 is shown on the BIW in Appendix B.2 Figure 72-Figure 91.

Loadcase:	Prediction		Full-analysis result
	Most prominent mode	Hotspot of prominent mode	
Lc 1	2	N221775	N221775
Lc 2	2	N221775	N221775
Lc 3	2	N221775	N221775
Lc 4	28	N187749	N221775
Lc 5	1	N62640	N93640
Lc 6	114	N106773	N299536
Lc 7	1	N62640	N93640
Lc 8	110	N106781	N299957
Lc 9	2	N221775	N221775
Lc 10	2	N221775	N221775
Lc 11	2	N221775	N221775
Lc 12	2	N221775	N221775
Lc 13	2	N221775	N221775
Lc 14	2	N221775	N221775
Lc 15	2	N221775	N221775
Lc 16	2	N221775	N221775

Table 4 Comparison of predicted and actual critical points

From Lc 1 - Lc 3 and Lc 9 – Lc 16 the prediction was correct, N221775 is the critical point (see Table 4).

Also, it can be noticed that in case when the prominent mode is 1 (Lc 5 and 7) the critical points are the same N93640. Suggesting a correlation between the prominent mode and the critical point.

In case of Lc 6 and 8, the hotspot IDs are different just like their corresponding modes. However, from Figure 72-Figure 76 in Appendix B.2, N106773 and N106781 they are located near to each other. The critical points are similarly close (N299536 and N299957), which can be also a sign of correlation.

The prediction in Lc 4 is entirely off, however since the critical point N221775 is the same as in all cases where mode 2 was prominent it can be hypothesized that the most damaging modeshape was 2 and not 28, despite being the most prominent.

### 4.3.3. Prominent modeshapes

Since correlations between prominent modes and critical points could only be assumed in several cases it is worthwhile to investigate the modeshapes and the location of hotspots in detail. Pictures from modeshapes with highlighted nodes can be found in the Figure 77-Figure 91 in Appendix B.2.

- Mode 1

The first modeshape can be mostly described by the sideway oscillation of the roof. This results in high stresses at the corners of the windshield's frame. Both the predicted N62640 and the actual N93640 critical points are at one of the windshield's corners. Therefore, if the number of hotspots were extended to include not just one node with the highest stress, but nodes from several highly stressed areas, the critical point could have been included.

Another interesting thing is to notice in which loadcase, mode 1 is or is not prominent. From Table 3 it is not prominent in Lc 1, Lc 2, Lc 6 and Lc 8-13. Which are the least rough roads, curbs, bumps, and the in-phase washboard. The commonality in these is that the road profiles do not generate substantial roll on the car. While the rest of the loadcases where mode 1 is prominent (rougher roads, cobblestone, out-of-phase washboard, and potholes) do. Therefore, it appears to be that if a loadcase generates rolling motion on this car the first modeshape will be excited, which will be a relevant source of damage.

- Mode 2

The investigation of modeshape 2 seems to be the most important one, since its hotspot N221775 is the critical point in 12 out of 16 loadcases (all rough roads, curbs, bumps, potholes). Moreover, it is a prominent shape in all but one loadcase (out-of-phase washboard). The modeshape can be best described by the vertical oscillation of the rear bumper. The hotspot is at one of the spot-welds keeping the structure together, which are all stress concentrators. It can be concluded that whenever the car is pitching or moved vertically, the modeshape is excited.

- Mode 28

The description of mode 28 is rather difficult to describe with words but the pictures in Figure 83-Figure 85 Appendix B.2.5 tell that most of deformation happens at the back of the car. And N221775 is a stress concentrator although it is far from being the most stressed spot. Here it is more difficult to find a correlation between road profiles and the excitation since this mode is only prominent in D class rough-road i.e. Lc 4.

Investigating which other modes contribute to the pseudo damage in Lc 4 (Figure 42) it can be said that the second highest pseudo damage comes from Mode 2, where N221775 is a hotspot. This suggests that Mode 28's correlation with D class rough road might be less relevant for the location of the critical point.

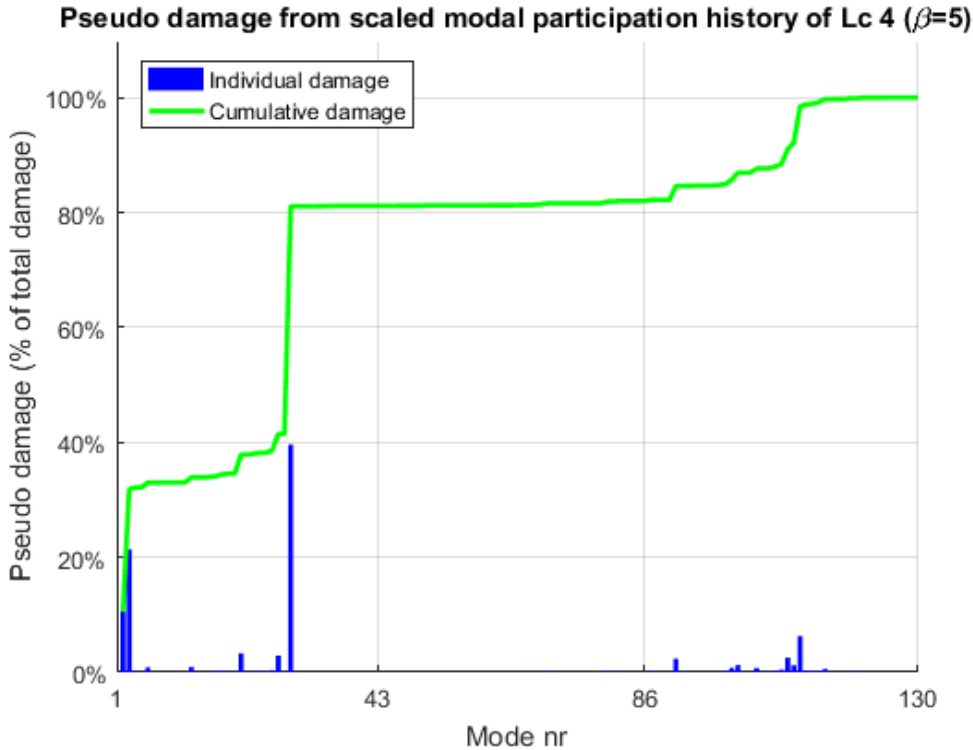


Figure 42 Pseudo damage from scaled modal participation history of Lc 4

Furthermore, interesting to note that Mode 28 despite being the most prominent modeshape in Lc 4, its natural frequency (139 Hz) contains almost the lowest power in the PSD of equivalent stress (at N221775). Therefore, this modeshape was hardly excited, because that would have resulted in higher response like the peak at 21 Hz which is the natural frequency of Mode 2. See Figure 41. This seems to confirm the previous hypothesis of Mode 2 being the most damaging despite not being the most prominent. From this it can be hypothesized that the active participation of mode 28 was mostly due to the mathematical formulation of MSM, and the interaction between  $q_i$ s was substantial in Lc 4.

Since Mode 2 was listed amongst the prominent modeshapes of Lc 4, the prediction could have been accurate if the considered number of hotspots was extended to include hotspots from all prominent modes.

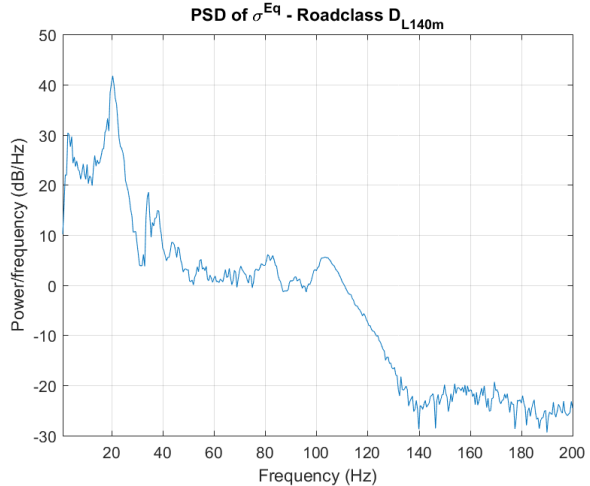


Figure 41 PSD of equivalent stress at critical point from Lc 4

- Mode 110 and 114

The remaining two modeshapes can be discussed together since they are quite similar. Both the hotspots and the critical points are in separate small areas of the BIW. Therefore, they can be handled as one critical area, or hotspot area. The oscillations of the body are mostly present at the

front suspension's connection points. The critical area includes one of these connection points. The previous argument of expanding the number of hotspots to highly stressed areas would have worked to capture the critical area but only from the stress contour of Mode 110. Mode 114 does not result in high stresses around the critical area, but it can be observed that whenever Mode 114 is present amongst the list of prominent modes, 110 is also present. Therefore, all hotspots from all prominent modes would have included all critical points in every investigated case. Although it is quite a larger list of nodes than the original 16, but it is still a reduction compared to the entire model nonetheless.

With a reduced model (less than 500 nodes) Figure 43 shows how the computational time of fatigue calculations compares to the full model. The number of loadcases presented is less than the total 16 because the computational times in remaining cases were not logged during the analyses of the full model. However, from just the partial data it is obvious that it is worthwhile reducing the number of evaluated nodes.

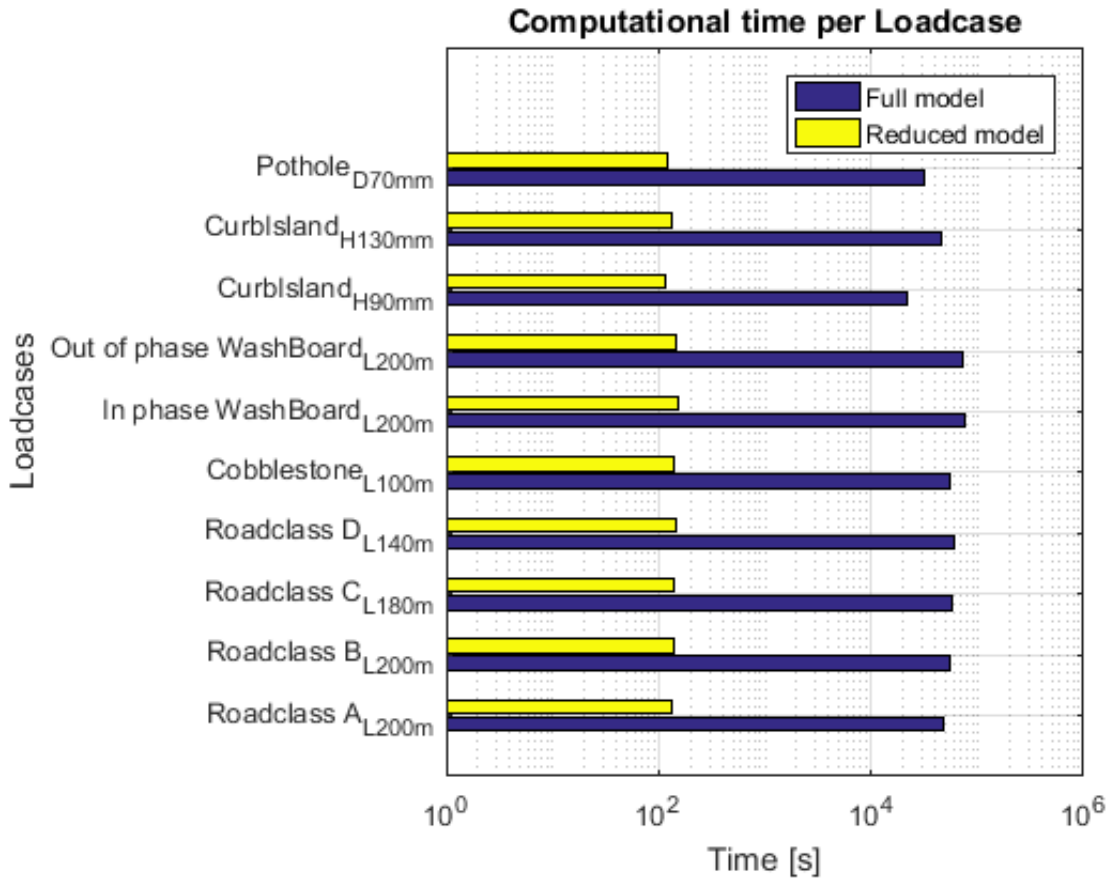


Figure 43 Computational time saving

#### 4.3.4. Damage

From Figure 44 the damage numbers from all loadcases are shown. The numbers were calculated by multiple methods. All results are based on FEMFAT's output of equivalent stress history. There are two cycle counting algorithms however, one implemented in FEMFAT and one implemented in the WAFO MATLAB toolbox [18]. In addition, more damage models were applied as well. From Lc 1 and 15 the amplitudes were so small that no damage was accumulated according to Miner's original model. And in these cases, there are noticeable differences between the elementary and the modified model. What is surprising is that by definition Miner's elementary model should always give higher damage than the modified, but the results from FEMFAT (which uses the modified model) do occasionally give higher damage. This is most certainly due to the difference between counting methods, which can be noticed from the rainflow matrices of the same stress history but counted with the two different methods, shown in Figure 45 and Figure 46.

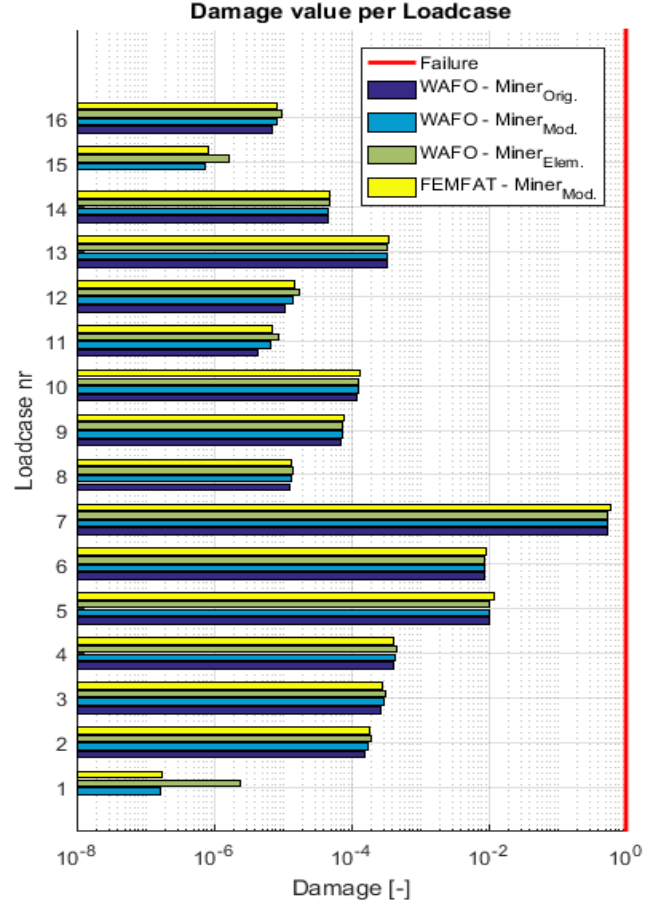


Figure 44 Fatigue Damage of BIW

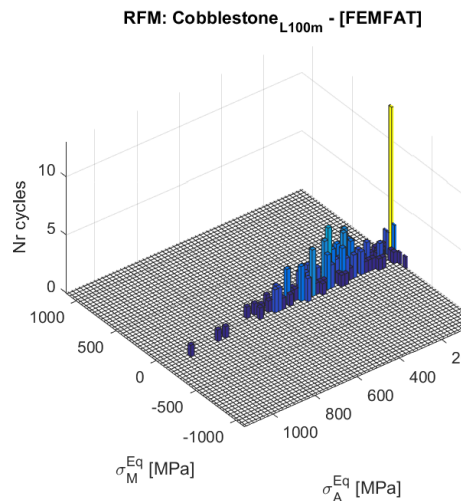


Figure 45 RFM from FEMFAT

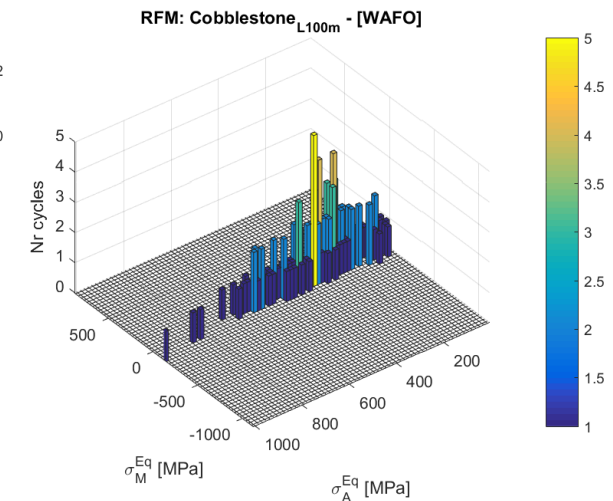


Figure 46 RFM from WAFO

Since FEMFAT's counting method is not published, in the following WAFO's rainflow counting algorithm will be used with Miner's modified damage model. The modified S-N curve parameters will be taken from FEMFAT. The resulting elementary S-N curves are shown in Figure 47. After the fatigue limit the second slope  $\beta'$  will be calculated in accordance with EUROCODE 3 as: [11]

$$\beta' = 2\beta - 1 \quad (30)$$

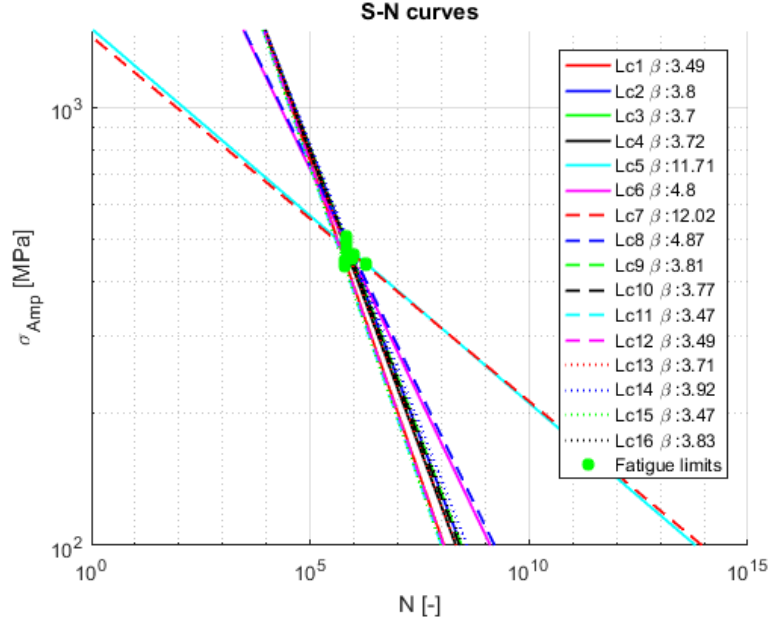


Figure 47 Modified S-N curves of critical points

Relative damage is calculated from Miner modified damage using Eq. (29) Which is now comparable with the previously calculated relative pseudo damage from Figure 37. The comparison is shown in Figure 48. The prediction of Lc 7 being the most severe loadcase can be confirmed, and some correlation can be perceived. However, it would be better to numerically express how good these estimations are.

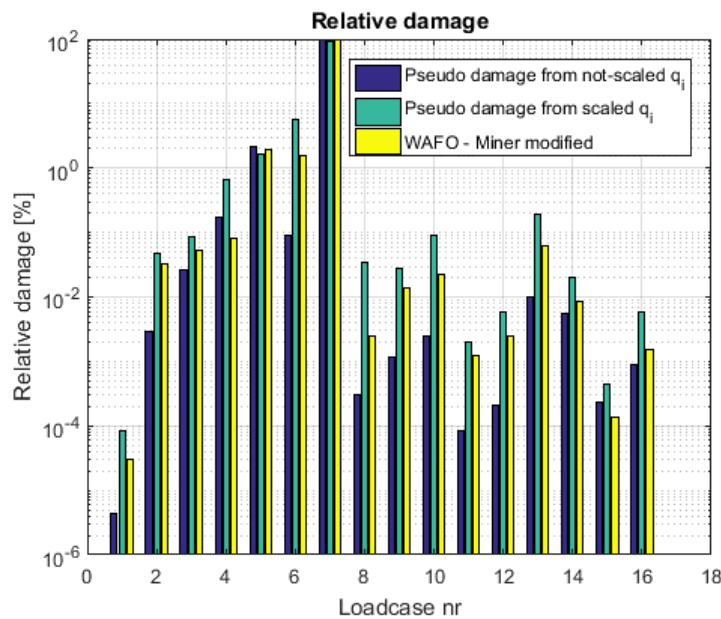


Figure 48 Miner modified dmg and Pseudo dmg from modal participation factors

The following equation is a distance measure between number A and B. [7] The benefit if expressing the difference this way is that  $f$  is symmetric to under and over estimation. B being twice as big results in the same  $f$  as being half as big as A. When the two numbers are equal  $f$  is 0.

$$f = \frac{A}{B} + \frac{B}{A} - 2 \quad (31)$$

Using this measure, the accuracy of the two sets of pseudo damages compared to the real Miner modified damage is shown in Figure 49. The scaled pseudo damage provides better approximation than the non-scaled ones. The worst value of it is  $f = 12$  which is an approximately 14 times over- or 1/14 under-shooting. In case of an existing reference loadcase this pseudo damage calculation could provide the first very rough estimate for the severity of a new load without calculating all elements' stress tensors or having knowledge of the modified S-N curve parameters.

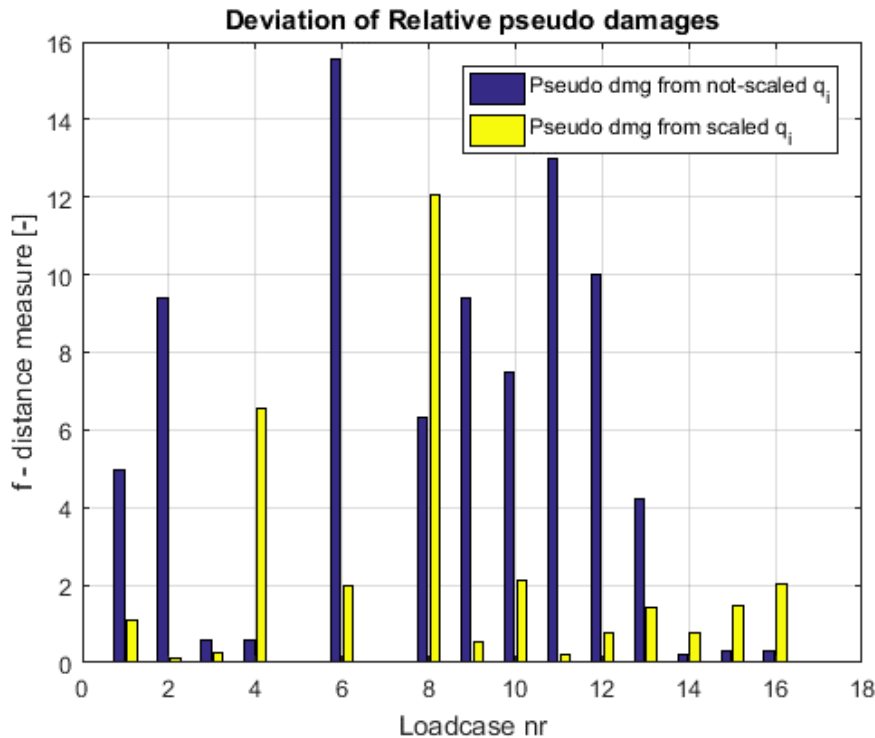


Figure 49 Accuracy of pseudo damage from modal participation factors

#### 4.4. Equivalent Pseudo damage definition

In the previous section the fatigue life of BIW was evaluated on several virtual roads. Evaluating customer targets e.g. driven distance in a specific region depends on the road types, road imperfections, driving styles of the region and so on. There is high variance amongst real loads which could be difficult to simulate and treat individually.

Furthermore, assumptions and simplifications are made regularly in modelling. For the example in case of the investigated BIW, structural elements were neglected such as doors and windshield. [4] The structural rigidity of the model is therefore affected. Structural damping parameters can influence the behaviour of a structure. [19] The FEA representation of spot welds can have effect on damage as they are common stress concentrators. [5]

Models can be improved by testing and changing parameters to fit data. Therefore, the evaluation of load severity must rely on measurements as well. Therefore, it is desirable to have a method which can evaluate the relative severity of loads based on measurements without the need to perfect a virtual model.

One method which does not rely on virtual models is pseudo damage. As detailed in Section 2.4 it is a suitable way to simplify data and compare loads from measurements. However, to have an adequate description from a structure the number of measured signals, i.e. channels, are usually high. In case of a hundred channels/accelerometers per measurement there are hundred pseudo damage numbers to compare. The desired conclusion is that how much more severe one loading/measurement is to another. Decision making based on hundreds of comparisons can be difficult. Therefore, building on to basic notion of pseudo damage (the reduction of data), it is now investigated if it is possible to have just one number per loadcase/measurement to compare their severity.

For this the previously evaluated BIW model and damage values will be taken as a reference. Then pseudo damage will be compared against it. Note that the previously created pseudo damage (see Figure 37) is not usable, since it is calculated from modal participation factors which are unmeasurable in real life. Therefore, acceleration data will be used.

During the MB analyses acceleration was logged at 34 nodes in all 6 degrees of freedom (3 translational and 3 angular). 30 nodes are located on the BIW which are presented in Figure 92–Figure 94 Appendix C.1. The remaining 4 was defined on the uprights to gather data from the unsprung mass as well. The entirety of 204 acceleration measurements i.e. channels are listed in Appendix C.1 Table 12 with their channel number, location, and acceleration component.

#### 4.4.1. Pseudo damage and stress

The use of acceleration for pseudo damage is quite common in practice. However, the entity that drives fatigue is stress. Making a connection between damage and acceleration without modelling the entire structure can lead to inaccuracies. Therefore, the commonalities and differences of stress and acceleration signals are investigated. Figure 50 shows the equivalent stress history from the critical point of Lc 11 and Figure 51 – Figure 52 show accelerations from two randomly selected channels Ch 45 and 105. Ch 45 is located at one connection point of the rear left suspension, while Ch 105 is at the near proximity of the engine mounts.

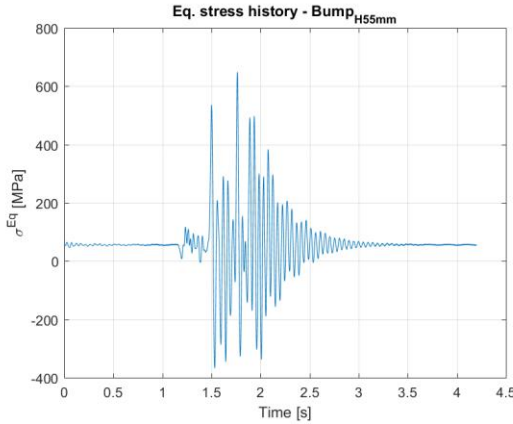


Figure 50 Equivalent stress history at critical point from Lc 11

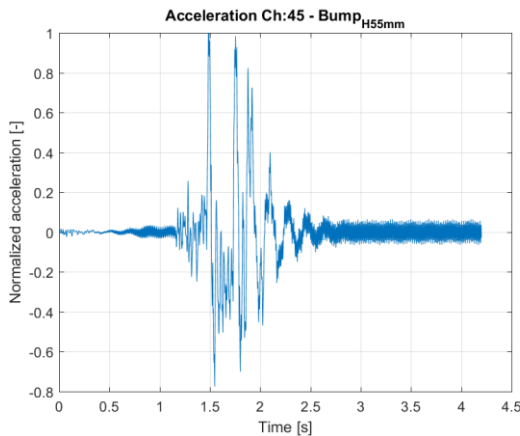


Figure 51 Acceleration history at channel 45 from Lc 11

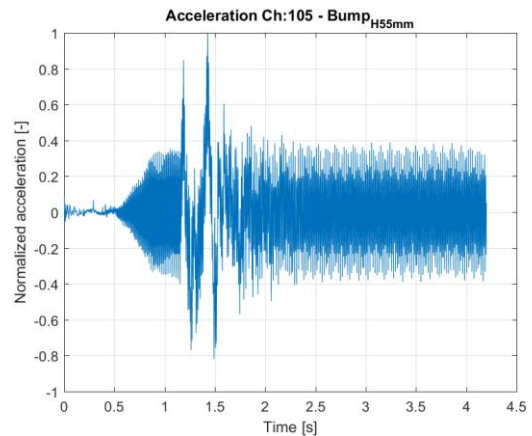


Figure 52 Acceleration history at channel 105 from Lc 11

The acceleration history is much noisier in case of Ch 105. This is probably due to the vibrations of the simulated engine. Since the critical point of Lc 11 is at the rear bumper the vibrations of the engine have little to no effect on its life. It is reasonable to think that since Ch 45 is closer it gives a better description of the stress. In Figure 53 and Figure 54 the PSDs are shown of the stress of critical point and acceleration of Ch 45. The peak frequency of the critical point is close to 20 Hz which is the natural frequency of the 2<sup>nd</sup> modeshape. The PSD of Ch 45, 20 Hz does contain rather high power, but it is not the highest peak. Presumably only an accelerometer on the bumper itself would have registered its oscillations.

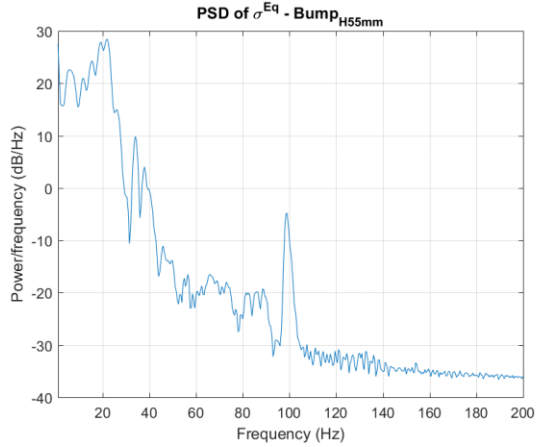


Figure 53 PSD of equivalent stress at critical point from Lc 11

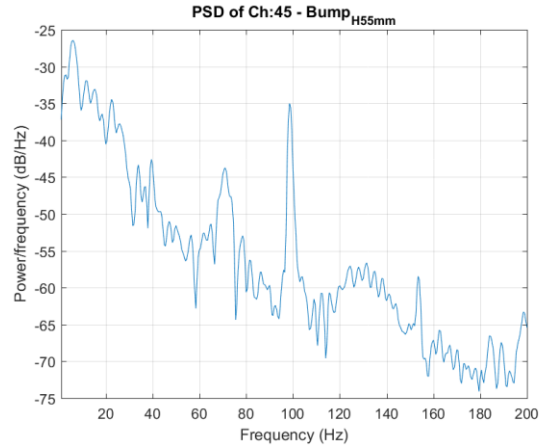


Figure 54 PSD of acceleration at channel 45 from Lc 11

Damage and pseudo damage are evaluated in the amplitude domain. Therefore, the most important representations of these signals are their rainflow matrices (Figure 55-Figure 57). The accumulation of equivalent stress cycles (Figure 55) is dense at low amplitudes levels, which is hardly damaging. The more damaging cycles are spread across different amplitude levels, becoming sparser at higher amplitudes. In this regard the RFM of normalized acceleration at Ch 45 (Figure 56) is rather similar. Although it has more variance regarding the mean values, bit is not the most dominant factor of damage. [2] Meanwhile Ch 105 (Figure 57) has much more cycles at higher amplitudes, therefore it overestimates the severity of the loadcase.

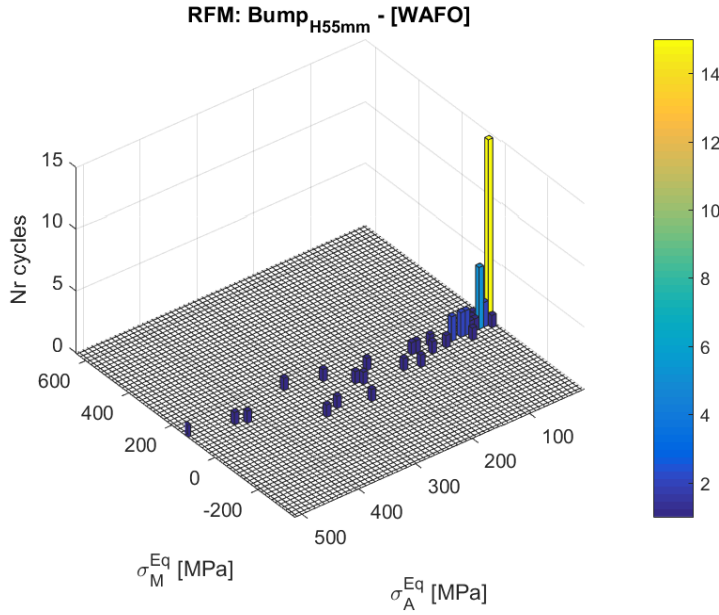


Figure 55 RFM of equivalent stress at critical point from Lc 11

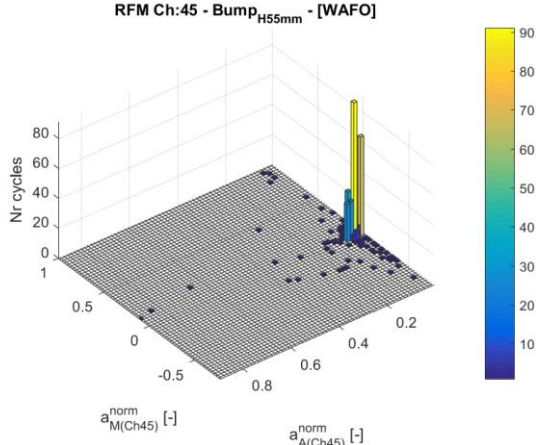


Figure 56 RFM of acceleration at channel 45 from Lc 11

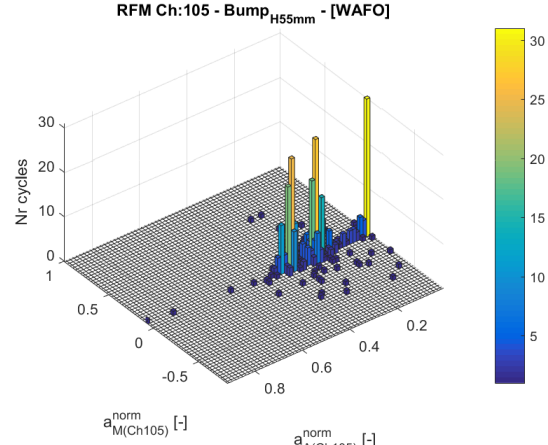


Figure 57 RFM of acceleration at channel 105 from Lc 11

It can be concluded that the location of accelerometers has a big impact on the results. It is possible that Ch 105 would prove to be the better descriptor of damage near the engine mounts, but it performs poorly for the rear bumper. The location of the critical point changes dependent on the loading, therefore even if one channel is a good descriptor of a set of loadcases it might give substantial errors in others. This could possibly skew the results. The knowledge of which channel to pay attention is therefore needed.

#### 4.4.2. Evaluation of channels

It is now investigated if there is a single channel that can give a good overall description damage. Figure 58 gives a picture of the distribution of relative pseudo damage values across all channels and loadcases. For the formulation of pseudo damage  $\beta=3$  was used in Eq. (32).

$$d_{ij} = \sum_k S_k(a_{ij})^\beta \quad (32)$$

Where

$d_{ij}$  - Pseudo damage of Ch  $i$ , from Lc  $j$

$a_{ij}$  - Acceleration signals of Ch  $i$ , from Lc  $j$

$i$  - Channel numbers

$j$  - Loadcase numbers

The definition of relative pseudo damage from Eq. (29) is modified as:

$$d_{ij}^{rel} = \left( \frac{1}{\sum_j d_{ij}} \right) d_{ij} \quad (33)$$

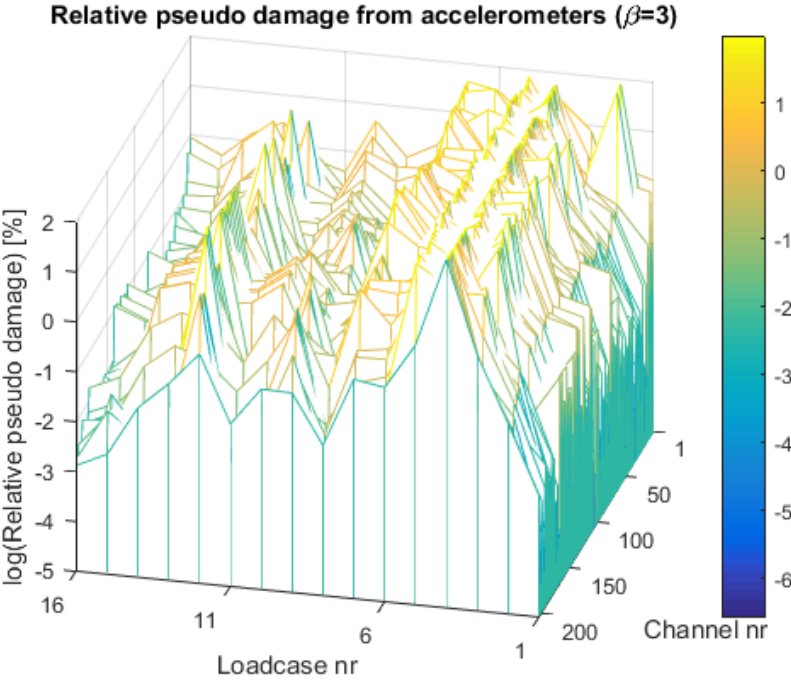


Figure 58 Relative pseudo damage from acceleration

Figure 59 shows the relative real damage values -  $D_j^{rel}$ .

$$D_j^{rel} = \left( \frac{1}{\sum_j D_j} \right) D_j \quad (34)$$

where

$D_j$  - Miner modified damage numbers

The use of relative damage preserves the ratio between the values of different loadcases. Therefore, the dark blue area can be interpreted as the desired outline of a cross section in the previous plot.

In Figure 58 there are several seemingly repeating cross sections. This can be due to the 6 different components of acceleration that is registered. Which are in different numerical ranges. In a single line event for example there is little lateral acceleration.

Another observation is that many channels register Lc 4 or Lc 5 as the most severe loadcase alongside to the actually most severe Lc 7. Furthermore, there are other noticeable peaks at loadcases where there should not be any. Therefore, there are several channels which cannot make

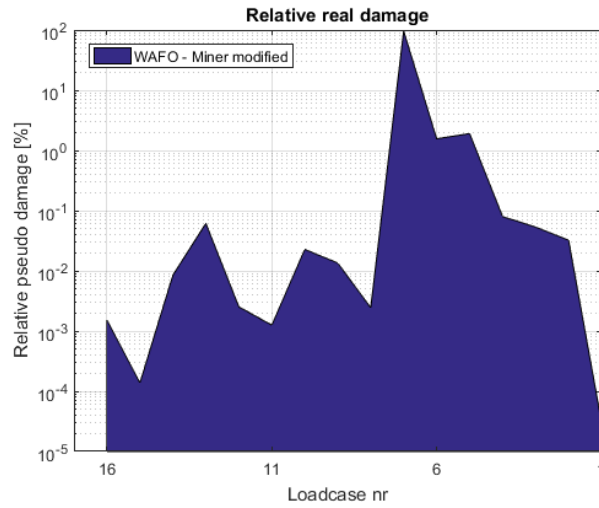


Figure 59 Relative Miner modified damage

Loadcases	Critical point	Channels A <sub>tY</sub> & A <sub>tZ</sub>
Lc 1-4 & Lc 9-16	N221775	Ch 194 & Ch 195
Lc 5 & Lc 7	N93640	Ch 140 & Ch 141
Lc 6 & Lc 8	N299536 & N299957	Ch 26 & Ch 27

Table 5 Channels located near to critical points

accurate comparison across all loads. However, due to the crowdedness of Figure 58 the good descriptions cannot be seen properly.

Focusing on a few channels, the relative pseudo damage is calculated from the lateral and vertical accelerometers selected near to the critical points. Table 5 lists these channels and their nearest critical point. The damage exponent is defined according to the recommended values for automotive and welded components from [7], which is 3 and 5. In addition the value of 12 is used which is the slope of several S-N curves from Figure 47.

Figure 60 shows the results from Ch 195, i.e. the vertical acceleration near to the rear bumper. In Lc 11 and 14 the agreement is quite good. However, the usability of a channel is best described by its worst estimation (for safety). In this case, the agreement between Ch 195's pseudo and real damage is quite inaccurate. The maximum of symmetric distance measures ( $f$  from Eq. (31), substituting  $D_j^{rel}$  for  $A$  and  $d_{195,j}^{rel}$  for  $B$ ) is in the magnitude of thousands, compared to the pseudo damage of modal participation factors where  $f_{max}$  was less than 12.

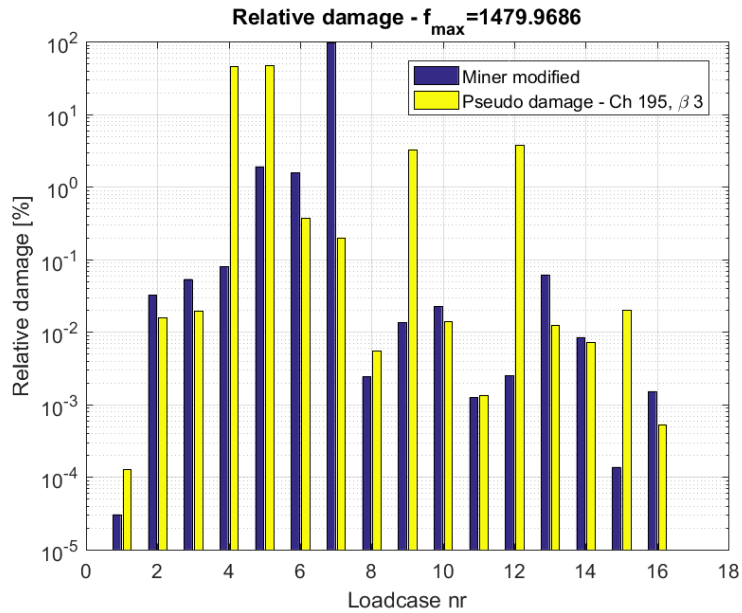


Figure 60 Comparison of Miner modified damage and Pseudo damage from channel 195

$f_{max}$  is calculated for the channels listed in Table 5. In addition, channels (out of all 204) with the best and worst  $f_{max}$  values (highlighted in green and orange) are presented in Figure 61.  $f_{max}=10$  is plotted in red as reference. This value represents approximately 12 times over or underestimation. It can be seen that no individual channel was able to meet this limit.

The selected channels, despite being close to the critical point, fail to be the best. Channel 29, angular accelerometer around Y axis from N5070001 (a connection point of the front left suspension) gives the best agreement  $f_{max}=37,46$ . Therefore, the proximity of a channel to a critical point is not the only factor that describes accuracy.

Furthermore, the inaccuracy of the best single channel, suggests that one channel alone cannot describe the whole loading domain.

In the following pseudo damage will be calculated from multiple channels.

Channels can be sorted in ascending order based on their  $f_{max}$  value. The first several channels can be regarded as the best ones. The best 12, 36, 102, and all 204 channels will now form sets which are separately evaluated. Note that the parameter value  $\beta$  can change the order of channels. Therefore, additional sets are defined for the multiple values of  $\beta$ .

The relative pseudo damage is now calculated (similarly as in Section 4.3.1 Eq. (27)) by just a simple summation on the different sets of channels, hoping that the combination of multiple channels will minimize the worst estimations. The assumption is made again that the damage potential of each channel is equal, therefore there are no weighting factors included in the sum. The results are presented in Table 6.

It can be concluded that the reduction of channels can improve the results. The use of best 12 channels with  $\beta=3$  proved to be the most accurate. However, it still has a worse  $f_{max}=47,9566$  value than the best individual Ch 29 with  $f_{max}=37,46$ . Also, in case of  $\beta=5$  the best set included 36 channels and not 12. It seems that for the best results more needs to be considered than just reducing the number of channels.

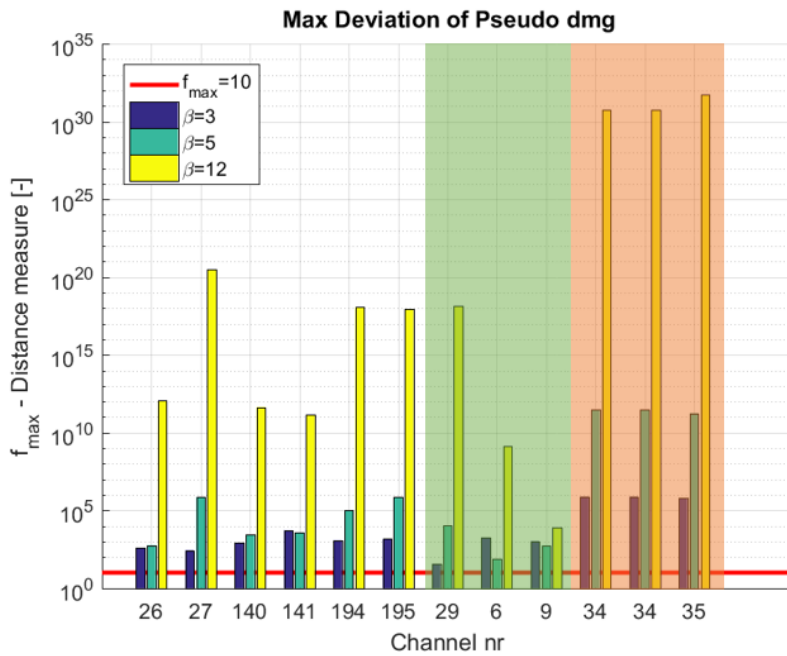


Figure 61  $f_{max}$  from selected Chs

$f_{max}$ table	best 12	best 36	best 102	All 204
3	47,9566	215,4058	779,9016	918,0431
5	426,3025	134,1979	3,06E+03	3,23E+04
12	7,35E+03	3,06E+06	6,58E+11	3,08E+15

Table 6  $f_{max}$  from summed pseudo dmgs of different sets of Chs

The set of all 204 channels with  $\beta=3$  are presented in Figure 62 and Figure 63.

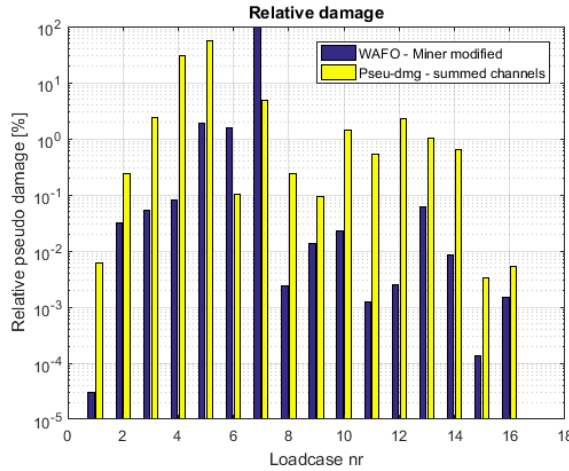


Figure 62 Comparison of Miner modified dmg and summed Pseudo dmg from all Chs

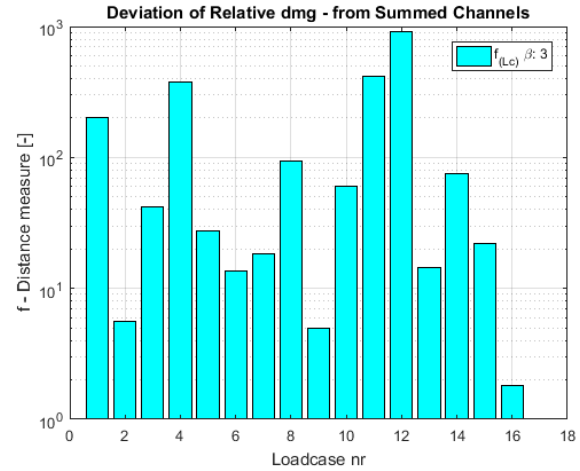


Figure 63 Deviation of summed Pseudo dmg from all Chs

The previously noticed overestimation of Lc 4 and 5 can be seen again. The biggest overestimation coming from Lc 12 which provides  $f_{max}=918$ . It is noticeable that in most loadcases the pseudo damage definition overestimates the real one. The exception is the most damaging Lc7 and the third most damaging Lc 6. These loadcases have such a high relative damage it seems that inaccuracies here skew the rest of the results. Figure 65 and Figure 64 show the same damage results, but the normalization excludes Lc 6 and 7 out of the total damage.

$f_{max}$  is now 19,15 which is better than any previous pseudo damage definition. Also, the real damage is not dominantly over or under estimated. It is clear that the accuracy of pseudo damage depends on the selection of channels, and the reduction of them. However, an additional factor is the 'size' or 'variety' of loadcase domain to which pseudo damage is applied. In the last case the included loadcases can be interpreted as the 'domain of the customer'. The removed loadcases (Lc 6 and 7) were the two variations of washboard. This is a road profile that is generally only present in test tracks, and not on common roads. The remaining rough roads, potholes, curbs, and bumps describe the everyday environment of a car.

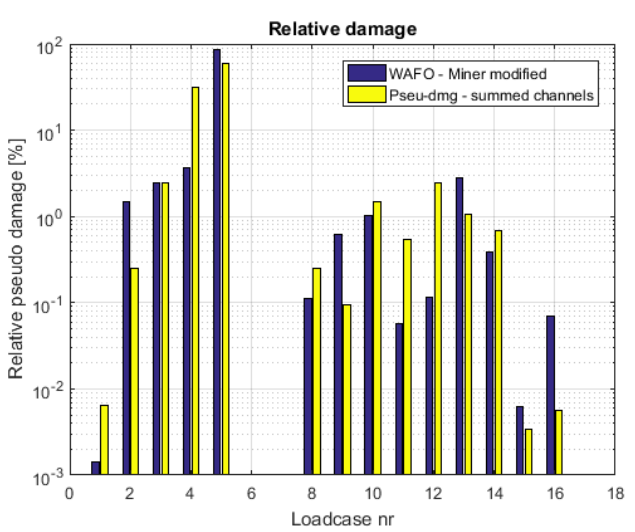


Figure 65 Miner modified dmg and summed Pseudo dmg from all Chs (reduced Lcs)

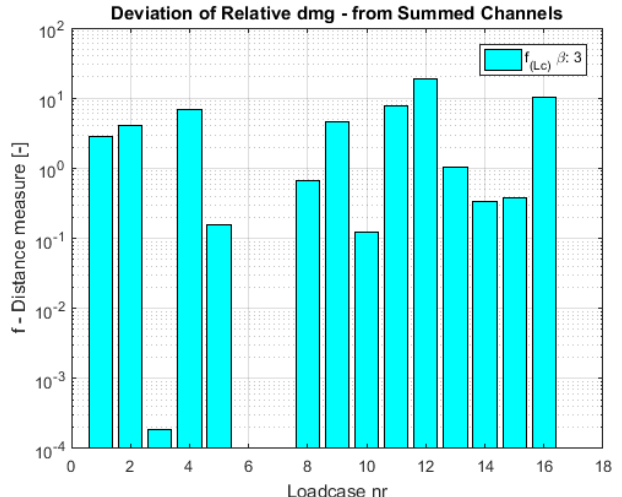


Figure 66 Deviation of summed Pseudo dmg from all Chs (reduced Lcs)

#### 4.4.3. Evaluation of loadcases

Now the loadcases are investigated how to divide them into different domains. The original aim of Section 4.4 was to be able to describe the relative severity of all possible loads by just one number per loadcase. The division of loads into different domains requires the knowledge about which domain a measurement is from. This might not be possible to tell so, alternatively, one can consider all possible domains. In this case one can have as many pseudo damage numbers (per loadcase) as the number of domains. However, this still can be considered as an improvement, since the number of domains is potentially much smaller than the number of channels.

The first aspect according to which loadcases can be divided into groups is the location of the critical points. In this case the evaluation of a domain gives information on the damage of a specific area. There are three distinct areas on the BIW where critical points are located. These three areas divide the loadcases into Group 2, 3 and 6 in Table 7

Another aspect that can divide the domains is the slopes of the modified S-N curves and the fatigue limits (Figure 47), since pseudo damage calculation is relying on  $\beta$ . Maybe numerically better results can be produced if in a limited domain the real damage has similar parameters. Figure 66 shows how the fatigue limits from each loadcase are grouped together into 4 different areas (A1-A4). The corresponding loadcases are Group 2, 3, 4 and 5. It can be noted that this grouping gave similar results to the previous one, since the modification of S-N curves is mainly based on stress concentration and geometry.

Another division is made based on the signal type of loads [20]. According the classification of road profiles, these are Random non-stationary in Group 7, Deterministic periodic in Group 8, and Deterministic single event in Group 9.

Finally, the loadcases can be divided based on if they force substantial roll on the car or not. Group 10 which does not, and Group 11 which does.

The first group was kept for the entire domain.

The best, worst, and average  $f_{max}$  values of individual channels from different domains are shown in Figure 67 and Table 8.

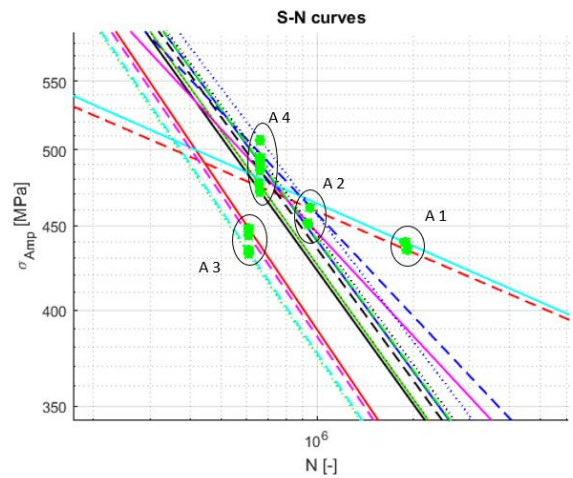


Figure 66 Modified S-N curves of critical points  
(enlarged from Figure 47)

Group	Loadcase nr
nr	
1	[1 2 3 4 5 6 7 8 9 10 12 13 14 15 16]
2	[6 8]
3	[5 7]
4	[1 11 12 15]
5	[2 3 4 9 10 13 14 16]
6	[1 2 3 4 9 10 12 13 14 15 16]
7	[1 2 3 4 5]
8	[6 7]
9	[8 9 10 11 12 13 14 15 16]
10	[1 2 6 8 9 10 11 12 13]
11	[3 4 5 7 14 15 16]

Table 7 Loadcase groups

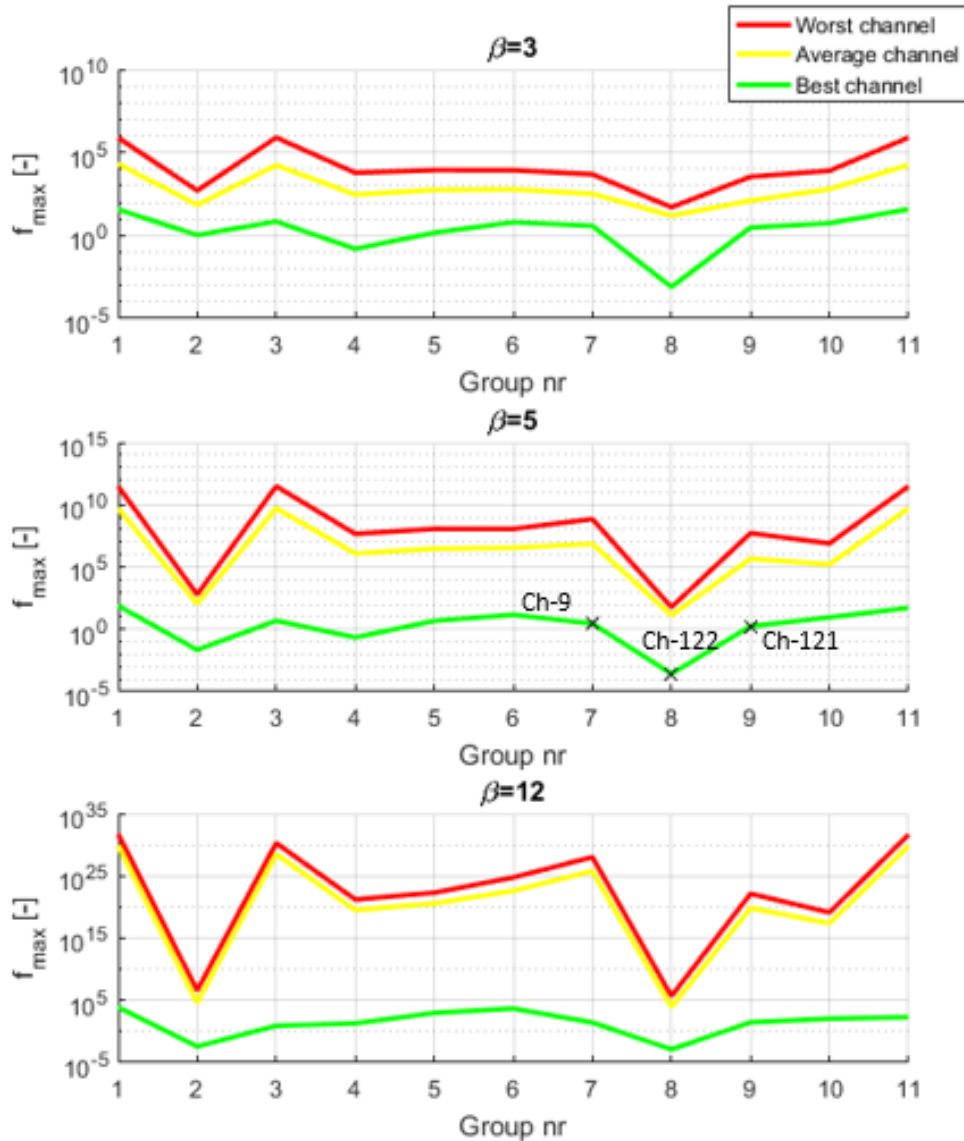


Figure 67 Best/Average/Worst channels across loadcase groups

In almost all cases the best  $f_{max}$  is better in a limited domain (Group 2-11) than in the full one (Group 1). It can be noticed that the lines of average values are much closer to the lines of worst channels. It can be concluded that well-correlating channels are rare, since the average channels concentrated at the proximity of worst values.

Groups 2-5 provide the good values from their respective best channels. It is interesting to note that in Group 2 the best value is evaluated with  $\beta=12$ . The use of this damage exponent in previous results usually provided bad estimations, but in this specific case  $f_{max}=0,004059$  which is the second-best value of them all.

The similar grouping based on the location of critical points provides somewhat worse agreement. Group 6 is the union of group 4 and 5. And it cannot give better  $f_{max}$  values, than the two Groups separately. This indicates that just the reduction of loadcases alone can improve results.

The advantage of load-signal type based grouping that these can be separated without having any special knowledge about the BIW. The evaluation of a measurement is possible by just the correct

interpretation of the signal. This grouping provided quite accurate results with Group 8 having the best  $f_{max}$  value 0,0002727.

The grouping based on rolling motion gives worse results than most other limited domains. The best channel is the same as in the full domain, therefore the better agreement compared to Group 1 is probably due to the smaller number of loadcases.

Groups	Best $f_{max}$	$\beta$	Channel number	Acceleration component t-translation r-rotation
Group 1	37,46	3	29	ArY@N5070001
Group 2	0,004059	12	186	ArZ@N524579
Group 3	4,93	5	3	AtZ@Upr_FL
Group 4	0,1587	3	31	AtX@N5050000
Group 5	1,49	3	29	ArY@N5070001
Group 6	6,404	3	21	AtZ@Upr_RR
Group 7	2,876	5	9	AtZ@Upr_FR
Group 8	0,0002727	5	122	AtY@N344598
Group 9	1,752	5	121	AtX@N344598
Group 10	5,55	3	29	ArY@N5070001
Group 11	38,48	3	29	ArY@N5070001

Table 8 Best  $f_{max}$  from loadcase groups

Looking at the location of measurements for the best channels (node IDs), 8 out of 11 times they are connection points of suspension and uprights. From this, the generalized conclusion could be that having measurements closest to the road produces better results. However, more data would be needed to confirm this. Also, the predictions can still be quite inaccurate.

An interesting thing to note is that in case of Group 2, the best value comes from a signal which is measured angular acceleration from under the rear-right seat of the car. It is also evaluated with  $\beta=12$ , that has not proved to be widely applicable. The selection of this specific parameters and signal location for two different load-signal types would be hard to generalize.

However, due to the finding of previous analyses, it is known that these loadcases are in the same group according to the location of critical points and modified S-N curves. Furthermore, in these cases 110 and 114 modes were deemed the most prominent which have close eigenfrequencies. Therefore, finding the commonality could be achieved by analysis from several angles.

In case data is available from tests or verified analyses, a parametrized pseudo damage model can be created. If the model can be accurate on the available data, its extension to new measurements can be investigated.

#### 4.4.4. Evaluation of parameters

In the following, it is again investigated how accurate one pseudo damage number can be that uses more channels. However, the parameters of each channel's pseudo damage are modified, so the results would fit on the real damage. Furthermore, this time it is only evaluated in case of Group 7-9.

From Table 6 it can be assumed that the summation of pseudo damages without weighing channel's individual relevance will most likely provide worse results than the best channel alone. This can be due to that half of the channels register angular acceleration, and their signals have different magnitudes than translational acceleration. This does not make an impact when evaluating relative pseudo damage from just one channel. However, smaller amplitude signals can be overpowered by others if they are not scaled before summation. Scaling the signals can be also interpreted as weighing their relevance in the sum. Therefore, weights will not be introduced but a scalar  $\lambda_i$  for individual signals will be used for this purpose. Another parameter that has a big impact is  $\beta$ , for which only 3 discrete values were used before, but now it can take any real value between 1 and 15. These parameters will be optimized for each channel to have the best possible agreement with real damage.

Several optimizations will be run with different sets of loadcase groups ( $G_l$ ) and different sets of channels ( $Ch_{lm}$ ) included.

The loadcases in  $G_l$  are defined by the previous groups in table 8.  $G_1$  is Group 1 i.e. Loadcase numbers: {1 ... 16}.

The channels in  $Ch_{lm}$  are a selection of  $m$  channels based on their individual  $f_{max}$  value evaluated in the corresponding  $G_l$ . (The best worst and average of these  $f_{max}$  values were shown in Figure 67.) The content of  $Ch_{lm}$  are the channel numbers that provide the lowest  $f_{max}$  calculated with any  $\beta$  in  $G_l$ , so the size of  $Ch_{lm}$  is  $m$ . For example,  $Ch_{7,1}$  is {9} since from Figure 67 the best one channel from  $G_7$  is Channel 9.

The optimization problem is formulated below

$$\begin{aligned} & \min_{\lambda, \beta} (f_{max}) \\ \text{s.t. } & \begin{cases} \lambda_i \in \mathbb{R}: 0 \leq \lambda_i \leq 1, & i \in Ch_{lm} \\ \beta_i \in \mathbb{R}: 1 \leq \beta_i \leq 15, & i \in Ch_{lm} \end{cases} \end{aligned} \quad (35)$$

Design variables:

$$\lambda = (\lambda_i)$$

$$\beta = (\beta_i)$$

where

from (31), (29), and (34)

$$f_{max} = \max \left( \frac{D_j^{rel}}{d_j^{rel}} + \frac{d_j^{rel}}{D_j^{rel}} - 2 \right) \quad (36)$$

$$d_j = \sum_i \sum_k \lambda_i * S_k(a_{ij})^{\beta_i}, \quad i \in Ch_{lm}, j \in G_l \quad (37)$$

$i \in Ch_{lm}$  – Set of channel numbers

$j \in G_l$  – Set of loadcase numbers

Since  $\lambda_i$  is allowed to be zero, therefore the number of channels that are included is optimized in a sense, when they are scaled to 0.

Optimizations were performed for  $m = 7, 8, 9$  and  $l = 12, 36, 102$  in MATLAB using a genetic algorithm [21]. The algorithm was modified by 3 parameters: NIND - number of individuals per subpopulations, MAXGEN - maximum number of generations, and GGAP - Generation gap (how many new individuals are created).

From several runs (with different configuration of optimization parameters) the best results are shown in Table 9, the corresponding optimization parameters are shown in Appendix D.1 Table 22.

In case of  $G_8$  there is no difference between the pseudo damage and the real damage, however in this group there are only 2 loadcases. Therefore, in such limited domain the good agreement is not surprising.

In case of the Random nonstationary, and Deterministic single event loads in  $G_7$  and  $G_9$  the results improved compared to the best individual channels from before, which is promising. However, to put the results into perspective  $f=0,114$  is approximately a 40% over or 30% under estimation of the target. This limit is met in  $G_9$  but could not be achieved in  $G_7$ . Therefore, the application of the parametrized pseudo damage models would need to take the accuracy of each group into account in a safety factor. This safety factor would need further analysis since the accuracy of the model might change on new measurements. However, it can be assumed that the model would not perform better on new measurements that it was not fitted into. Therefore, Table 10 can describe how accurate a parametrized pseudo damage model can be in terms of real damage.

Table of $f_{max}^*$	$G_7$	$G_8$	$G_9$
$Ch_{l,12}$	1.358677420700428	0	0.251351569499340
$Ch_{l,36}$	1.360380355800833	0	0.109045511061222
$Ch_{l,102}$	1.543264847853714	0	0.090590095672108

Table 9 Optimum objective values

Over/Under estimations	$G_7$		$G_8$		$G_9$	
	Over est.	Under est.	Over est.	Under est.	Over est.	Under est.
$Ch_{l,12}$	+202,85 %	-66,98 %	+0 %	-0 %	+64,25 %	-39,12 %
$Ch_{l,36}$	+203,04 %	-67,00 %	+0 %	-0 %	+38,92 %	-28,02 %
$Ch_{l,102}$	+223,41 %	-69,08 %	+0 %	-0 %	+34,97 %	-25,91 %

Table 10 Over and under estimations of optimized pseudo damage

The visualization of absolute damage and optimized pseudo damage values from  $Ch_{l,36}$  are in Figure 68-Figure 70. The lists of optimum pseudo damage parameters are in Appendix D.1 Table 13-Table 21.

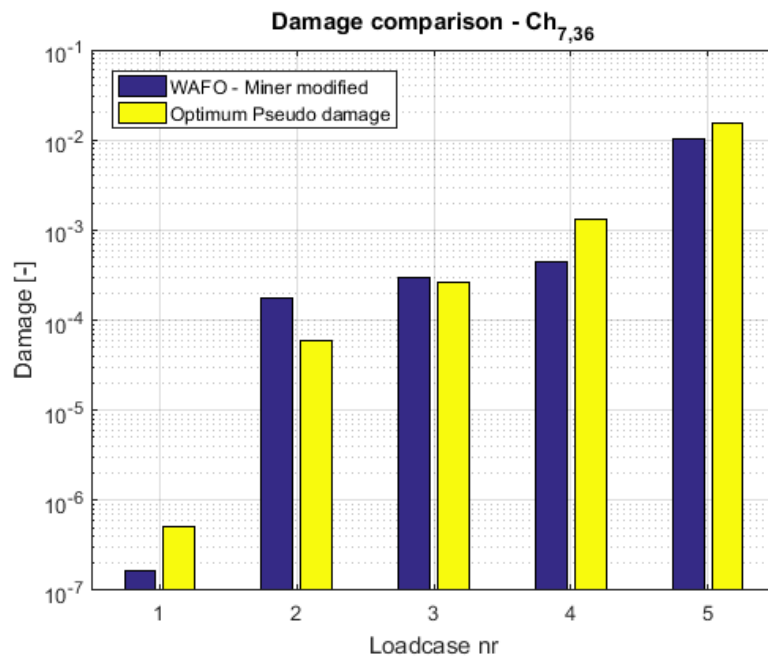


Figure 68 Comparison of Miner modified dmg and parametrized Pseudo damage from Ch<sub>7,36</sub>

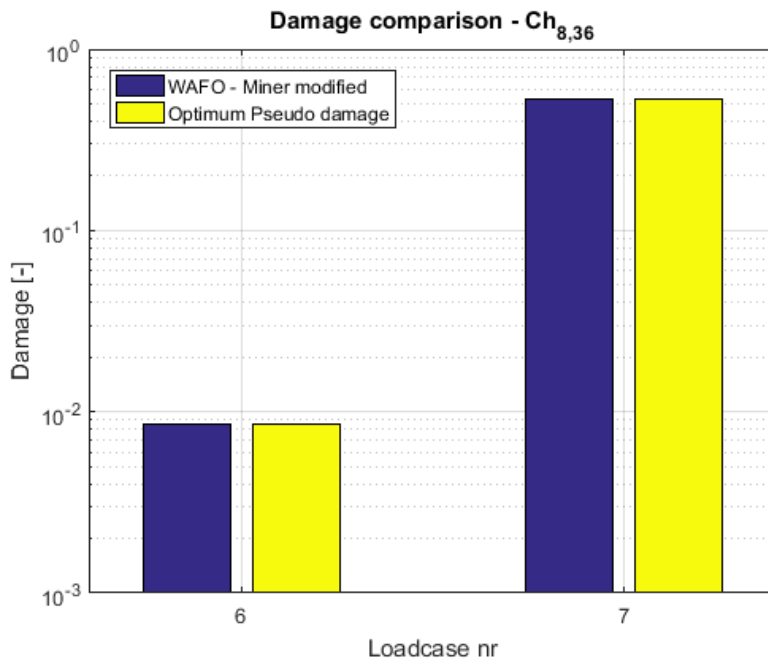


Figure 69 Comparison of Miner modified dmg and parametrized Pseudo damage from Ch<sub>8,36</sub>

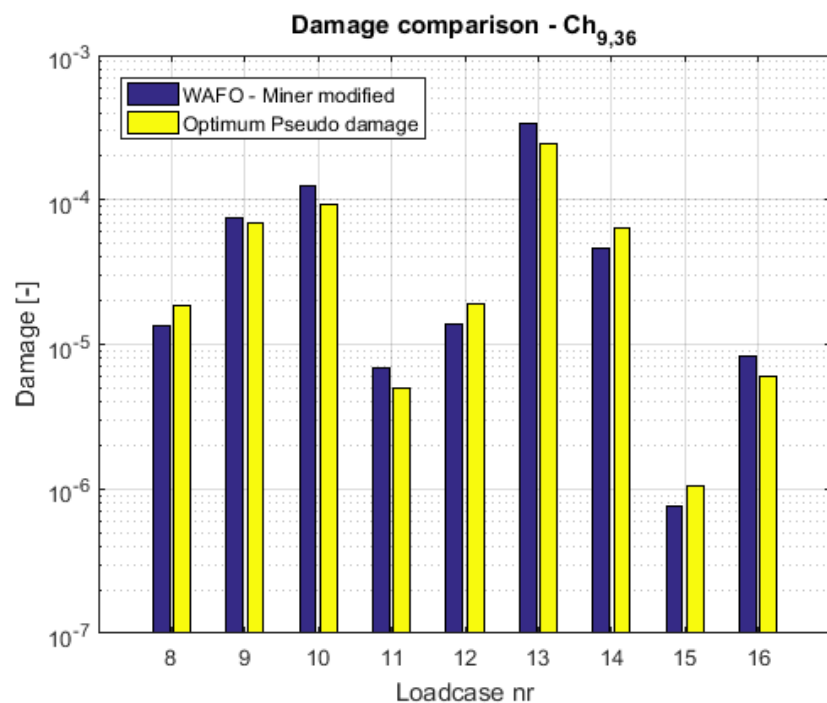


Figure 70 Comparison of Miner modified dmg and parametrized Pseudo damage from Ch<sub>9,36</sub>

## 5. Conclusion

This thesis aimed to elaborate on how to implement different methods for fatigue life calculations and examine their merits and limitations.

In Section 2.1 multiple methods were introduced from stress calculation, all of which had merits in simplifying complex models.

The same methods were evaluated in Section 3. The differences between them were investigated and revealed. QSSM was underestimating loads when vibrations were involved, FRA is best suited to random long signals, and finally MSM was deemed to be the most suitable for the later analysis of BIW, as it captured vibrational effects and could accurately handle short transient loads.

The investigation of modal participation factors using of pseudo damage gave a prediction on the location of critical points, and a definition of most prominent modeshapes of the deformed body. The prediction of critical points was good, which has the potential for saving computational time by model reduction. Also, this information combined with the most prominent modeshapes can give insight into the nature of failure. This could guide a designer during the development phase of a vehicle.

The damage calculation on BIW from MSM using virtual proving grounds captured the damage potential of structural vibrations (see Section 4.3.4), therefore it can be a useful tool when designing a vehicle for durability. However, before the final evaluation of meeting design targets the accuracy of vehicle model needs to be verified as it is affected by numerous parameters (mentioned in Section 1.4 d)).

Possibilities to relate severity of loadcases to each other by just one pseudo damage number was examined throughout Section 4.4. Pseudo damage numbers calculated from acceleration had big variation dependent on the selected channels and parameters. There were no clear generalizable approaches how to select channels or which parameters to use for evaluating load severity accurately. However, this was improved by optimization of parameter values and selection of channels and loadcases. This parametrization of a pseudo damage model requires references when the real damage is known, to fit the model into that. In case of a beforementioned verified vehicle model exists, this can be achieved. However, in this case using the verified model is most certainly the most accurate way to evaluate measurements. Therefore, according to the author one pseudo damage number is not sufficient to evaluate fatigue life of a component. Thus, its domain of applicability should remain in data reduction and comparisons between measurements using multiple pseudo damage numbers.

In conclusion, the goals of this thesis formulated in Section 1.2 by the judgement of the author were achieved. From Sections 2.1.1-2.1.3, and 3.2-3.4 the reader could make a better selection and implementation of the investigated methods to evaluate stress for a vehicle body. The findings of Section 4.3 could help to calculate damage efficiently, due to accurate predictions of critical points. Meanwhile the results of Section 4.4 warn the reader to the limitations of extensive data reduction with pseudo damage, while detailing the possibilities for improvements. Hopefully, these finding will provide useful to an engineer who is planning to undertake durability analysis for a vehicle.

## 6. Future work

The notion of pseudo damage is based on data reduction while preserving fatigue related aspects. [7] The pseudo damage parametrization did improve its relation to fatigue. It is yet to be investigated if usual use-cases for pseudo damage such as accelerated testing (with track mixing) or investigation of customer load distribution [7] can benefit from a parametrized pseudo damage. Performing these activities with parametrized and non-parametrized models in a virtual environment where the actual results are controlled would provide a base of comparison.

The fidelity of the parametrized pseudo damage model also need to be investigated since it's presumed use-case must be outside of the results it was fitted into. This can be achieved by the generation of new loadcases i.e. road profiles in the existing multi-body model and investigation of the predicted and actual results.

## References

- [1] Wikipedia contributors, "Effects of the car on societies," [Online]. Available: [https://en.wikipedia.org/w/index.php?title=Effects\\_of\\_the\\_car\\_on\\_societies&oldid=838625803](https://en.wikipedia.org/w/index.php?title=Effects_of_the_car_on_societies&oldid=838625803). [Accessed 26 06 2018].
- [2] T. Dahlberg and A. Ekberg, Failure Fracture Fatigue: An Introduction, Studentlitteratur AB, 2002.
- [3] D. A. Halfpenny and M. F. Kihm, "Rainflow cycle counting and acoustic fatigue analysis techniques for random loading," in *RASD 2010*, Southampton, 2010.
- [4] D. Y. M. Reddy and S. Padmanabhan, "Virtual Full Vehicle Durability Testing of a passenger car," Department of Applied Mechanics Chalmers University of technology, Göteborg, 2017.
- [5] A. B. Ofner, "Evaluation and parametrization of finite-element representations of spot welds for durability analysis of vehicle BIW," Carinthia University of Applied Science, Villach, 2018.
- [6] G. Moore, Interviewee, *Gordon Moore: The Man Whose Name Means Progress, The visionary engineer reflects on 50 years of Moore's Law*. [Interview]. 30 03 2015.
- [7] P. Johannesson and M. Speckert, Guide to load analysis for durability in vehicle engineering, Fraunhofer-Chalmers Research Centre for Industrial Mathematics: John Wiley & Sons, Ltd, 2014.
- [8] P. O'Connor, Test Engineering, A Concise Guide to Cost-effective Design, Development and Manufacture, Chichester, : Wiley, 2005.
- [9] Siemens Product Lifecycle Management Software Inc., "Basic Dynamic Analysis User's Guide," [Online]. Available: [https://docs.plm.automation.siemens.com/data\\_services/resources/nxnastran/10/help/en\\_US/tocExt/pdf/basic\\_dynamics.pdf](https://docs.plm.automation.siemens.com/data_services/resources/nxnastran/10/help/en_US/tocExt/pdf/basic_dynamics.pdf). [Accessed 10 06 2018].
- [10] R. D. Cook, D. S. Malkus, M. E. Plesha és R. J. Witt, Concepts and applications of finite element analysis, Wiley & Sons. Inc., 2002.
- [11] Magna International Inc., "FEMFAT user manual," St. Valentin, 2015.
- [12] C. Gaier, B. Unger and J. Vogler, "Theory and Applications of FEMFAT - A FE-Postprocessing Tool for Fatigue Analysis.", in *7th International Fatigue Congress*, Beijing, P.R. China, 1999.
- [13] Z. Lv, H.-Z. Huang, S.-P. Zhu, H. Gao and F. Zuo, "A modified nonlinear fatigue damage accumulation model," *International Journal of Damage Mechanics*, vol. 24, pp. 168-181, 2015.

- [14] Y.-L. Lee, J. Pan, R. Hathaway and M. Barkey, *Fatigue Testing and Analysis: Theory and Practice*, Butterworth-Heinemann, 2005.
- [15] Siemens Product Lifecycle Management Software Inc., "Quick Reference Guide," [Online]. Available:  
[https://docs.plm.automation.siemens.com/data\\_services/resources/nxnastran/10/help/en\\_US/tocExt/pdf/QRG.pdf](https://docs.plm.automation.siemens.com/data_services/resources/nxnastran/10/help/en_US/tocExt/pdf/QRG.pdf). [Accessed 10 06 2018].
- [16] U. Sellgren, *COMPONENT MODE SYNTHESIS - A method for efficient dynamic simulation of complex technical systems*, Stockholm: Department of Machine DesignThe Royal Institute of Technology (KTH), 2018.
- [17] F. Tyan, Y.-F. Hong, S.-H. Tu and W. S. Jeng, "隨機路面之產生 Generation of Random Road Profiles," *Journal of Advanced Engineering*. 4., pp. 1373-1378, 2009.
- [18] WAFO group, *WAFO - a Matlab Toolbox for Analysis of Random Waves and Loads*, Lund: Lund University, 2011.
- [19] K. Bladh, "Virtual full vehicle durability testing of a coach," KTH Industrial Engineering and Management Machine Design, Stockholm, 2012.
- [20] K. Shin and J. K. Hammond, *Fundamentals of Signal Processing for Sound and Vibration Engineers*, West Sussex PO19 8SQ, England: John Wiley & Sons, Ltd, 2008.
- [21] Chipperfield, A. a. Fleming, P. a. Pohlheim, H. a. Fonseca and Carlos, Genetic algorithm toolbox for use with MATLAB, Citeseer, 1994.

# Appendix A

## A.1. Modes and frequencies of constrained beam

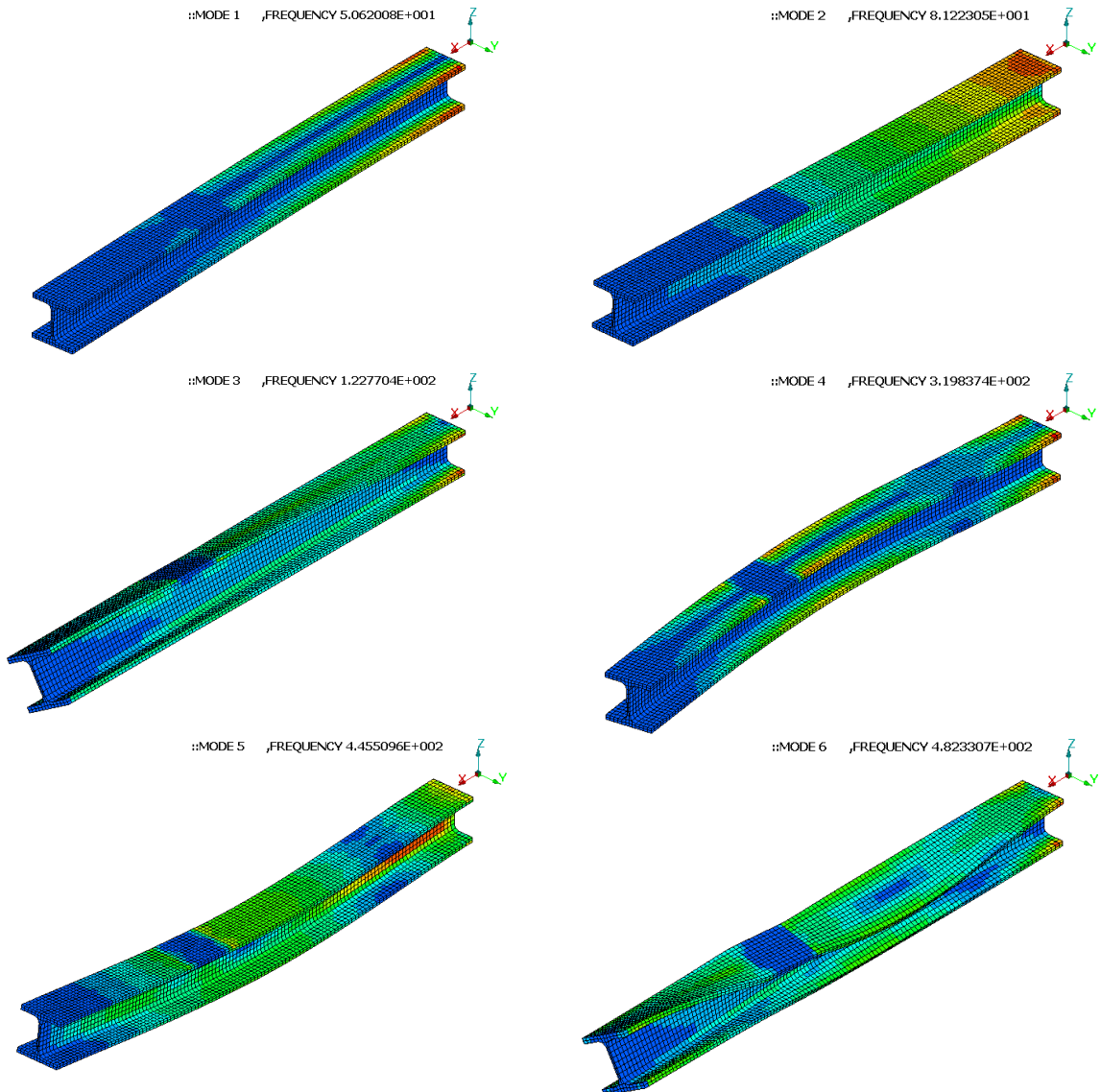


Figure 71 Modes and frequencies of constrained beam

## Appendix B

### B.1. Modes and frequencies of BIW

Mode	Frequency	Mode	Frequency	Mode	Frequency	Mode	Frequency
<b>1</b>	1,89E+01	<b>41</b>	2,86E+02	<b>81</b>	1,00E+03	<b>121</b>	3,43E+03
<b>2</b>	2,12E+01	<b>42</b>	2,93E+02	<b>82</b>	1,02E+03	<b>122</b>	3,74E+03
<b>3</b>	2,69E+01	<b>43</b>	3,00E+02	<b>83</b>	1,04E+03	<b>123</b>	3,87E+03
<b>4</b>	2,73E+01	<b>44</b>	3,20E+02	<b>84</b>	1,20E+03	<b>124</b>	3,88E+03
<b>5</b>	2,76E+01	<b>45</b>	3,26E+02	<b>85</b>	1,22E+03	<b>125</b>	3,94E+03
<b>6</b>	3,14E+01	<b>46</b>	3,48E+02	<b>86</b>	1,23E+03	<b>126</b>	4,01E+03
<b>7</b>	3,50E+01	<b>47</b>	3,52E+02	<b>87</b>	1,31E+03	<b>127</b>	4,10E+03
<b>8</b>	3,58E+01	<b>48</b>	3,62E+02	<b>88</b>	1,33E+03	<b>128</b>	4,23E+03
<b>9</b>	3,61E+01	<b>49</b>	3,76E+02	<b>89</b>	1,38E+03	<b>129</b>	4,31E+03
<b>10</b>	3,74E+01	<b>50</b>	3,89E+02	<b>90</b>	1,41E+03	<b>130</b>	5,49E+03
<b>11</b>	3,90E+01	<b>51</b>	4,04E+02	<b>91</b>	1,45E+03		
<b>12</b>	4,83E+01	<b>52</b>	4,09E+02	<b>92</b>	1,52E+03		
<b>13</b>	5,40E+01	<b>53</b>	4,21E+02	<b>93</b>	1,53E+03		
<b>14</b>	5,60E+01	<b>54</b>	4,25E+02	<b>94</b>	1,53E+03		
<b>15</b>	6,43E+01	<b>55</b>	4,56E+02	<b>95</b>	1,58E+03		
<b>16</b>	6,49E+01	<b>56</b>	4,77E+02	<b>96</b>	1,60E+03		
<b>17</b>	6,90E+01	<b>57</b>	4,87E+02	<b>97</b>	1,62E+03		
<b>18</b>	7,96E+01	<b>58</b>	5,23E+02	<b>98</b>	1,69E+03		
<b>19</b>	8,87E+01	<b>59</b>	5,32E+02	<b>99</b>	1,70E+03		
<b>20</b>	9,78E+01	<b>60</b>	5,69E+02	<b>100</b>	1,82E+03		
<b>21</b>	9,87E+01	<b>61</b>	5,86E+02	<b>101</b>	1,88E+03		
<b>22</b>	1,03E+02	<b>62</b>	6,10E+02	<b>102</b>	1,89E+03		
<b>23</b>	1,05E+02	<b>63</b>	6,29E+02	<b>103</b>	1,93E+03		
<b>24</b>	1,10E+02	<b>64</b>	6,85E+02	<b>104</b>	1,98E+03		
<b>25</b>	1,21E+02	<b>65</b>	7,11E+02	<b>105</b>	2,04E+03		
<b>26</b>	1,24E+02	<b>66</b>	7,18E+02	<b>106</b>	2,21E+03		
<b>27</b>	1,37E+02	<b>67</b>	7,30E+02	<b>107</b>	2,22E+03		
<b>28</b>	1,39E+02	<b>68</b>	7,34E+02	<b>108</b>	2,31E+03		
<b>29</b>	1,43E+02	<b>69</b>	7,44E+02	<b>109</b>	2,32E+03		
<b>30</b>	1,62E+02	<b>70</b>	7,66E+02	<b>110</b>	2,33E+03		
<b>31</b>	1,67E+02	<b>71</b>	7,95E+02	<b>111</b>	2,41E+03		
<b>32</b>	1,82E+02	<b>72</b>	8,00E+02	<b>112</b>	2,50E+03		
<b>33</b>	2,03E+02	<b>73</b>	8,06E+02	<b>113</b>	2,50E+03		
<b>34</b>	2,05E+02	<b>74</b>	8,35E+02	<b>114</b>	2,55E+03		
<b>35</b>	2,13E+02	<b>75</b>	8,48E+02	<b>115</b>	2,69E+03		
<b>36</b>	2,30E+02	<b>76</b>	8,67E+02	<b>116</b>	2,77E+03		
<b>37</b>	2,39E+02	<b>77</b>	8,95E+02	<b>117</b>	3,04E+03		
<b>38</b>	2,46E+02	<b>78</b>	9,36E+02	<b>118</b>	3,26E+03		
<b>39</b>	2,59E+02	<b>79</b>	9,57E+02	<b>119</b>	3,35E+03		
<b>40</b>	2,70E+02	<b>80</b>	9,84E+02	<b>120</b>	3,39E+03		

Table 11 Modes and frequencies of BIW

## B.2. BIW hotspots, critical points, and prominent modes

### B.2.1. Hotpots

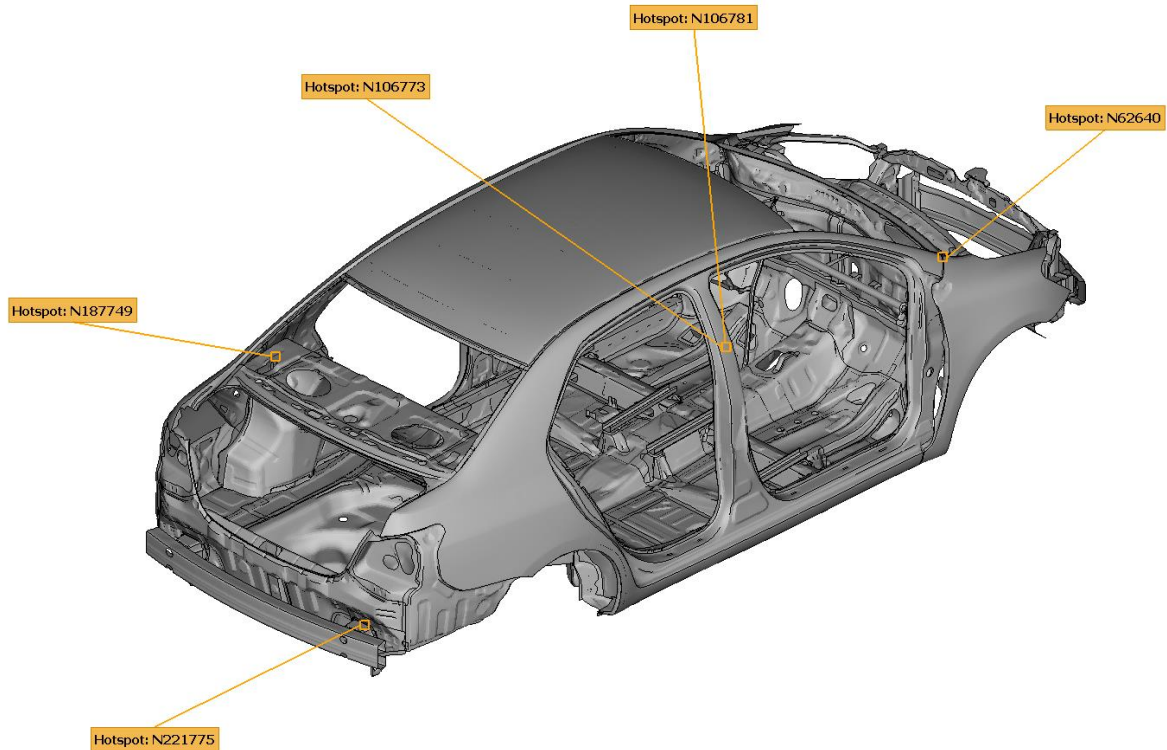


Figure 72 Hotspots of BIW

### B.2.2. Critical points

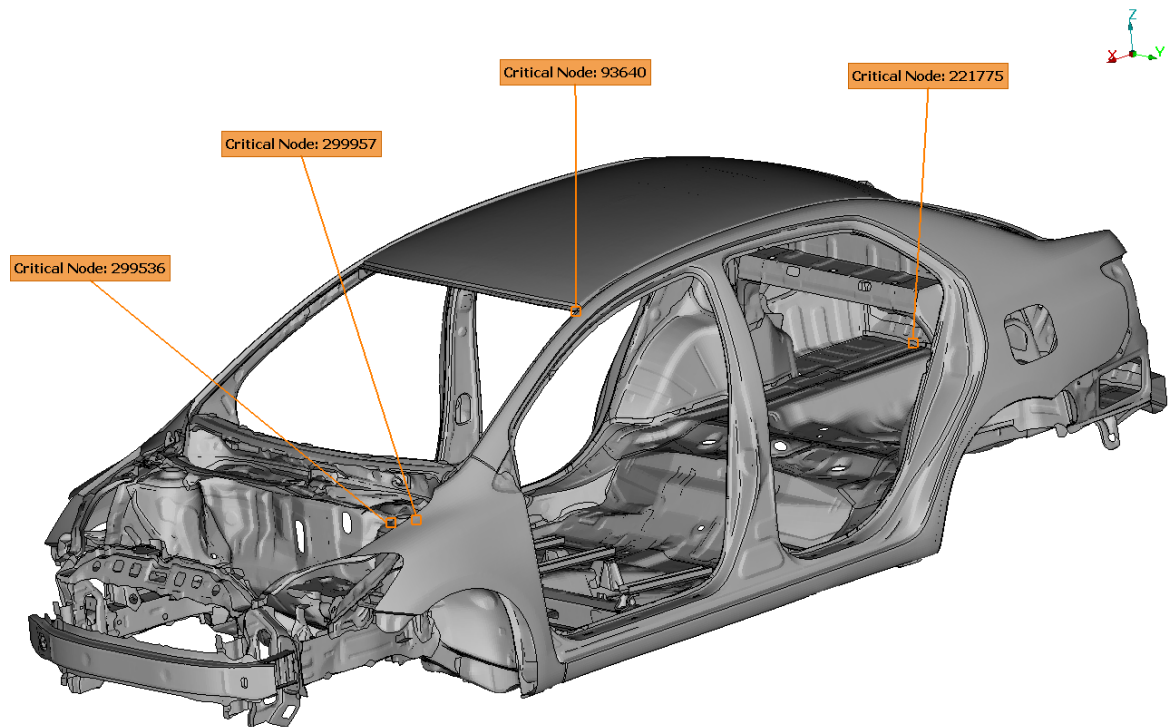


Figure 73 Critical points of BIW (1/4)

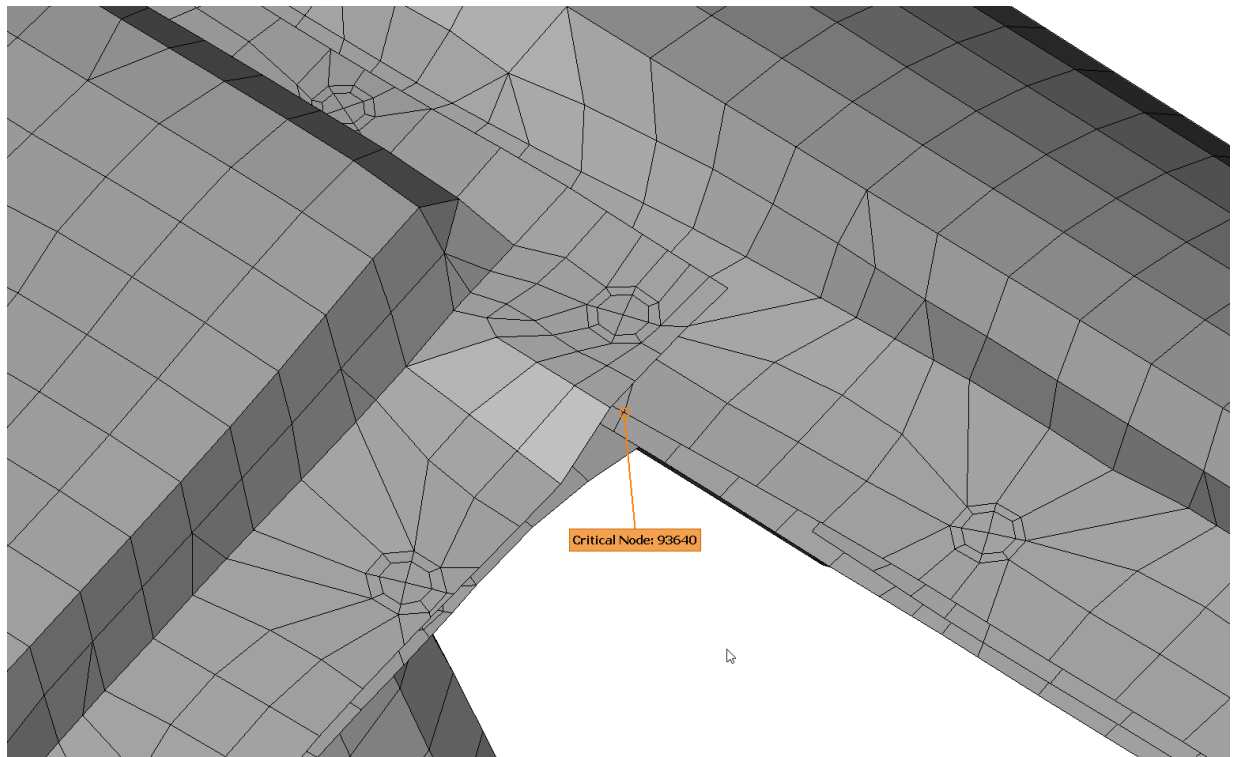


Figure 74 Critical points of BIW (2/4)

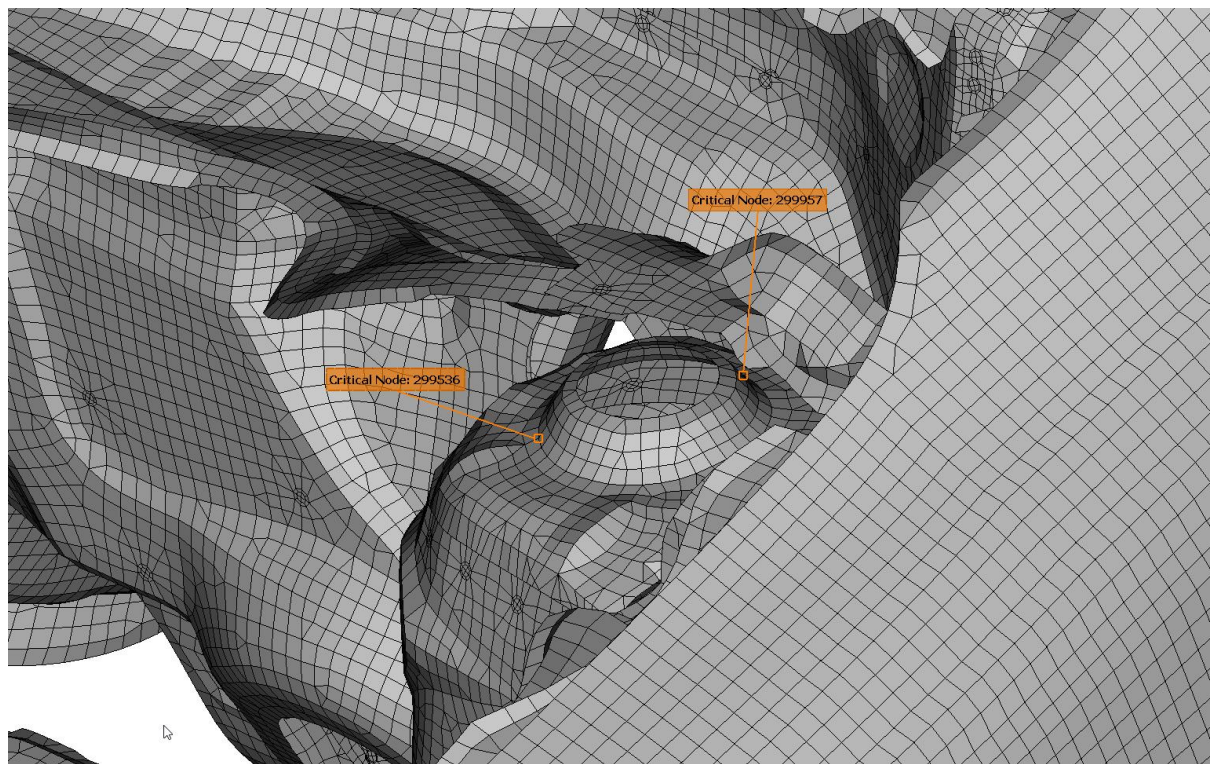


Figure 75 Critical points of BIW (3/4)

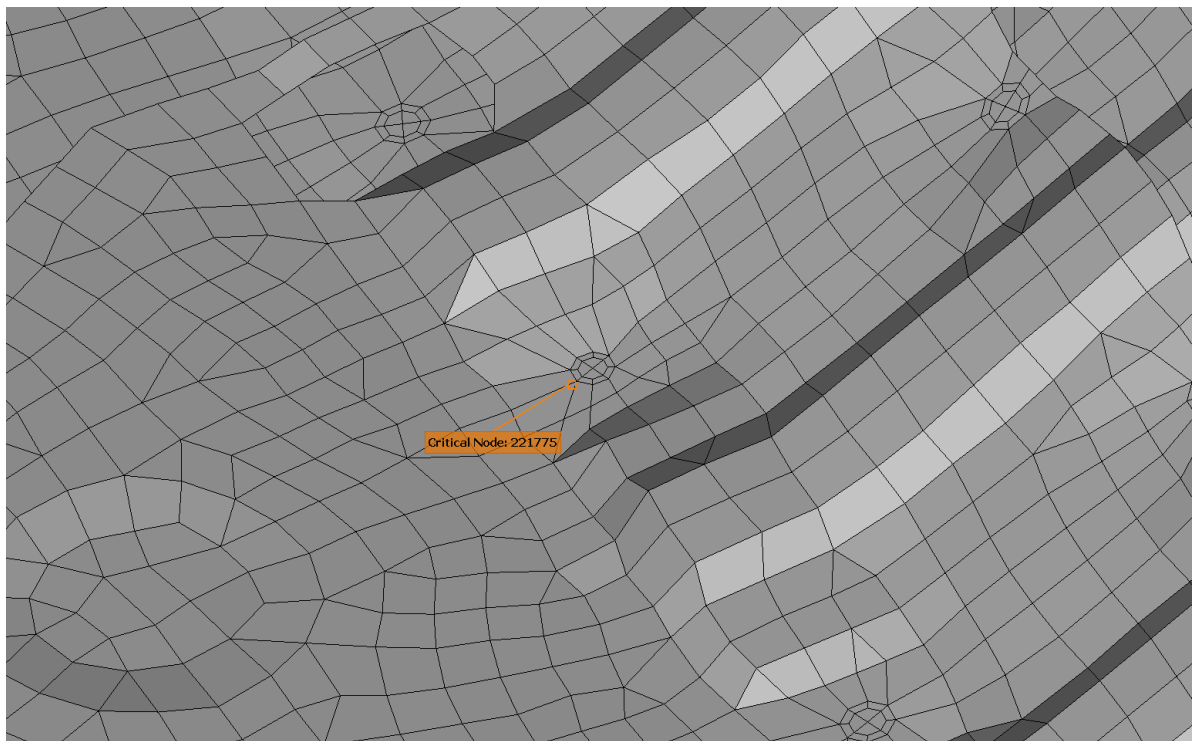


Figure 76 Critical points of BIW (4/4)

### B.2.3. Mode 1

Contour:  
deformation  
State:  
Undeformed

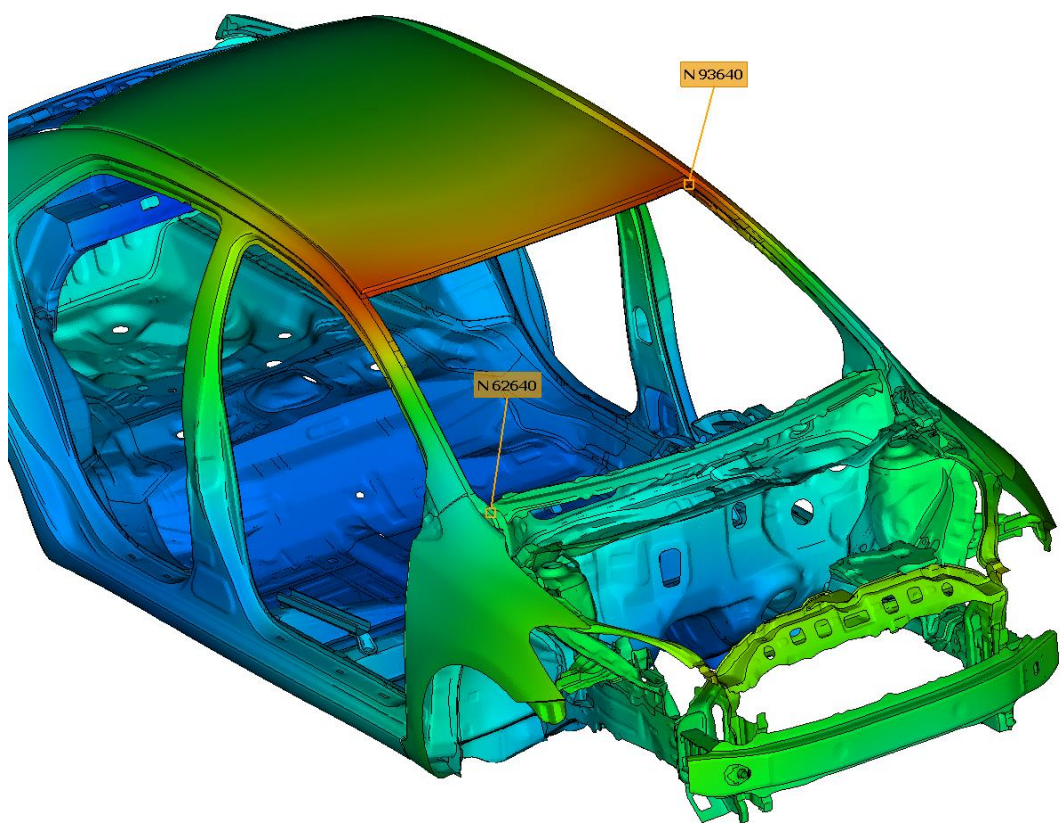


Figure 77 Mode 1 with hotspot and critical point (1/3)

Contour:  
deformation  
State:  
Deformed

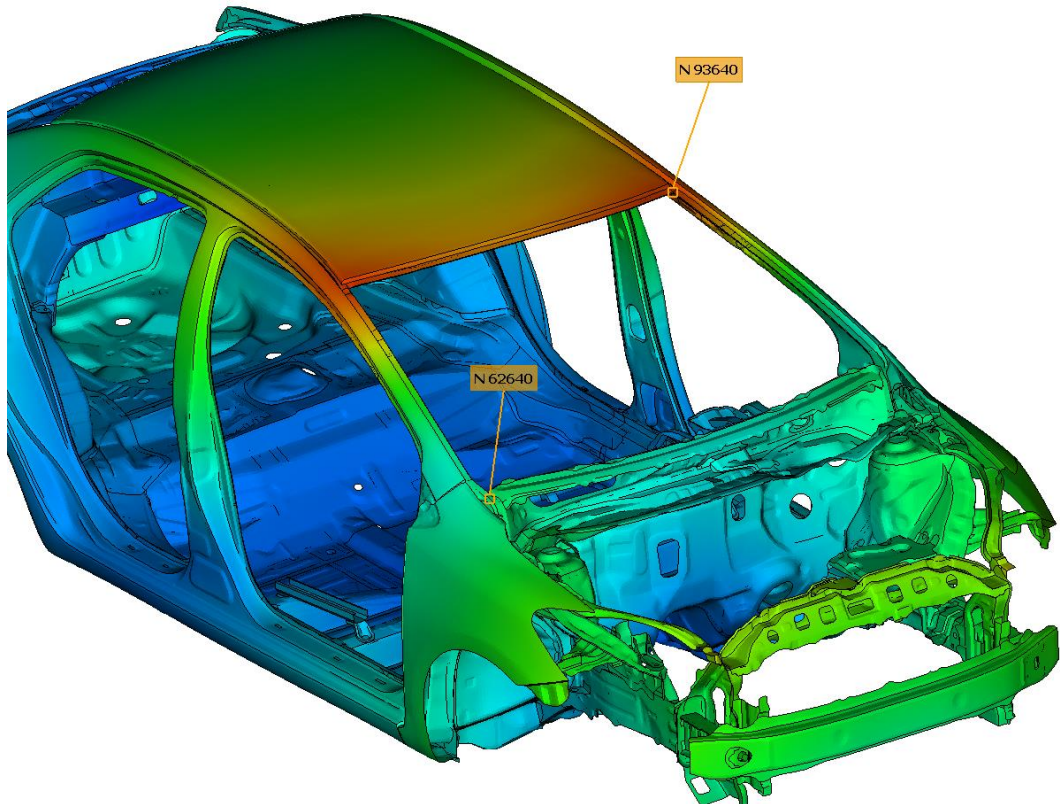


Figure 78 Mode 1 with hotspot and critical point (2/3)

Contour:  
Von Mises  
stress  
State:  
Undeformed

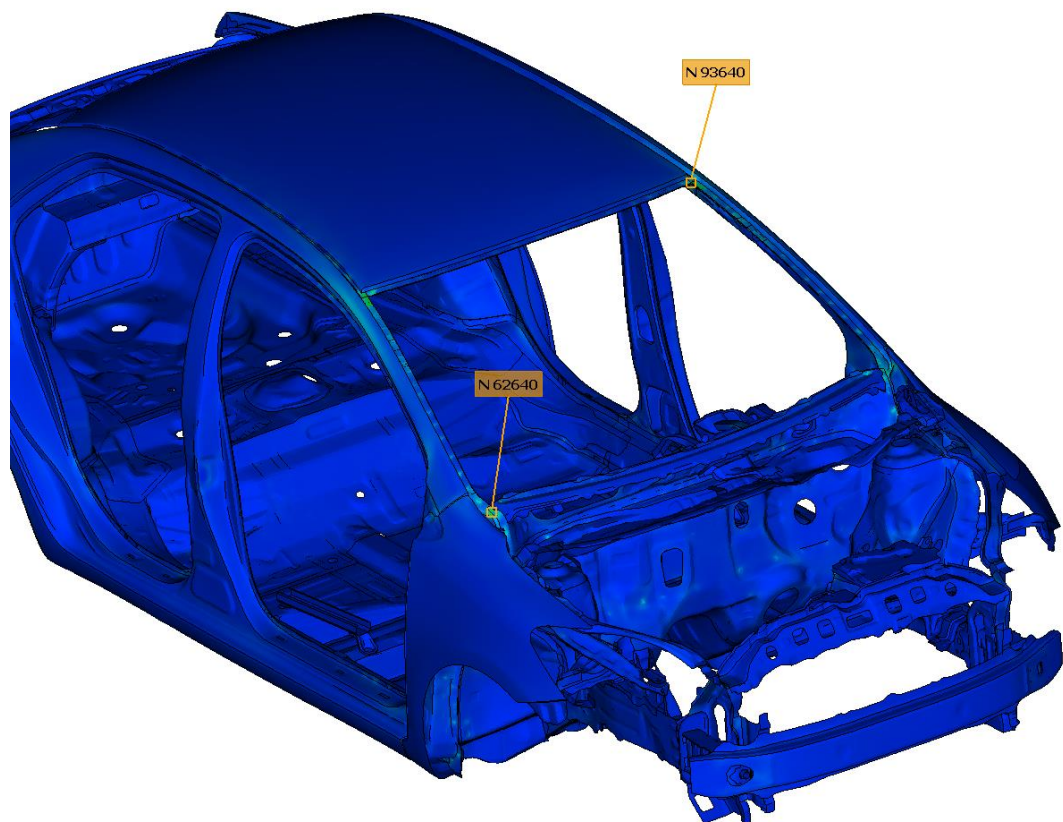


Figure 79 Mode 1 with hotspot and critical point (3/3)

#### B.2.4. Mode 2

Contour:  
deformation  
State:  
Undeformed

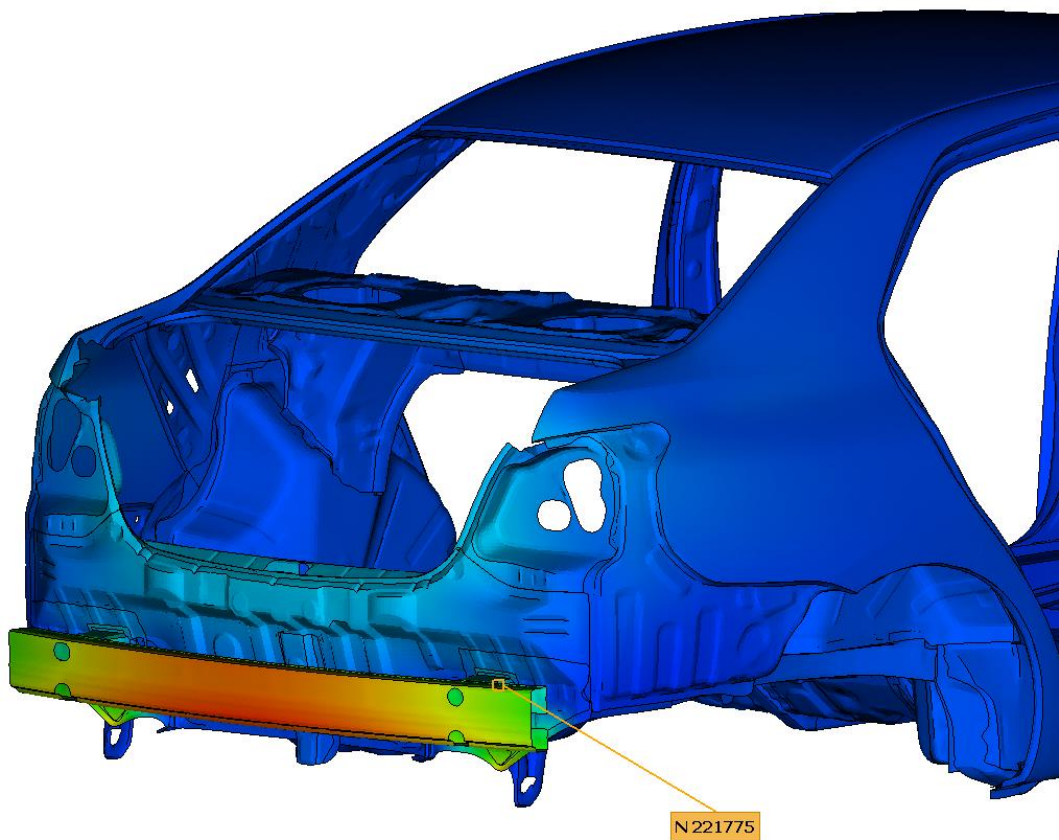


Figure 80 Mode 2 with hotspot and critical point (1/3)

Contour:  
deformation  
State:  
Deformed

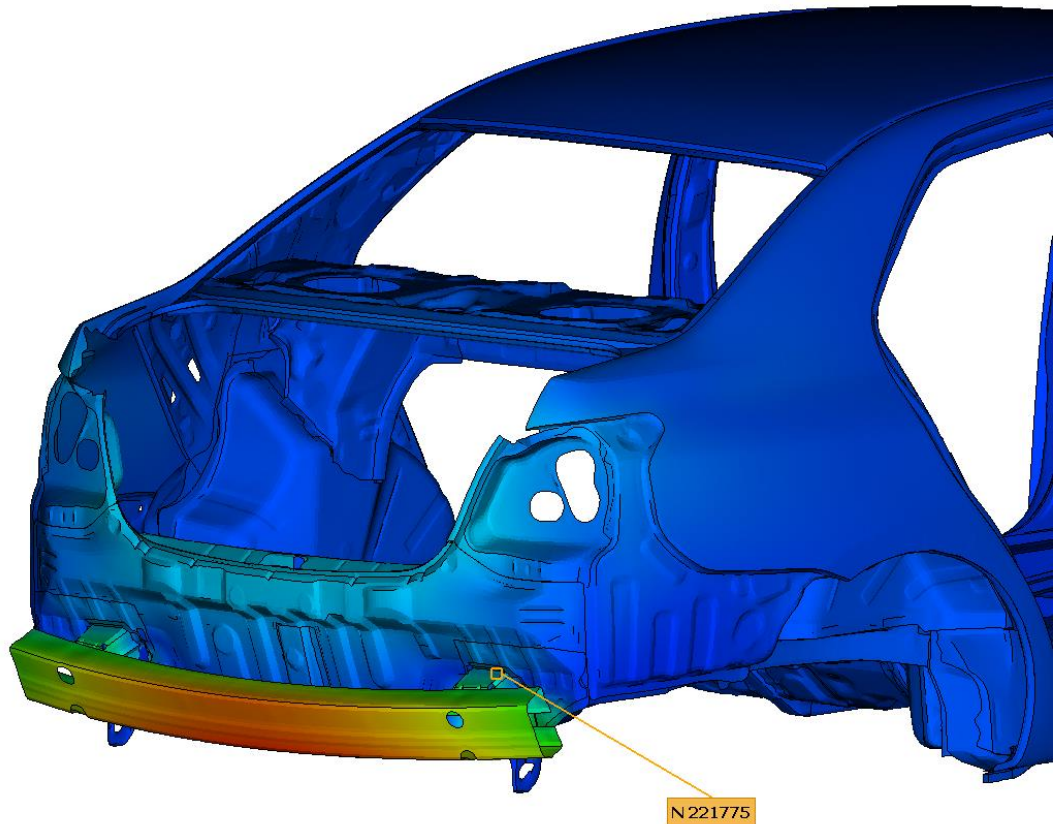


Figure 81 Mode 2 with hotspot and critical point (2/3)

Contour:  
Von Mises  
stress  
State:  
Undeformed

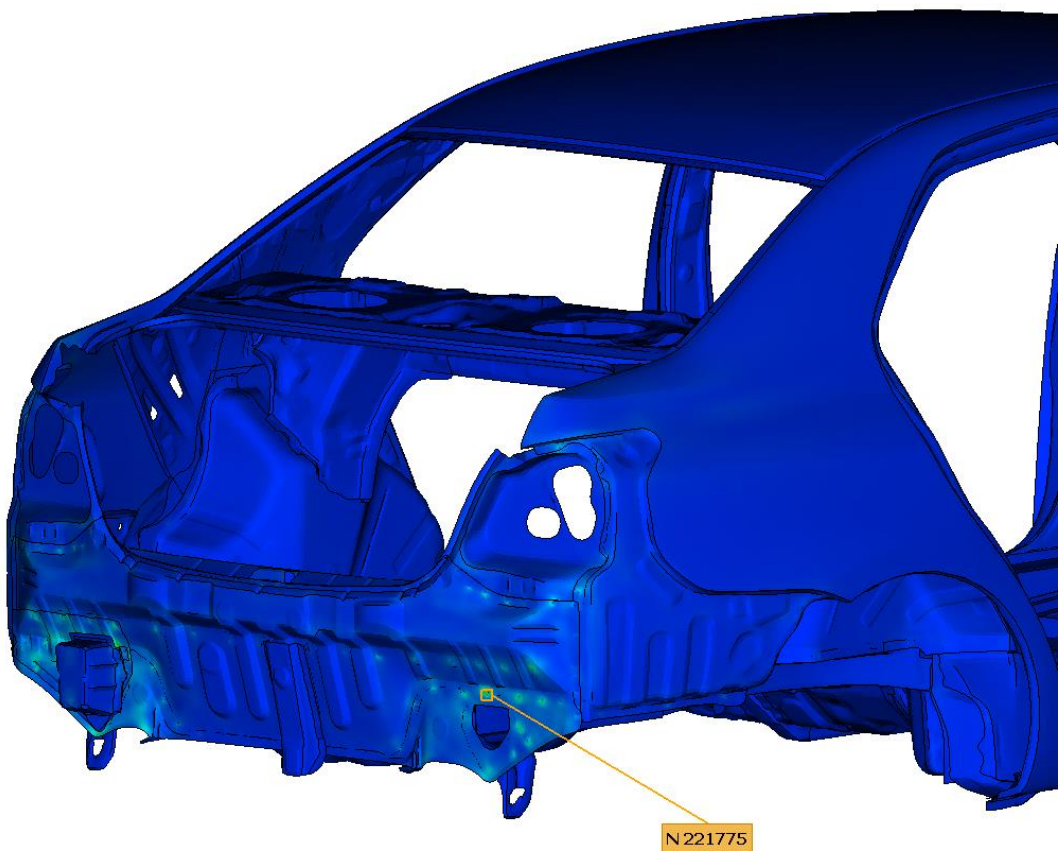


Figure 82 Mode 2 with hotspot and critical point (3/3)

### B.2.5. Mode 28

Contour:  
deformation  
State:  
Undeformed

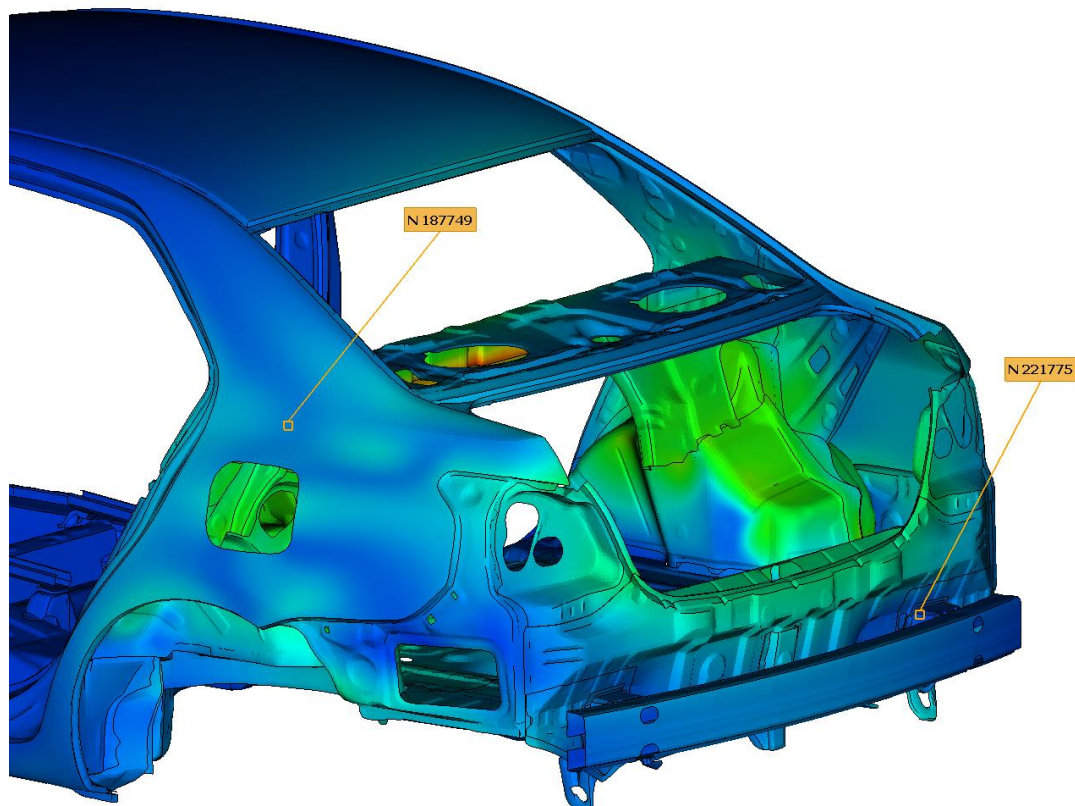


Figure 83 Mode 28 with hotspot and critical point (1/3)

Contour:  
deformation  
State:  
Deformed

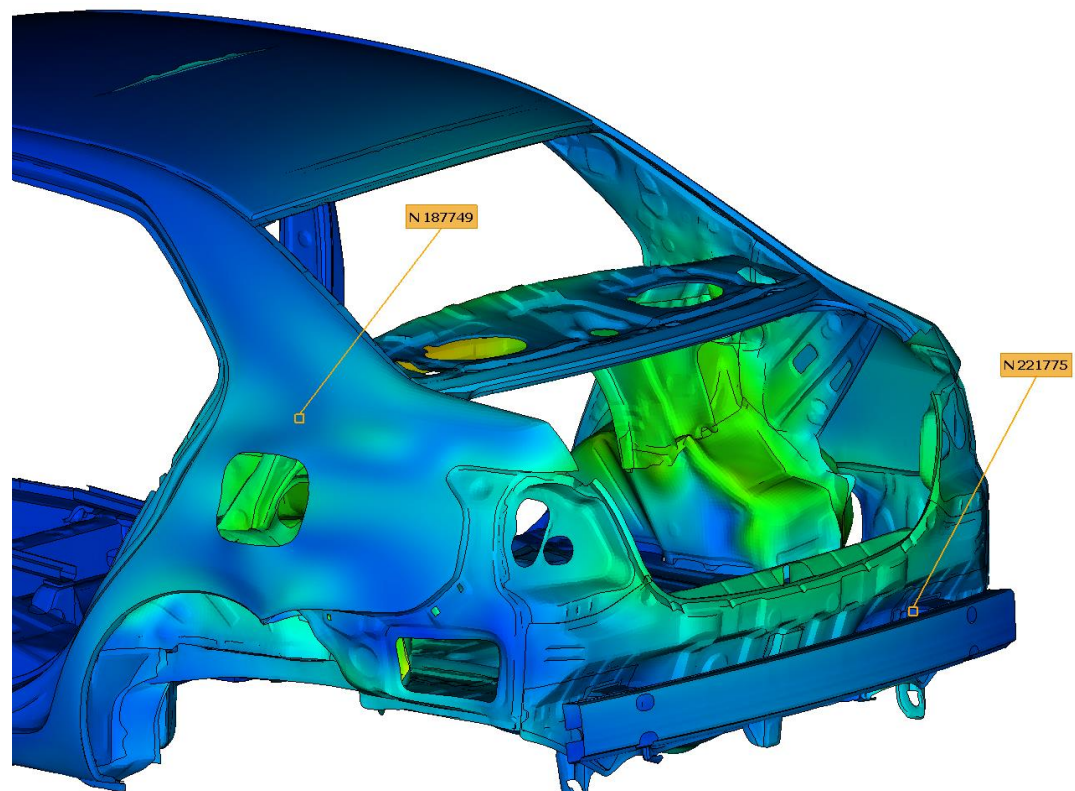


Figure 84 Mode 28 with hotspot and critical point (2/3)

**Contour:**  
**Von Mises**  
**stress**  
**State:**  
**Undeformed**

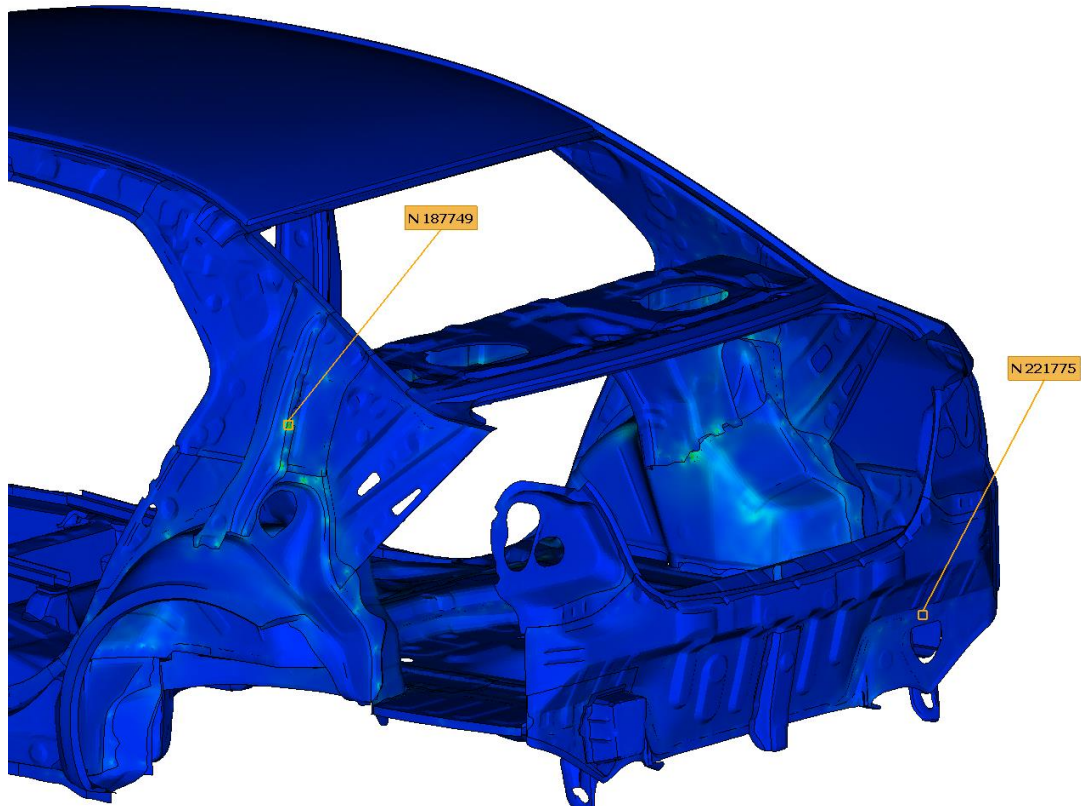


Figure 85 Mode 28 with hotspot and critical point (3/3)

### B.2.6. Mode 110

Contour:  
deformation  
State:  
Undeformed

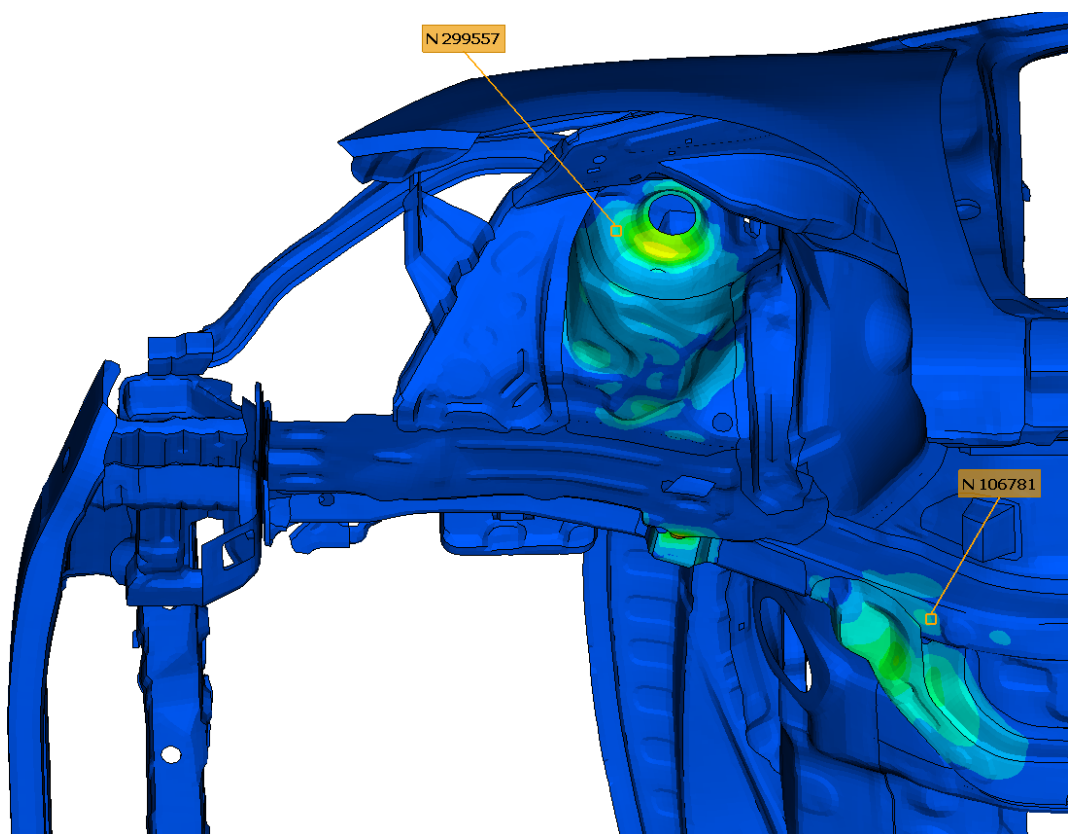


Figure 86 Mode 110 with hotspot and critical point (1/3)

Contour:  
deformation  
State:  
Deformed

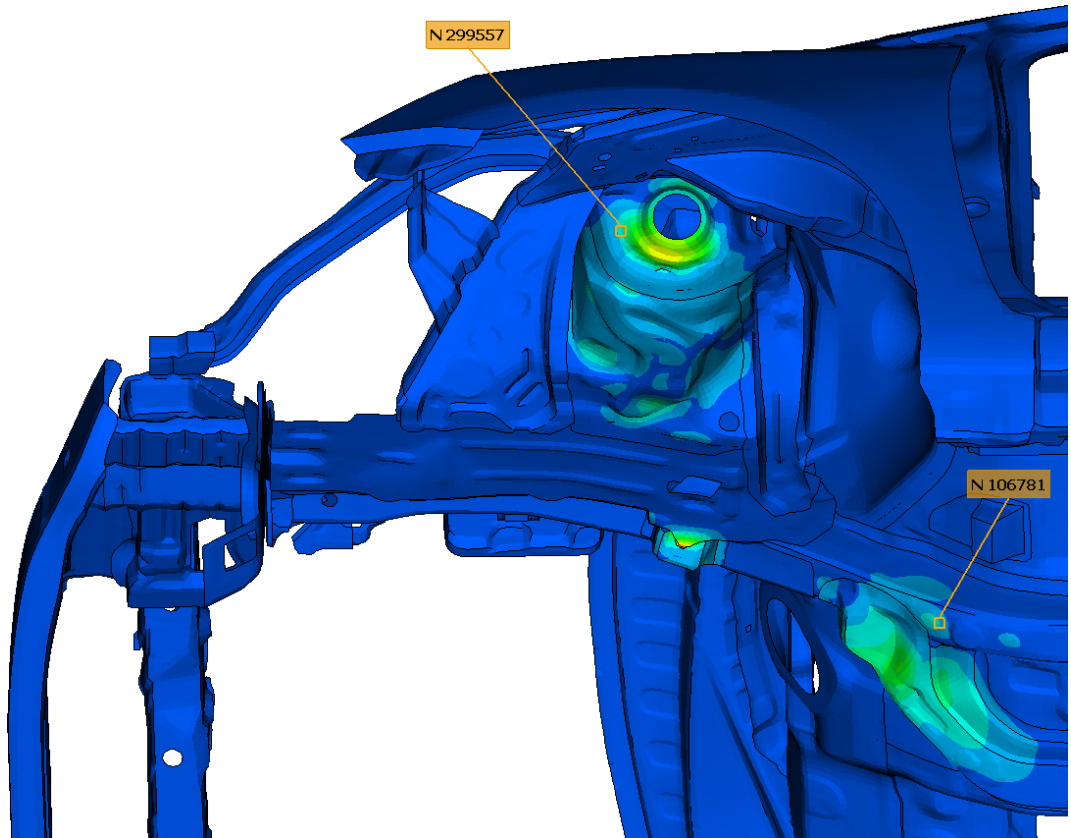


Figure 87 Mode 110 with hotspot and critical point (2/3)

Contour:  
Von Mises  
stress  
State:  
Undeformed

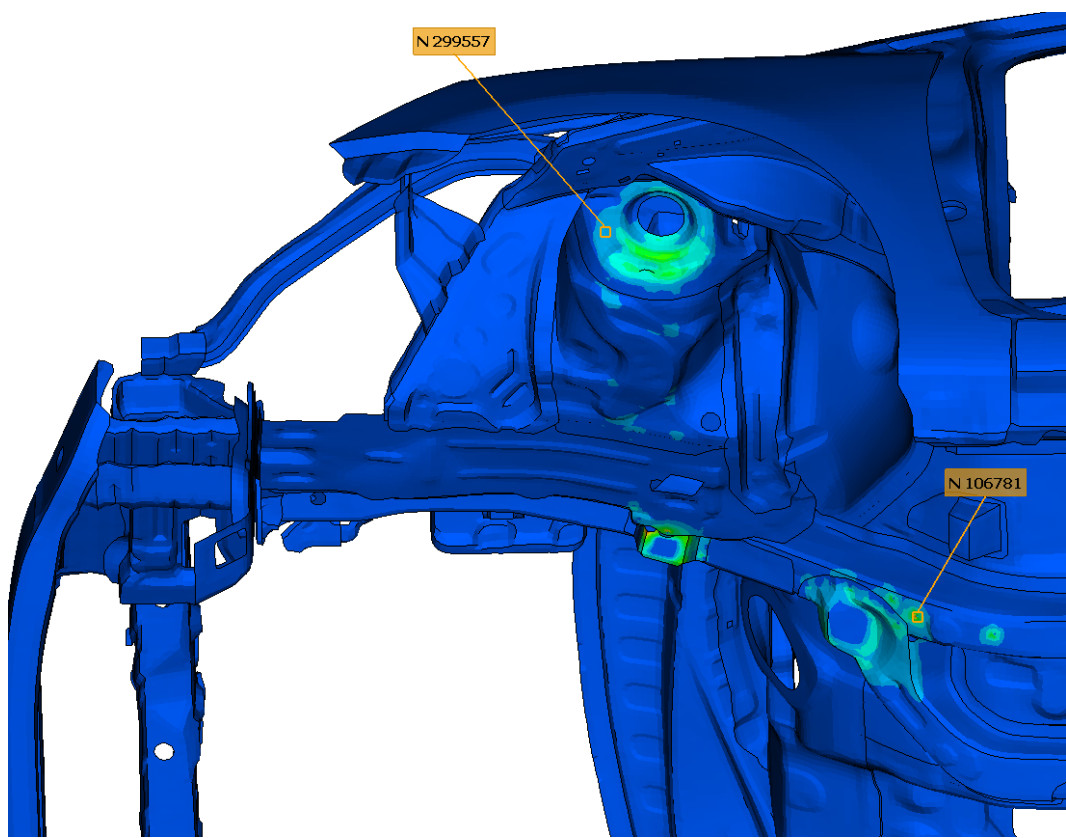


Figure 88 Mode 110 with hotspot and critical point (3/3)

### B.2.7. Mode 114

Contour:  
deformation  
State:  
Undeformed

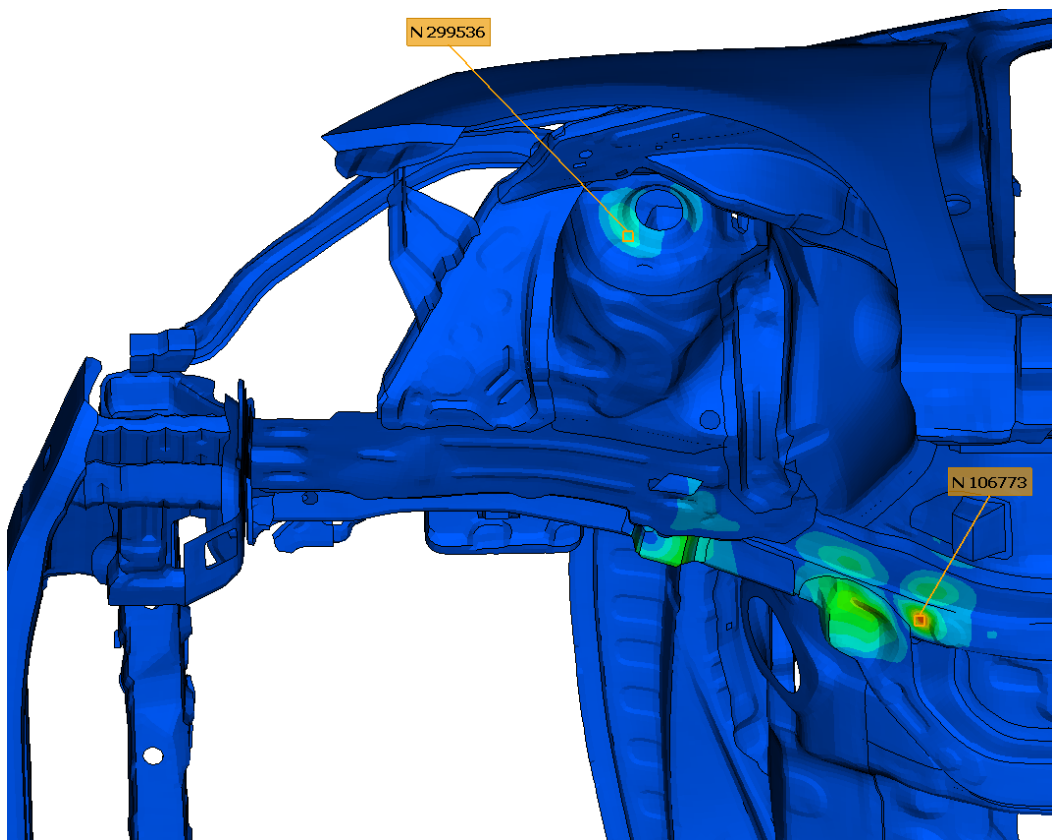


Figure 89 Mode 114 with hotspot and critical point (1/3)

Contour:  
deformation  
State:  
Deformed

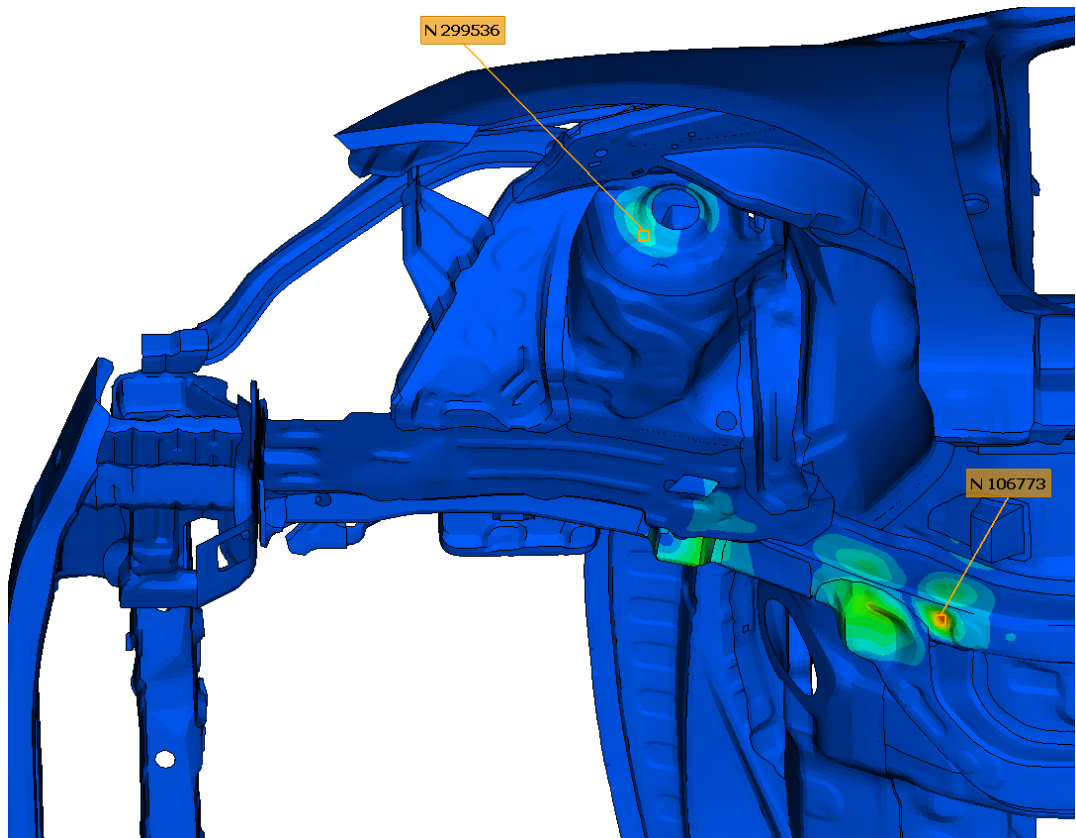


Figure 90 Mode 114 with hotspot and critical point (2/3)

Contour:  
Von Mises  
stress  
State:  
Undeformed

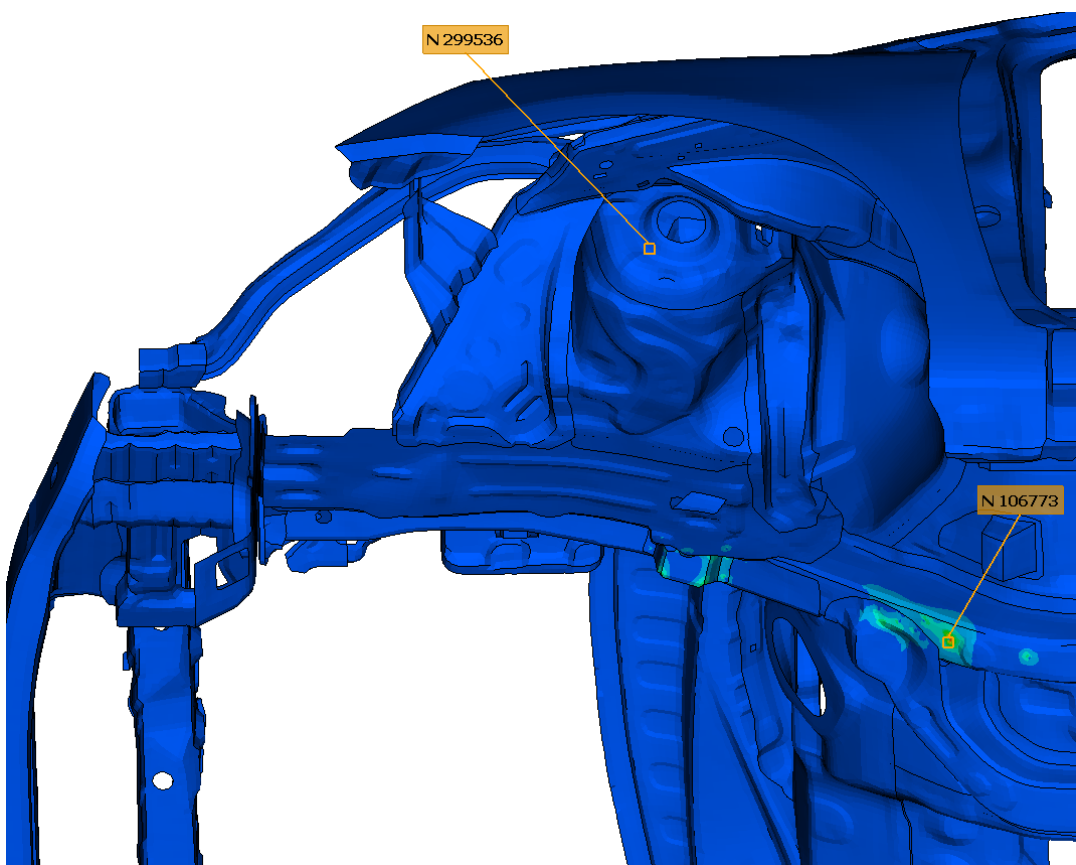


Figure 91 Mode 114 with hotspot and critical point (3/3)

# Appendix C

## C.1. Accelerometer locations and channels

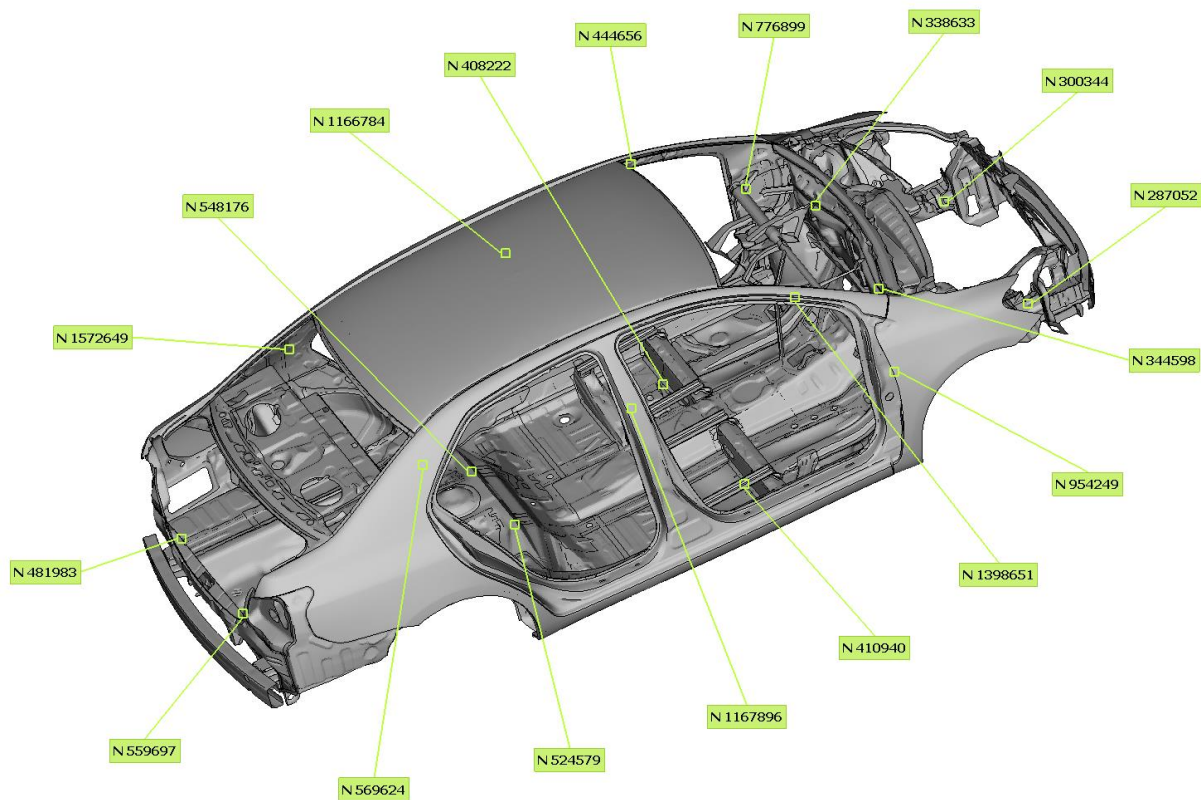


Figure 92 Locations of accelerometers (1/3)

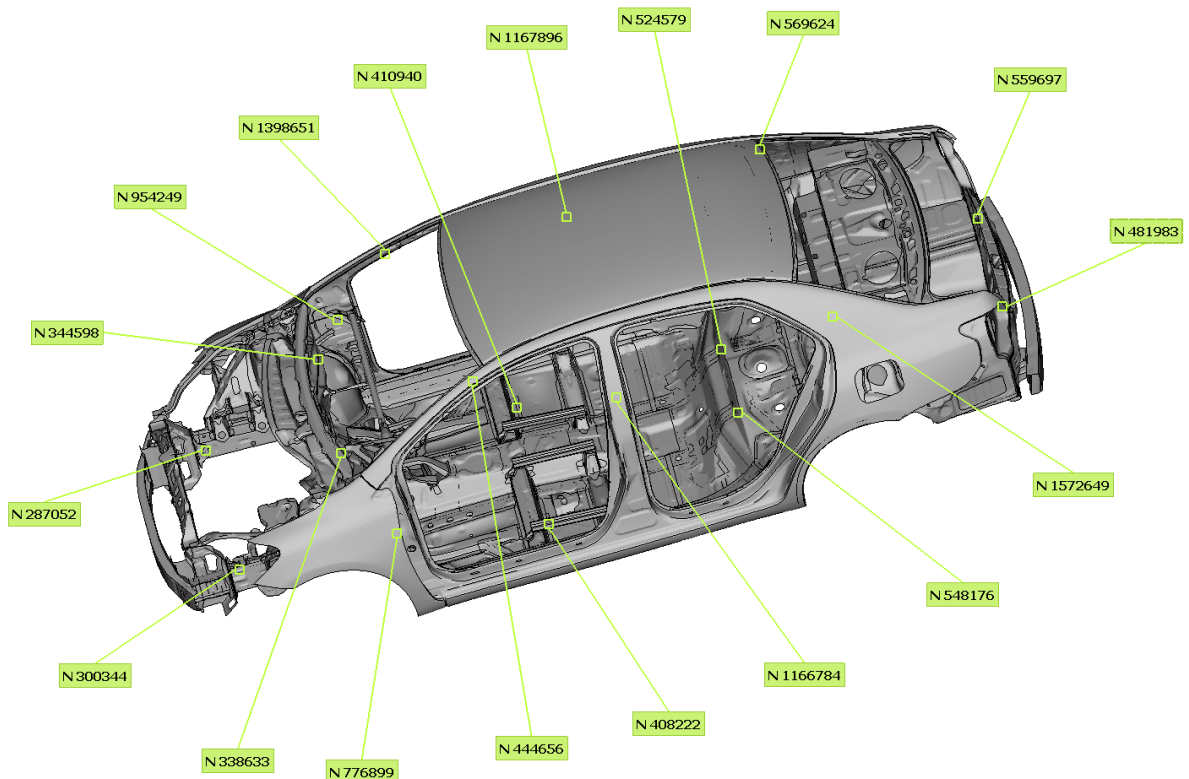


Figure 93 Locations of accelerometers (2/3)

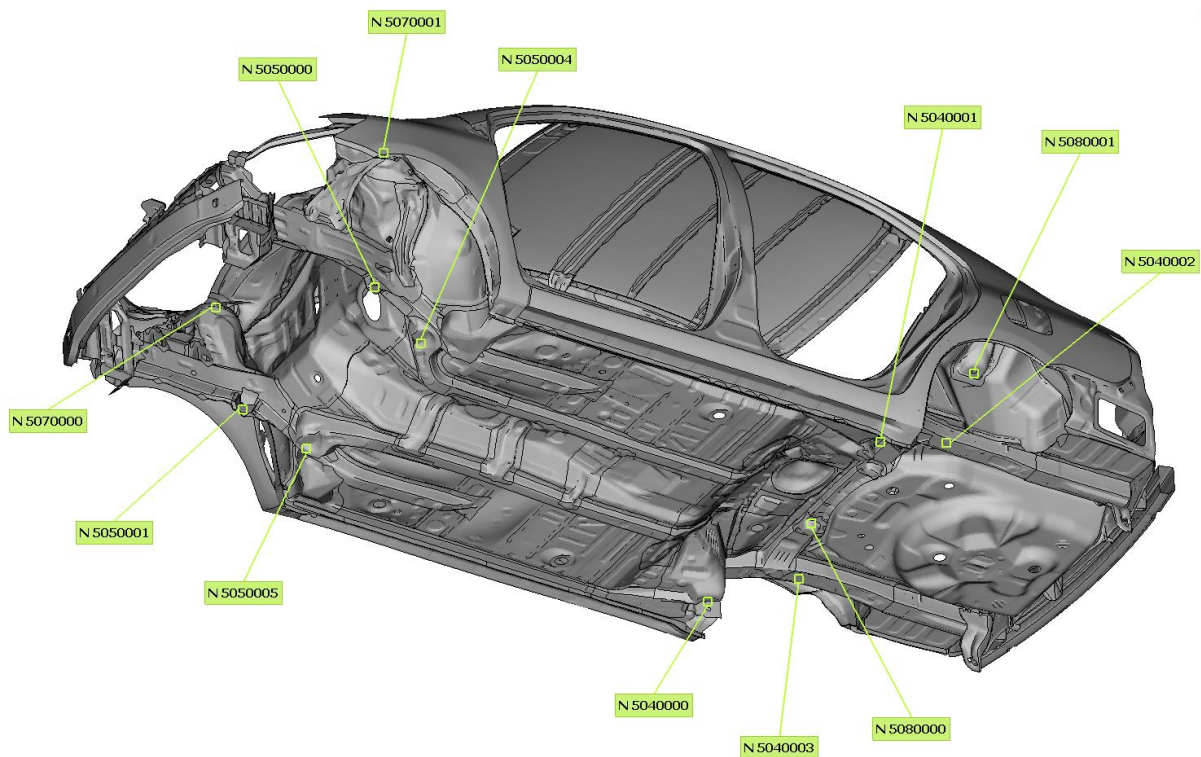


Figure 94 Locations of accelerometers (3/3)

Channel nr	Location	Acceleration component t-translation r-rotation	Channel nr	Location	Acceleration component t-translation r-rotation
1	Upright Front_L	tX	43	N5040002	tX
2	Upright Front_L	tY	44	N5040002	tY
3	Upright Front_L	tZ	45	N5040002	tZ
4	Upright Front_L	rX	46	N5040002	rX
5	Upright Front_L	rY	47	N5040002	rY
6	Upright Front_L	rZ	48	N5040002	rZ
7	Upright Front_R	tX	49	N5080001	tX
8	Upright Front_R	tY	50	N5080001	tY
9	Upright Front_R	tZ	51	N5080001	tZ
10	Upright Front_R	rX	52	N5080001	rX
11	Upright Front_R	rY	53	N5080001	rY
12	Upright Front_R	rZ	54	N5080001	rZ
13	Upright Rear_L	tX	55	N5040001	tX
14	Upright Rear_L	tY	56	N5040001	tY
15	Upright Rear_L	tZ	57	N5040001	tZ
16	Upright Rear_L	rX	58	N5040001	rX
17	Upright Rear_L	rY	59	N5040001	rY
18	Upright Rear_L	rZ	60	N5040001	rZ
19	Upright Rear_R	tX	61	N5050001	tX
20	Upright Rear_R	tY	62	N5050001	tY
21	Upright Rear_R	tZ	63	N5050001	tZ
22	Upright Rear_R	rX	64	N5050001	rX
23	Upright Rear_R	rY	65	N5050001	rY
24	Upright Rear_R	rZ	66	N5050001	rZ
25	N5070001	tX	67	N5050005	tX
26	N5070001	tY	68	N5050005	tY
27	N5070001	tZ	69	N5050005	tZ
28	N5070001	rX	70	N5050005	rX
29	N5070001	rY	71	N5050005	rY
30	N5070001	rZ	72	N5050005	rZ
31	N5050000	tX	73	N5070000	tX
32	N5050000	tY	74	N5070000	tY
33	N5050000	tZ	75	N5070000	tZ
34	N5050000	rX	76	N5070000	rX
35	N5050000	rY	77	N5070000	rY
36	N5050000	rZ	78	N5070000	rZ
37	N5050004	tX	79	N5040000	tX
38	N5050004	tY	80	N5040000	tY
39	N5050004	tZ	81	N5040000	tZ
40	N5050004	rX	82	N5040000	rX
41	N5050004	rY	83	N5040000	rY
42	N5050004	rZ	84	N5040000	rZ

Channel nr	Location	Acceleration component t-translation r-rotation	Channel nr	Location	Acceleration component t-translation r-rotation
85	N5040003	tX	127	N338633	tX
86	N5040003	tY	128	NN338633	tY
87	N5040003	tZ	129	N338633	tZ
88	N5040003	rX	130	N338633	rX
89	N5040003	rY	131	N338633	rY
90	N5040003	rZ	132	N338633	rZ
91	N5080000	tX	133	N1398651	tX
92	N5080000	tY	134	N1398651	tY
93	N5080000	tZ	135	N1398651	tZ
94	N5080000	rX	136	N1398651	rX
95	N5080000	rY	137	N1398651	rY
96	N5080000	rZ	138	N1398651	rZ
97	N287052	tX	139	N444656	tX
98	N287052	tY	140	N444656	tY
99	N287052	tZ	141	N444656	tZ
100	N287052	rX	142	N444656	rX
101	N287052	rY	143	N444656	rY
102	N287052	rZ	144	N444656	rZ
103	N300344	tX	145	N410940	tX
104	N300344	tY	146	N410940	tY
105	N300344	tZ	147	N410940	tZ
106	N300344	rX	148	N410940	rX
107	N300344	rY	149	N410940	rY
108	N300344	rZ	150	N410940	rZ
109	N954249	tX	151	N408222	tX
110	N954249	tY	152	N408222	tY
111	N954249	tZ	153	N408222	tZ
112	N954249	rX	154	N408222	rX
113	N954249	rY	155	N408222	rY
114	N954249	rZ	156	N408222	rZ
115	N776899	tX	157	N1167896	tX
116	N776899	tY	158	N1167896	tY
117	N776899	tZ	159	N1167896	tZ
118	N776899	rX	160	N1167896	rX
119	N776899	rY	161	N1167896	rY
120	N776899	rZ	162	N1167896	rZ
121	N344598	tX	163	N1166784	tX
122	N344598	tY	164	N1166784	tY
123	N344598	tZ	165	N1166784	tZ
124	N344598	rX	166	N1166784	rX
125	N344598	rY	167	N1166784	rY
126	N344598	rZ	168	N1166784	rZ

Channel nr	Location	Acceleration component t-translation r-rotation	Channel nr	Location	Acceleration component t-translation r-rotation
<b>169</b>	N569624	tX	<b>187</b>	N548176	tX
<b>170</b>	N569624	tY	<b>188</b>	N548176	tY
<b>171</b>	N569624	tZ	<b>189</b>	N548176	tZ
<b>172</b>	N569624	rX	<b>190</b>	N548176	rX
<b>173</b>	N569624	rY	<b>191</b>	N548176	rY
<b>174</b>	N569624	rZ	<b>192</b>	N548176	rZ
<b>175</b>	N1572649	tX	<b>193</b>	N559697	tX
<b>176</b>	N1572649	tY	<b>194</b>	N559697	tY
<b>177</b>	N1572649	tZ	<b>195</b>	N559697	tZ
<b>178</b>	N1572649	rX	<b>196</b>	N559697	rX
<b>179</b>	N1572649	rY	<b>197</b>	N559697	rY
<b>180</b>	N1572649	rZ	<b>198</b>	N559697	rZ
<b>181</b>	N524579	tX	<b>199</b>	N481983	tX
<b>182</b>	N524579	tY	<b>200</b>	N481983	tY
<b>183</b>	N524579	tZ	<b>201</b>	N481983	tZ
<b>184</b>	N524579	rX	<b>202</b>	N481983	rX
<b>185</b>	N524579	rY	<b>203</b>	N481983	rY
<b>186</b>	N524579	rZ	<b>204</b>	N481983	rZ

Table 12 Accelerometer channels

## Appendix D

### D.1. Results of optimization

$f_{max}^* = 1.358677420700428$		
$Ch_{7,12}$	$\lambda_i^*$	$\beta_i^*$
4	0	14,99125
9	9,71E-06	4,980318
25	0	7,9979
28	7,64E-10	3,887478
30	1,56E-06	14,87369
116	0	10,46458
118	2,31E-11	15
120	2,44E-10	14,67765
127	9,94E-13	10,09259
130	0	1,277488
132	1,08E-12	6,514354
152	0	14,56201

Table 13 Parameters of optimized pseudo damage definition from  $Ch_{7,12}$

$f_{max}^* = 1.360380355800833$		
$Ch_{7,36}$	$\lambda_i^*$	$\beta_i^*$
3	3,23E-07	5,490054
4	1,98E-10	1,00015
9	9,71E-06	4,979434
15	6,73E-08	6,287481
25	8,54E-10	14,22836
26	3,27E-08	1,328867
28	5,47E-07	3,008519
30	1,43E-14	1,694844
38	8,64E-10	1,040514
39	1,10E-07	11,97839
61	3,04E-10	2,355087
63	4,49E-07	2,362405
66	1,43E-07	14,56331

67	4,14E-10	7,708415
68	1,59E-07	2,418322
69	8,34E-09	14,9058
75	1,62E-06	13,21716
87	5,34E-11	2,00336
102	0	1,13701
115	2,98E-08	1,295229
116	8,63E-10	1,143585
117	0	1,001812
118	3,30E-06	7,596345
120	2,04E-05	10,5394
127	1,06E-08	12,85161
128	1,14E-07	2,936581
130	8,75E-07	4,89802
132	8,32E-08	2,631775
140	3,25E-08	5,210847
142	3,55E-11	2,523828
152	0	1,097531
153	8,03E-09	2,131463
154	3,06E-10	14,42113
164	6,75E-08	3,720738
166	2,74E-11	8,447918
192	7,46E-06	5,610345

Table 14 Parameters of optimized pseudo damage definition from  $Ch_{7,36}$

$f_{max}^* = 1.543264847853714$		
$Ch_{7,102}$	$\lambda_i^*$	$\beta_i^*$
1	1,30E-07	5,306271
3	3,48E-07	13,73999
4	2,06E-06	5,666461
9	9,29E-06	4,964521
10	4,50E-07	9,422079
14	5,32E-06	2,12685
15	1,36E-07	4,09167
19	1,18E-06	14,80444
20	3,62E-06	2,163216

21	1,32E-07	6,260728
23	8,37E-07	12,66762
25	1,21E-07	14,10731
26	1,50E-08	2,463043
28	5,54E-06	12,68737
30	1,20E-06	2,71984
38	1,00E-06	10,24283
39	1,03E-06	8,47158
43	2,16E-06	14,998
44	9,36E-07	14,99025
45	4,89E-07	5,039024
46	1,51E-07	14,41508
47	1,02E-05	13,06098
49	7,43E-07	12,71906
51	4,17E-09	2,185271
55	4,65E-07	12,82027
56	7,35E-07	12,49373
57	2,94E-08	13,5416
58	2,16E-09	5,303201
59	4,51E-07	10,95913
61	2,23E-06	11,11378
62	3,72E-07	14,40031
63	1,02E-06	10,10771
66	7,49E-07	7,083854
67	6,82E-07	14,15423
68	1,05E-07	3,81429
69	2,61E-06	12,36893
71	6,26E-06	14,7741
72	1,59E-05	14,87032
73	6,75E-07	6,782085
74	5,21E-07	5,544736
75	5,43E-08	13,87493
78	1,77E-06	9,188461
79	2,37E-06	10,04524
80	1,50E-06	14,05432
81	7,33E-07	10,93782
85	1,93E-06	9,036242
87	3,78E-07	14,96242
88	2,73E-06	13,90431

89	2,70E-06	3,293166
91	1,37E-06	8,83472
93	1,77E-07	10,28147
96	1,56E-06	13,29807
98	2,94E-07	14,79716
102	8,47E-08	12,38507
104	2,90E-07	14,51427
109	1,36E-07	11,07548
110	5,38E-07	14,38258
111	4,11E-07	14,60122
114	3,68E-09	12,78179
115	3,15E-08	6,370703
116	3,07E-07	6,949781
117	2,60E-08	14,4768
118	5,35E-06	6,841535
120	1,26E-06	10,38494
121	8,89E-08	14,58662
122	2,62E-07	14,24928
123	3,10E-08	4,277017
126	1,88E-08	10,51419
127	3,87E-07	3,455252
128	1,83E-06	13,79786
130	1,61E-06	6,737259
132	2,32E-06	10,38767
133	2,80E-07	10,67239
134	1,17E-08	13,23761
138	1,12E-06	9,522102
140	3,26E-09	2,15025
142	1,35E-07	6,610144
145	5,98E-07	3,295227
147	7,97E-08	5,904292
149	1,19E-06	3,482635
152	4,95E-08	6,984771
153	2,05E-08	12,46733
154	5,96E-07	12,43264
164	4,82E-08	5,211981
166	2,25E-07	10,24298
171	4,17E-07	8,965737
174	2,39E-06	7,434753

175	1,77E-08	4,330686
177	8,70E-08	11,65252
181	1,13E-06	5,241904
182	9,67E-06	2,194763
183	1,48E-07	11,49703
184	1,03E-07	5,786845
185	1,73E-06	9,677534
187	1,08E-06	14,22038
188	3,94E-08	2,862716
189	7,03E-07	14,63854
190	1,24E-06	12,53474
192	3,85E-07	14,82087
193	2,51E-09	7,269797
198	2,01E-06	7,205117
199	6,76E-07	14,88726

Table 15 Parameters of optimized pseudo damage definition from  $Ch_{7,102}$

$f_{max}^* = 0$		
$Ch_{8,12}$	$\lambda_i^*$	$\beta_i^*$
2	1,68E-06	1,371234088
10	1,45E-06	14,99998604
32	7,63E-07	1,003811757
69	3,58E-13	1,696055742
105	1,87E-06	1,019921453
122	0	2,361586959
140	0	14,99946711
142	3,46E-05	3,032251265
152	0	1
154	0	1,022744961
164	2,10E-07	1,07109567
166	0	6,844809082

Table 16 Parameters of optimized pseudo damage definition from  $Ch_{8,12}$

$f_{max}^* = \mathbf{0}$		
$Ch_{8,36}$	$\lambda_i^*$	$\beta_i^*$
2	2,91E-07	1,281861505
10	2,88E-11	1
12	3,66E-05	14,37849404
20	5,42E-06	13,04323609
32	1,20E-05	1,007019786
33	1,13E-06	1,269974213
39	9,37E-06	1,041369877
44	1,48E-07	7,939521014
48	5,19E-08	1,639763055
55	6,86E-07	11,82703019
69	3,69E-11	2,042366823
83	7,78E-06	8,393641555
85	2,19E-06	1
86	2,11E-05	1,034177724
91	4,69E-06	1
97	4,22E-07	1,819953714

Table 17 Parameters of optimized pseudo damage definition from  $Ch_{8,36}$

$f_{max}^* = \mathbf{0}$		
$Ch_{8,102}$	$\lambda_i^*$	$\beta_i^*$
2	1,66E-05	5,637230657
4	1,92E-05	9,157802795
5	4,45E-06	9,996009646
6	1,03E-06	10,82279945
7	1,29E-06	10,24771059
8	1,78E-05	6,700114126
10	4,19E-06	10,38453495
12	9,93E-06	11,56618783
13	1,35E-05	6,226079628
14	4,87E-07	13,4516805
15	6,09E-06	3,925921804
16	1,93E-05	8,388097324
20	1,30E-05	8,450713559

25	1,23E-05	13,03587512
26	1,77E-05	13,608508
27	1,69E-05	13,54538628
28	9,89E-06	1,373268167
30	1,01E-05	13,93322218
32	1,90E-05	10,85271764
33	2,27E-06	14,99538364
37	1,98E-05	5,995795944
38	1,68E-05	14,35386089
39	5,73E-08	8,096146611
42	9,47E-08	13,59211577
44	7,34E-06	7,271383811
48	3,21E-07	14,36074945
50	8,41E-06	8,82358779
54	2,00E-07	1,992013777
55	1,56E-05	1,658512804
56	1,53E-05	1,052503267
60	1,53E-05	4,224767914
63	9,33E-06	8,353126204
64	6,18E-06	5,420586631
68	1,89E-05	13,10149556
69	1,16E-05	10,75261038
70	1,68E-05	10,80251273
71	1,35E-05	10,20856005
73	2,28E-06	12,94385994
75	8,99E-06	14,99996744
76	7,85E-06	2,248064726
79	1,81E-05	8,100959563
81	4,97E-06	3,706011331
83	1,69E-05	10,81247712
85	4,08E-06	5,441679779
86	1,32E-05	2,848617544
87	5,83E-06	2,23480246
89	1,71E-05	13,77270483
90	2,00E-05	13,40236979
91	1,65E-05	8,008699156
93	2,56E-06	3,290107581
97	1,86E-05	10,31821286
98	1,99E-06	1,663043545

99	9,42E-06	3,497351554
100	2,00E-05	6,50035303
105	1,70E-05	1,901168833
110	1,24E-06	11,18763145
112	5,74E-06	6,412741918
115	9,67E-06	9,418306411
116	8,21E-06	4,219808189
117	5,46E-06	1,225378514
118	1,10E-05	10,06299748
120	1,70E-05	7,26513578
121	6,26E-06	4,858482504
122	9,36E-06	1,919289898
123	1,52E-07	10,43378607
124	1,44E-05	14,16941686
127	0	6,653717667
128	6,72E-07	10,41865887
130	1,98E-05	2,552676538
132	5,64E-06	11,50916731
136	6,44E-06	13,97718051
139	1,40E-05	4,196459483
140	5,57E-08	1,531059417
141	5,73E-06	12,79854335
142	2,06E-06	1,757698984
143	1,73E-05	13,6737827
144	8,80E-06	9,581005703
145	1,10E-05	13,78665641
146	7,95E-07	10,01875577
150	1,12E-05	2,659239721
152	0	12,47573536
153	5,87E-07	1,953223882
154	1,93E-05	6,177808388
155	2,97E-08	13,95825021
156	1,82E-05	13,47858306
159	8,37E-07	5,707254287
160	1,03E-05	11,74263369
162	6,75E-06	8,916377734
163	1,21E-05	3,706677953
164	6,78E-07	4,466927066
165	1,20E-05	2,368532651

166	4,02E-06	1,42123427
167	1,60E-05	6,323139167
168	1,20E-05	8,720799176
180	1,36E-05	1,022418566
182	2,32E-06	4,72445996
185	1,76E-05	4,373043354
186	1,14E-05	4,667892305
188	1,20E-05	6,788419796
190	1,47E-05	6,471372239
200	1,06E-05	9,888197686
204	8,38E-06	10,38174149

Table 18 Parameters of optimized pseudo damage definition from  $Ch_{8,102}$

$f_{max}^* = 0.251351569499340$		
$Ch_{9,12}$	$\lambda_i^*$	$\beta_i^*$
25	5,43E-09	13,66453879
31	4,06E-07	14,99996305
45	0,00E+00	15
73	7,05E-06	15
79	2,35E-09	4,458026182
82	8,91E-05	7,77435679
85	0,00E+00	1,005516352
91	7,45E-06	14,99898398
115	9,07E-11	1,065269466
121	1,82E-05	4,757090427
145	5,27E-06	14,99541878
193	9,68E-06	2,374579323

Table 19 Parameters of optimized pseudo damage definition from  $Ch_{9,12}$

$$f_{max}^* = 0.109045511061222$$

<i>Ch<sub>9,36</sub></i>	$\lambda_i^*$	$\beta_i^*$
2	0,00E+00	15
4	5,49E-05	14,03436187
8	0,00E+00	9,734375205
12	1,58E-11	1,004001196
13	0,00E+00	15
23	3,29E-14	5,603898256
25	9,17E-19	1,001988307
30	2,54E-13	1,006935777
31	3,77E-07	1,000016913
39	2,53E-05	15
43	5,52E-18	3,571268471
45	0,00E+00	14,96077204
49	1,34E-20	12,84104088
51	0,00E+00	15
55	0,00E+00	1
56	7,04E-23	6,248057212

Table 20 Parameters of optimized pseudo damage definition from Ch<sub>9,36</sub>

$$f_{max}^* = 0.090590095672108$$

<i>Ch<sub>9,102</sub></i>	$\lambda_i^*$	$\beta_i^*$
1	6,28E-06	8,700186576
2	9,38E-06	6,911082182
3	2,55E-08	9,256416342
4	7,93E-06	6,532483688
6	1,35E-05	8,716159439
7	5,68E-06	5,487135347
8	3,40E-06	3,405925584
9	2,22E-07	14,36652001
12	1,27E-05	8,536127833
13	4,20E-06	8,512873632
14	5,21E-06	4,921599958
15	2,17E-07	5,003747408
16	1,51E-05	14,81560525

17	1,34E-05	8,294967431
20	8,32E-09	9,735769539
21	1,24E-06	5,845165918
22	3,72E-06	14,50334497
23	6,51E-07	7,934278827
25	8,84E-06	9,740160474
26	1,11E-05	5,769486686
27	9,13E-07	14,97537964
28	7,03E-06	3,317676212
29	1,42E-05	8,068541974
30	1,89E-05	10,98575983
31	2,35E-06	6,227582411
32	6,86E-07	14,22930624
33	3,32E-06	5,639092588
36	3,34E-06	14,31142268
37	1,63E-05	13,19880167
39	1,79E-05	11,98510885
43	2,88E-06	14,79463794
45	1,29E-05	14,85136335
49	1,04E-05	7,465743352
50	6,88E-06	13,14110694
51	1,20E-05	7,157502421
54	5,47E-06	7,400786544
55	9,62E-06	13,744235
56	1,63E-05	10,72860794
57	7,73E-06	5,578394069
59	2,05E-06	5,350359858
61	1,90E-06	5,951371911
62	1,99E-05	5,989952097
63	2,16E-06	5,255499185
67	8,92E-06	12,15407078
68	1,09E-05	11,58118115
69	2,10E-08	4,261358294
71	8,06E-06	12,49268574
73	1,13E-05	14,02657478
74	7,03E-07	11,79252263
75	2,31E-06	14,87957978
78	1,64E-05	13,27035979
79	1,06E-05	13,64473951

80	2,00E-05	6,172628279
81	1,30E-05	9,843992869
82	9,02E-06	13,99583788
83	9,44E-06	4,06132874
85	1,27E-05	12,04506595
86	2,00E-05	4,12494413
87	1,39E-05	11,31303575
89	1,44E-05	7,741568015
91	1,11E-06	14,51373659
92	5,41E-06	10,01338586
93	8,89E-06	8,517607189
98	2,25E-07	6,808733214
103	4,92E-06	12,21593455
108	7,90E-06	3,888718325
109	9,61E-06	8,872960841
110	3,55E-06	11,39695561
111	4,19E-06	14,25022019
114	1,44E-05	14,81046428
115	5,53E-06	4,909786688
116	3,03E-06	14,74706432
117	8,34E-06	6,455632544
118	1,55E-05	4,750356464
119	4,78E-06	3,023689744
120	1,88E-05	14,81091168
121	9,41E-06	4,221657714
126	2,00E-05	8,788258438
127	6,15E-06	14,29591325
128	2,00E-05	7,206402897
129	1,01E-06	5,063153773
130	2,00E-05	8,268186262
131	4,10E-06	6,524384706
132	1,03E-06	7,74585489
138	5,03E-06	6,314033791
140	4,58E-07	5,333682501
142	8,75E-06	7,756139067
144	1,86E-05	5,899881105
145	1,27E-05	9,271694561
152	3,33E-06	6,903417177
153	1,72E-06	6,746058343

154	8,76E-06	8,859460133
156	1,95E-05	14,96824056
164	3,61E-08	9,332843668
166	2,73E-06	7,725566293
168	1,79E-05	11,51349604
180	8,62E-07	7,324584947
181	8,33E-06	10,24119586
183	5,94E-06	13,21079457
193	1,01E-05	8,253200333
199	8,63E-06	11,80125966
204	1,38E-05	14,73277429

Table 21 Parameters of optimized pseudo damage definition from  $Ch_{9,102}$

Optimization parameters	$G_7$	$G_8$	$G_9$
$Ch_{l,12}$	NIND=60 MAXGEN=500 GGAP=0,9	NIND=60 MAXGEN=500 GGAP=0,9	NIND=60 MAXGEN=1000 GGAP=0,9
$Ch_{l,36}$	NIND=60 MAXGEN=1000 GGAP=0,9	NIND=60 MAXGEN=2000 GGAP=0,9	NIND=60 MAXGEN=2500 GGAP=0,9
$Ch_{l,102}$	NIND=150 MAXGEN=2500 GGAP=0,9	NIND=60 MAXGEN=1000 GGAP=0,9	NIND=100 MAXGEN=1000 GGAP=0,9

Table 22 Optimization parameters

NIND - number of individuals per subpopulations

MAXGEN - maximum number of generations

GGAP - Generation gap (how many new individuals are created)